Manufacturing Methods for High Density Micro-Channel Arrays

by

Luke Sosnowski

Submitted to the Department of Mechanical Engineering
in partial fulfillment of the requirements for the degree of

Master of Science in Mechanical Engineering

at the

MASSACHUSETTS INSTITUTE OF TECHNOLOGY

May 2000
[June 2000]

©Massachusetts Institute of Technology 2000. All rights reserved.

Author ....
Department of Mechanical Engineering
May 18, 2000

Certified by ....
Ian W. Hunter
Professor of Mechanical Engineering and Professor of BioEngineering
Thesis Supervisor

Accepted by ....
Ain A. Sonin
Chairman, Department Committee on Graduate Students

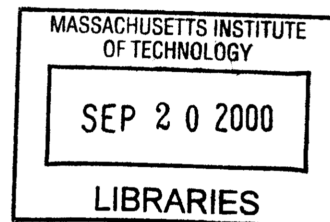
MASSACHUSETTS INSTITUTE OF TECHNOLOGY
SEP 2 0 2000
LIBRARIES
ARCHIVES

Manufacturing Methods for High Density Micro-Channel Arrays

by

Luke Sosnowski

Submitted to the Department of Mechanical Engineering
on May 18, 2000, in partial fulfillment of the
requirements for the degree of
Master of Science in Mechanical Engineering

Abstract

This thesis explores two distinct methods of micro-array manufacture for high throughput pharmaceutical scanning. The first method, impact shaping of polymers, is a novel, inexpensive way to form large numbers of small channels or wells in plastics. The impact method uses the kinetic energy from a ram to punch holes into a polymer sample without melting the bulk of the workpiece. The second method is electrical discharge machining (EDM) of silicon, which machines high aspect ratio holes arranged in high density arrays on silicon wafers. The method may be viewed as complementary to current plasma etching techniques and lithography. Several testing platforms were devised for the creation of the plastic well arrays based on the high speed ram principle. A modified Charmilles Roboform 30 machine was used to create the silicon arrays. While creating high volume manufacturing methods for will required additional work, both processes were fundamentally successful, producing individual arrays of acceptable quality. Both methods hold promise for manufacture of accurate, inexpensive, and useful replacements for current plate technology.

Thesis Supervisor: Ian W. Hunter
Title: Professor of Mechanical Engineering and Professor of BioEngineering

Acknowledgments

Many people have been instrumental in helping me finish this thesis, and I cannot thank them enough. My thesis advisor, Professor Ian Hunter, originated the idea of the high speed ram, and guided me through the difficult sections of the project. His amazing breadth and depth of knowledge in mechanical engineering and physical sciences immensely enriched my MIT experience. I am honored to have worked with him.

I also had the good fortune to work with many great graduate students and researchers. Peter Madden spent an inordinate amount of time teaching me on topics ranging from mathematics to CNC milling, and also provided invaluable critiques on my design work and writing. His brother John Madden, even though busy writing his own PhD thesis, took time to explain the operation of the electron microscope, DSC, and TG-FTIR systems. Colin Brenan came up with with the idea of using silicon together with EDM, and thus added two chapters to my thesis. Tanya Kanigan figured out a way to actually put my arrays to use, thus giving my thesis' claims justification. Matt Graham was merciless in his constructive critique of my writing, and thus made me pull together my dilapidated writing style.

My fellow members of the BioInstrumentation and BioMechanics Laboratories provided a great atmosphere for work, and were in fact 'the' world for the last few months of this project. Max Berniker was a constant source of motivation for finishing this thesis, and were it not for his constant hounding I would have started writing much later. Steve Buerger, Brian Crane, James Tangora, Robert David, Patrick Anquetil, and Brandon Rohrer were a most amazingly talented group of people. Thanks for sharing your time with me.

I could not imagine going through MIT without good friends. Rachel Cunningham was always there to go to talk about things unrelated to MIT, or go of for a book hunt in Boston. My friends from the outing club, Hector Briceno, Dave Andersen, Mike Freedman and Robert Zeithammer were always there if I needed to leave town for the weekend and forget about MIT.

Contents

1 Introduction **12**

1.1 Overview 12

1.2 High Throughput Pharmaceutical Scanning 13

1.3 Prototype Processes 15

1.3.1 Plastic Impact Forming 15

1.3.2 Silicon Micromachining 16

2 Impact Shaping Process **18**

2.1 Impact Process Description 18

2.1.1 Theoretical Model 19

2.1.2 Energy Requirements 20

2.1.3 Plastic Selection 22

2.2 Experiment Design 23

3 Ram Design and Manufacturing **25**

3.1 Functional Requirements 25

3.2 Design Concepts 25

3.2.1 Rotational Hammer 26

3.2.2 Linear Motor Ram 26

3.2.3 Pneumatic Ram 27

3.2.4 Linear Gravity Ram 27

3.2.5 Velocity Amplifier 27

3.2.6 Linear Ram Revision 28

3.3 Bearing Selection 29
3.4 Spine 30
3.5 Air Piping 33
3.6 Sled 34
3.7 Anvil 36
3.8 Impact Limiter 39

4 Pin Arrays **41**

4.1 Functional Requirements 41
4.2 Stress Analysis 42
4.3 Material Selection 46
4.4 Pin Array Design 47
4.4.1 Pin Design 47
4.4.2 Array Design 48
4.4.3 Tool Holding 48
4.5 Pin Array Manufacturing 49
4.5.1 EDM Wire Method 49
4.5.2 Heat Treatment 50
4.5.3 Machining Time Estimates 51

5 Impact Forming Results **52**

5.1 Initial Ram Results 52
5.1.1 High Speed Photography 52
5.1.2 Failure Analysis 53
5.2 Results for Revised Ram 53
5.2.1 Failure modes 54
5.2.2 Array Inset Fit 58
5.2.3 Melting Model Verification 58
5.3 Polymer Selection 59

6 Silicon EDM Machining 61

6.1 Traditional Silicon Machining Processes 61

6.1.1 Wet Etching 62

6.1.2 Dry Etching Processes 62

6.2 EDM Machining Method 63

6.2.1 Overview 63

6.3 Electrode Manufacture 65

6.4 Experimental Setup 67

6.4.1 Oil Based Machining 67

6.4.2 Erosion Patterns 68

6.4.3 Silicon Resistance 68

6.4.4 Silicon Fluid Based Machining 72

6.4.5 Water Based Machining 75

7 EDM Manufacturing Results 76

7.1 Erosion Rates 76

7.2 Surface Finish 77

7.3 Electrode Wear 78

7.4 Silicon Array Cleaning 80

7.5 Applications 81

8 Conclusions and Recommendations for Future Work 83

A Plastics 85

B CAD Drawings 89

B.1 Ram Final Version - All Drawings 89

B.1.1 Ram Head Assembly Drawings 89

B.1.2 Ram Head Part Drawings 93

B.1.3 Ram Structure Part Drawings 107

B.1.4 Array Inserts 114

B.2 EDM Array Components 117

C Programs **119**

C.1 Matalab 119

List of Figures

2-1 Melt zone formation 19

3-1 Rotational hammer concept 26
3-2 Linear motor concept 27
3-3 Gravity powered ram 28
3-4 Linear air bushing specifications 29
3-5 Complete ram layout 31
3-6 Sled mounting details 34
3-7 Sled assembly with air manifold 36
3-8 Anvil assembly 38

4-1 Buckling failure of pins 43
4-2 Array insert - final version 43
4-3 Strike pin and array assembly 49
4-4 Limitations on EDM-cut slot width 50

5-1 High speed camera footage - ram 53
5-2 High speed camera footage - broken pins 54
5-3 Surface defects resulting from bent pins 55
5-4 Radial flow of polymer 56
5-5 Characteristic breakage due to radial flow 57
5-6 Radial pin bending pattern 58
5-7 A successful array in polycarbonate 59

6-1 50×50 electrode made from copper 66

6-2 Grid-based sinking erosion pattern 69
6-3 Superposition-based erosion pattern 69
6-4 Continuous resistance model of a wafer 70
6-5 Element of a resistive network 71
6-6 Resistance increase to superposition-patterning 73
6-7 Power decrease due to superposition-patterning 73
6-8 Silicon fluid based machining setup 74

7-1 4 wells/mm^2 and 36 wells/mm^2 silicon arrays 77
7-2 Parasitic discharges through carbon 78
7-3 Surface roughness of EDM-machined silicon 79
7-4 Alignment jig and prototype arrays 81
7-5 Alignment jig for prototype arrays 82

A-1 Polymer Data - Delrin 86
A-2 Polymer Data - Nylon 87
A-3 Polymer Data - Polycarbonate 88

B-1 Complete Ram Head Assembly 90
B-2 Complete Ram Head Assembly 91
B-3 Complete Ram Head Assembly 92
B-4 Cover Plate 94
B-5 Ram Head Case 95
B-6 Ram Head Case 96
B-7 Ram Head Case 97
B-8 Impact Absorber - Sacrificial Anvil 98
B-9 Release Spring of Stopper Swing Arm 99
B-10 Multi-Impact Preventing Stopper Swing Arm 100
B-11 Stopper Pillow Block 101
B-12 Stopper Spring Retaining Pin 102
B-13 Ram Strike Pin 103

B-14 Test Sample Support Plate 104
B-15 Anvil Base 105
B-16 Anvil Bracket 106
B-17 Ram/Bearing Pylon 108
B-18 Bottom Guide Bracket 109
B-19 Bottom Guide Bracket 110
B-20 Top Guide Bracket 111
B-21 Top Guide Bracket 112
B-22 Cable Pulley 113
B-23 Punch Inset - 10×10 Array - 0.9 mm Pins 115
B-24 Punch Inset - 10×10 Array - 0.9 mm Pins 116
B-25 100 Hole Silicon Array Alignment Block 118

List of Tables

1.1 Comparison of high density arrays to current technologies 14

2.1 Impact heat penetration depth for selected polymers 22

4.1 Heat treatment of D-2 steel 51

6.1 Erosion Resistance Index C_m 64

A.1 Material properties of selected polymers 85

Chapter 1

Introduction

1.1 Overview

This work focuses on the development of novel methods for manufacture of micro-well and micro-channel arrays for use in pharmaceutical research. Under the direction of Professor Ian Hunter, the project began in 1998 at the Bio-Instrumentation Laboratory of the MIT Mechanical Engineering Department. This thesis was part of a larger project whose goal was to improve the traditional methods of drug discovery and drug screening. The improvements would result in faster, more efficient and ultimately less expensive methods to find new drugs.

Initial stages of the drug discovery process rely heavily on screening a compound for interactions against an established library of chemicals. This search might involve several million possible chemical combinations and is both time consuming and expensive. Current automation systems use a plate technology which is wasteful in terms of space and reagents and which is not optimized for handling large numbers of reactions in parallel [30].

One possible improvement to the screening process lies in the miniaturization of the system used to hold samples. High throughput scanning techniques have the potential to increase the sample density and lower chemical consumption, thus cutting costs and speeding up the screening process. While there are many challenging mechanical and chemical aspects to be addressed in size reduction, this thesis will

focus upon methods to reliably manufacture high precision arrays of channels and wells in two particular materials: thermoplastics and silicon. These arrays aim to replace the current low density well plate technology commonly used in pharmaceutical research. As shown in Table. 1.1, the desired array sample density is up to three orders of magnitude higher than those currently used. In order to effectively compete with the current low density arrays the new arrays need to be relatively inexpensive. While the smaller amounts of reagents used and higher densities already make the new arrays inherently less expensive on a per-sample basis, a cost effective method of manufacturing must be found.

Two distinct methods of micro-array manufacture are explored. Impact forming of polymers is investigated as a novel method to form large arrays of small channels or wells in polymers and a viable alternative to injection molding. The method is capable of creating feature sizes and feature types not easily achievable with traditional injection molding techniques at a fraction of the cost. A manufacturing platform based on a high speed ram is devised for the optimization of the process of forming the plastic well arrays. The impact method is optimized for plate material and desired well or channel depth and shape. The other method explored is electrical discharge machining (EDM) of silicon. In preliminary studies EDM of silicon has been shown as a fast and potentially inexpensive method to produce high aspect ratio channels and wells. A modified Charmilles Roboform 30 EDM machine is used to create the silicon arrays. Effects of alternative dielectric fluids on machining speed and surface finish are investigated. Both methods hold promise for manufacture of inexpensive replacements for current plate technology.

1.2 High Throughput Pharmaceutical Scanning

While drug companies might try to design drugs using only theoretical predictions of chemical interactions, predicting the effects of a given chemical on any given protein or system is still quite difficult. The systems involved are simply too complex to accurately model on even the most powerful modeling software. Instead, drug com-

Table 1.1: Comparison of high density arrays to current technologies

Wells per array	Well Density($\frac{wells}{mm^2}$)	Volume of assay(μL)	Arrays per test
96	~ 0.01	100	2273
384	~ 0.04	20	568
1536	~ 0.15	4	142
10000	4	< 0.02	22
100000	36	< 0.006	3

**Based on 200,000 compounds. Source: "Future Considerations in HTS", [30]*

panies maintain extensive libraries of compounds that have interesting biochemical properties. These libraries might contain hundreds of thousands or millions of unique compounds, each a possible basis for a new drug. The drug discovery process is then reduced to a shotgun process. To find a new drug, the first component necessary is a protein or receptor that is known to be part of the process that the drug will attempt to control. This chemical of interest is incorporated in a liquid solution that usually also incorporates some means to detect a reaction. This combination of a base compound plus a detector is called an assay. The assay is then reacted with each chemical or chemical combination from the libraries. The samples are scanned for reactions, which usually manifest themselves in various levels of easily detectable activity, such as flourescence. The few flourescent samples are then evaluated for their interactions in subsequent steps that will hopefully result in a patentable and marketable drug.

The millions of reactions that are required to make this process work are now generally carried out in standard 96 well plates that measure about 100 by 125 millimeters. Loading of the wells is usually done by robots that fill the wells one at a time. The wells hold a few fractions of a milliliter of reagents. After the reactions are complete, the reagents are examined either in-situ or the contents of several well plates can be moved in small quantities onto a glass in an array arrangement. This secondary plating step is usually done by robots as well.

Micro-array technology improves this process in several ways. Through an increase in well density, the overall size of the system is reduced. The decrease in size also means that smaller amounts of the sometimes expensive library compounds and assay

will be used for the experiment. The arrays can be filled with a single fluid by immersion and capillary action. Mixing occurs by stacking arrays on top of one another. The stacking and self loading nature of the arrays [23] eliminates at least one and possibly more of the loading steps. Finally, the reacted compounds can be scanned in-situ, using an optical system, completely eliminating the need for final plating. Consequently, the use of micro-arrays makes the drug search process both faster and less expensive.

1.3 Prototype Processes

1.3.1 Plastic Impact Forming

Injection molding and compression forming have been widely used to create miniature features. One good example of small features that can be created with traditional molding techniques are electronic connector assemblies. These techniques work well for features down to sub-millimeter scale, but then only with relatively low aspect ratios. The production of a large array of channels or wells poses some unique challenges that make injection molding manufacturing quite difficult. In both injection and compression molding the entire workpiece is subject to heating and cooling, leading to shrinking when the part is cooled. This shrinking is likely to be non-uniform, as anisotropy in the plastic produces warping and non-uniformities in channel alignment. Since it is critical for alignment that the location of particular wells be precisely the same between different arrays, the injection molding method cannot produce satisfactory results. In addition, for large array size, the fragility of individual pins needs to be taken into account. Uniform shrinkage of the array towards the center of the injection cavity will stress and possibly break the pins on the outer edges of the array. Polycarbonate, a material often used for biomedical applications, has a coefficient of thermal expansion of 44 μm/m/K. For a 120 ^{o}C drop in temperature that occurs during cooling, the array will shrink about 0.5 mm in length and width. This may be enough to permanently damage the injection molding tools.

The process presented in this thesis relies on ramming a hard die into a relatively soft plastic at speeds large enough to produce localized melting of the material. Specifically, the pin needs to transfer enough kinetic energy into the plastic to melt it into a negative of the die. The key to the ramming process effectiveness is that it does not rely on heating of the entire workpiece. The impact process only affects a small portion of the plastic in the immediate vicinity of the wells, and thus side-steps the problems associated with uniform and non-uniform workpiece shrinkage. Since the features molded into the plastic are small, and energy contained in the ram can all be transferred into melting of the plastic, the energy requirements are low. It is estimated that for an a 10k array the energy required is as low as 5 Joules. In addition, the process does not require the expensive 150-ton press normally used in injection molding.

1.3.2 Silicon Micromachining

Silicon EDM machining has been investigated by various other researchers [27, 21, 28] for the purpose of creating a method supplementary to the traditional lithography and plasma etching methods (See Sec 6.1). EDM machining has been widely used in toolmaking to produce intricate dies for injection molding. In that venue, EDM is generally known as a slow, expensive, but accurate process for material removal. The process is well suited for machining very small runs of parts from very hard materials, such as dies used for injection molding of plastics or extrusion of metals. The 'slow' and 'expensive' assumptions are valid when the metals in question are steel or tungsten carbide, the materials used for most industrial tools. However, thanks to to a combination of physical properties such as low thermal conductivity, low thermal capacity and low melting temperature, silicon can be eroded much faster than any of the 'traditional' EDM metals. Furthermore, silicon is bio-compatible and can be treated to change its surface properties. These factors in addition to the ready availability of inexpensive wafers made for the electronics industry, make silicon an attractive choice for the future generation of high density microarrays.

In Chapters 6 and 7 this thesis outlines methods which were used to manufac-

ture channel arrays in silicon. Densites of up to 36 holes per square millimeter were attained through the use of superposed-pattern erosion. Array sizes up to 10 thousand holes were obtained, with various degrees of surface finish. As predicted, the EDM method is shown to be a good complement to the standard micro-scale silicon processing techniques, although it faces certain limitations if oil based dielectrics are used.

Chapter 2

Impact Shaping Process

Injection molding is by far the most common method for creating small, detailed plastic parts. While the feature types that are possible with injection molding are similar to those that are needed in micro-channel array manufacturing, the injection molding process faces several limitations. The feature size of the wells on the array is on the order of hundreds of microns. However, the overall size of the array is several centimeters. Plastic shrinkage may damage the mold. Furthermore, the injection molding machines that need to be used for this process are expensive and bulky. This section discusses an alternate method for forming arrays of wells or channels into a polymer.

2.1 Impact Process Description

A punch array is made whose pins are negative forms of the wells that need to be created. The array is driven into into a polymer sample at high speed by a ram. When the pins impact on the polymer, kinetic energy is dissipated as heat and work. The much harder material of the die penetrates into the plastic creating local high pressure spot, and either melts the polymer or displaces it by plastic deformation. After a dwell of three milliseconds the array will withdraw, leaving a finished set of channels or wells. The bulk of the plastic is never melted. In addition, the process does not require a bulky press, and instead relies on a small impulse force source, in

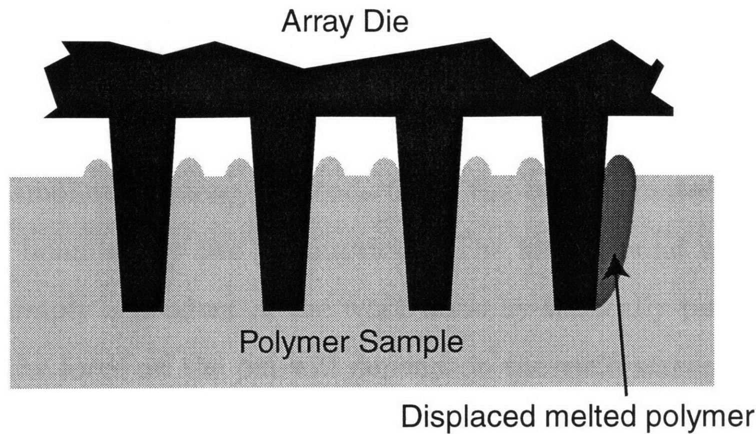

Figure 2-1: During the entry of pins into the sample, melted zones form immediately next to the pins. The depth of this zone is dependent on the velocity of the pin.

this case a form of a ram.

2.1.1 Theoretical Model

Two processes were considered as possible for the extraction of plastic during impact. The first process involves localized melting of the plastic around the pin due to friction and pressure. The plastic is immediately heated to the point of melting or vaporization, and ejected outward round the pin. The second process involves a more wide-spread yielding and plastic flow of the polymer, resulting in a lateral displacement of material around the pin. A simple visualization of the impact is shown in Fig. 2-1.

The first process is favored if the heat affected zone within the plastic is shallow, and the only way for the displaced polymer to escape is through the ejection process. This also implies that the viscosity of the molten polymer would be low enough to permit flow in a narrow space. Unlike the ejection process, the displacement process occurs when the penetration of heat into the plastic is large enough that the heat may be dissipated, and cause melting of part or the entire wall surrounding the individual wells. While the process is too complex to be modeled completely, some simple

predictions can be made and later corroborated by experimental evidence.

2.1.2 Energy Requirements

Displacement of plastic out of the well requires the delivery of energy by the pin. The exact amount of energy depends upon the type of material that is being used, but can be bounded by two assumptions. The lower bound energy required for the process is simply a product of the work done by statically pushing the pin into the polymer. The force on the pin will depend on the yield strength of the plastic. The energy E is the force times the distance, or in this case

$$E = \sigma_Y A_{pin} h_{pin}, \tag{2.1}$$

where σ_Y is the compressive yield strength of the polymer, A_{pin} is the frontal area of the pin, and h_{pin} is the depth to which the pin is embedded in plastic. The product $\sigma_Y A_{pin}$ is the force on each pin during this process. As an example, when a standard pin array (see Section 4.4.1) is used in polycarbonate, the load on each pin is 1.2 N, and the associated energy required to form this array is 0.11 J. By extension, the energy required to form a 10000 well would be 11 J.

Lower bound limit of the work required to form the well may be found using an energy conservation argument. Since the plastic that is displaced from the well will have to transition at least to a liquid form, the energy required for the formation of the well will be equivalent to the energy necessary to melt and displace the polymer from the well and its vicinity. Assuming an ejection mechanism for material removal, where only the well volume is melted and displaced, the energy required can be calculated using the following equation:

$$E = M_{well}[c(T_{final} - T_{ini}) + H_{fusion} + H_{vapor}], \tag{2.2}$$

where M_{well} is the mass of the material being displaced, c is the specific heat, T_{final} is the final temperature, T_{ini} is the starting (room) temperature and H_{fusion}

and H_{vapor} are the heat of fusion and heat of vaporization/decomposition, respectively. Note that H_{fusion} and H_{vapor} are greater than zero only if the final temperature is sufficiently high. For all practical purposes, the plastic is likely to melt but not decompose. The heat of decomposition is simply too high for this process to occurs (see Appendix A). Using this criterion, the maximum required energy is 0.0035 J per pin or 35 J for an array of 10,000. The resulting force is 3.8 N per pin. The force may be higher if a larger volume of polymer than contained in the well needs to be heated during the impact.

Thermal penetration may increase the volume that needs to be heated. Thermal penetration in this case is defined as the depth of the melting front around the pin. If we assume that the layer of plastic immediately next to the pin is heated to its decomposition temperature, the melt front will advance while the pin is being rammed into the plastic. After the process is complete, no more heat is generated at the metal/plastic interface, and metal, which is about twenty times more thermally conductive than plastic, efficiently cools the well interior, preventing further melting and solidifying the plastic around it.

The depth of the melt front can be calculated using the complementary error function equation [25]:

$$\frac{T - T_0}{T_s - T_0} = erfc\left(\frac{x}{(4\alpha\, t)^{0.5}}\right), \tag{2.3}$$

where T is the initial temperature (in Kelvin), T_0 is the melting temperature, T_s is the source or interface temperature, x is the depth into the material, α is the thermal diffusivity of the polymer, and t is the event duration. Given the temperatures and α from polymer tables, and the event time from the known impact velocity, it is possible to calculate the maximum depth of the melting front, in this case at the top surface of the array. Table 2.1 shows solutions to Eqn. 2.3 for polymers used in these experiments and for various drop heights. Note that for the most commonly employed drop height of 0.5 m, the thermal penetration is on the order of 300 μm, which is enough to completely melt the walls around each well. While a drop from

full height of 5 m looks more promising in this respect, it was never attempted due to impact strength problems of the ram bearings. If the whole volume of the plastic around the pin is expected to reach melting temperature, the energy dissipated and force on the pin will increase significantly. For polycarbonate, the relevant values will be 0.03 J and 33 N, respectively. This can be considered the worst case scenario for that particular pin size, and the pins should be designed to withstanding that force.

The solutions used in Table 2.1 were found using tabulated values[1] for the complementary error function [25].

Table 2.1: Impact heat penetration depth for selected polymers

Drop Height (m)	t (msec)	Polycarbonate (μm)	PTFE (μm)	Delrin (μm)
9.79	0.13	139	227	130
4.15	0.2	172	282	162
2.67	0.25	193	315	181
1.86	0.3	211	345	198
1.06	0.4	244	398	229
0.48	0.6	298	488	280
0.28	0.8	345	563	323
0.19	1	385	630	362
0.06	2	545	891	511

2.1.3 Plastic Selection

Several plastics were analyzed in the process of selecting the optimum candidate for impact processing. While a few of the impact tests utilized polymers whose properties make them inherently well suited for impact forming, it was found that some of those polymers are not suitable for biological applications. Specifically, acetal and Nylon were eliminated because of their high hygroscopicity. Since swelling due to contact with water is unacceptable in a micro-array application, these materials are not suited for the experiments. However, the experimental data is included because both

[1] A programming bug was discovered in Maple [4] and Mathcad [5] while attempting to solve Eqn. 2.3. The bug produces a complex number when asked to solve for x in the *erfc* function of Eqn. 2.3. The newest versions of Maple and Mathematica [6] seem to have corrected this error.

materials show promise in the extrusion process, and may be useful for different applications. Polymethyl Methacrylate (PMMA), a plastic extensively used in biomedical industry, was rejected because its of brittleness which caused extreme pin buckling during impact. In the end, polycarbonate and Polytetrafluoroethylene (Teflon,PTFE) were chosen as the most promising polymers because of their low hygroscopicity and high toughness.

Data for particular plastics is available in literature [19, 16]. Yet in spite of the ready availability, sources conflict to give a wide range of possible values for a particular polymer. These discrepancies are most likely due to actual variations of the same polymer, which is made in many varieties. Consequently, some of the properties of the particular polymer used in the experiment were verified on a Perkin Elmer [12] Differential Scanning Calorimeter (DSC) or a PE Thermogravimetric Analyzer. The properties of the polymers used or considered are listed in Appendix A.

The ideal plastic for this application has a low specific heat, low heat of fusion, requiring little energy to form it. Moderately high tensile strength and good ductility ensure lower loads on the pins themselves and should prevent plastic cracking during the process. A low coefficient of thermal expansion should prevent pins from being stuck inside the heated plastic, and minimize geometric deformations of the array itself. Of the plastics examined, polycarbonate was chosen as the best candidate.

2.2 Experiment Design

The theories and equations developed in the preceding sections need to be tested and refined. Since no commercial product was found to that fulfilled the energy and velocity requirements as stated earlier in this section, a dedicated experimental platform had to be constructed. For this purpose, a prototype ram was designed and built. Multiple pin array configurations were tested as dies to try shape to several different polymers. Effects of pin material, pin length and taper on the different material types were be tested. The process was fine tuned and compared with the predictions made earlier in this section. The three chapters that follow outline the the

design and manufacturing processes involved in building the ram, the various array configurations tested, and finally the test results obtained with the described setup.

Chapter 3

Ram Design and Manufacturing

3.1 Functional Requirements

As described in the previous chapter, the ram has to meet several requirements. The energy used during the collision is significant and must be properly controlled in order for the punching process to be successful. At the moment of impact, pins of the array must have adequate momentum to be driven into the plastic and adequate velocity to melt the plastic at the same time. The pins need to be constrained from motion that could cause their breakage. Since this is a prototype process, provisions must be made for easily replacing a broken die (pin array). A method must also exist for extracting embedded pins from the plastic sample.

The following sections outline the steps taken to design and manufacture individual components, and details any unusual processes that were used during the manufacturing. All the parts used for the kinetic ram were built in house with extensive use of the laboratory machine shop. The part and assembly drawings may be found in in Appendix B.

3.2 Design Concepts

Based on the functional requirements, several possible design concepts were developed and evaluated. The final design was chosen on the merits of simplicity. Later re-design

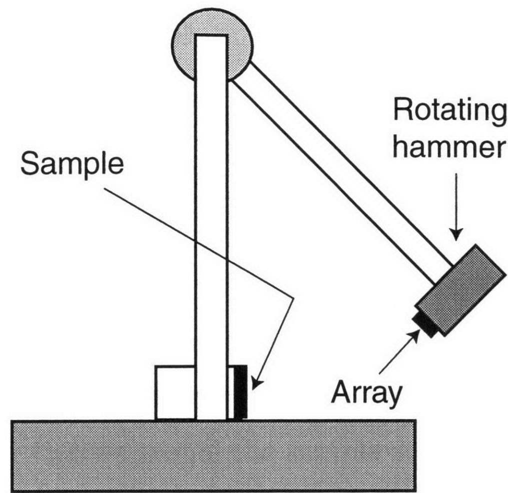

Figure 3-1: The rotational hammer concept uses potential energy of a weight on a pendulum arm.

was required to remedy problems found during testing.

3.2.1 Rotational Hammer

This concept is pendulum-like device where the array is placed at the end of a swing arm (see Fig. 3-1). Powered by gravity, the swing arm is driven into a stationary plastic sample. This approach is simple and elegant, but is limited in the amount of energy it can store by the length of the swing arm and its weight. In order to achieve a significant velocity, the swing arm would need to be quite long, making the machine bulky. In addition, a long swing arm would bend like a beam and would subject the head to deflection upon impact. Finally, the impact trajectory would not be linear, causing possible pin breakage.

3.2.2 Linear Motor Ram

This concept is ram powered by a linear motor (See Fig. 3-2). Linear motors are an expensive choice for accelerating the ram. In order to achieve the desired acceleration of about 50-100 m/s^2 in a reasonably sized package, the motors needed to be extremely powerful and thus massive and expensive. In addition, it was unclear that the linear

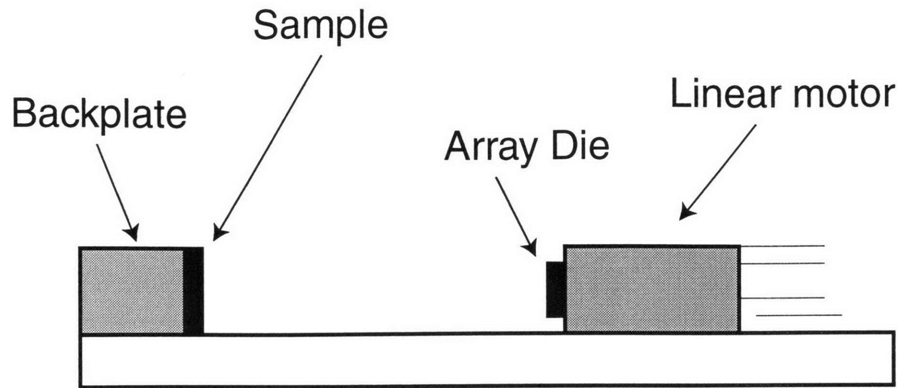

Figure 3-2: Linear motors propel the sample stage at high acceleration.

motors would be suitable for impact applications, necessitating a setup with a separate break-away array driver module and extra rail space for the motors themselves to decelerate. Thus the linear motor setup was abandoned in favor of a simpler design.

3.2.3 Pneumatic Ram

A pneumatic ram was considered, but rejected due to the difficulties associated with velocity control of a pneumatic setup.

3.2.4 Linear Gravity Ram

A vertical drop of 5 meters will accelerate an object to 10 m/s. A linear ram with low friction bearings can use gravity to accelerate to the desired speed, within limits imposed by height. Given that the lab space available for this experiment was approximately 5 meters high, this solution seemed simplest and most robust, and was chosen over the others (See Fig. 3-3).

3.2.5 Velocity Amplifier

A set of velocity amplifiers was considered for the gravity ram in order to obtain increased impact velocity from a given drop height. The velocity amplifier would consist of several stacked sliding blocks of decreasing mass, heaviest on top. The

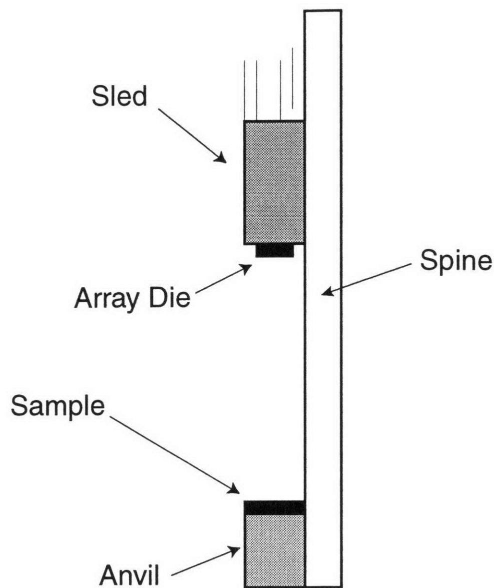

Figure 3-3: A sled is driven by gravity over a long drop. This concept was adopted for the project because of its simplicity.

blocks would slide on the same rail as the main ram sled, but be separated from one another by a thin layer of compressed air. Upon sled impact, a series of collisions would transfer momentum to the lowest, smallest block. Assuming elastic collisions for the metal to metal contact, a three level amplifier of this sort may achieve a factor of 2.4 velocity increase at the cost of lowering the impact mass by a factor of eight. The higher velocity could be useful to lower the impact duration, possibly decreasing the radius of the heat affected zone around the pins. However, this set-up was judged too complex and unnecessary given the already high velocity available with a 5 m drop.

3.2.6 Linear Ram Revision

Due to difficulties with the initial ram concept, described in more detail in Section 5.1, the ram was modified to serve only as an energy source (a hammer) for the shaping process. All the high precision components were moved into a rigid assembly that allows translation along the vertical axis. This set-up reduces lateral forces on the pins.

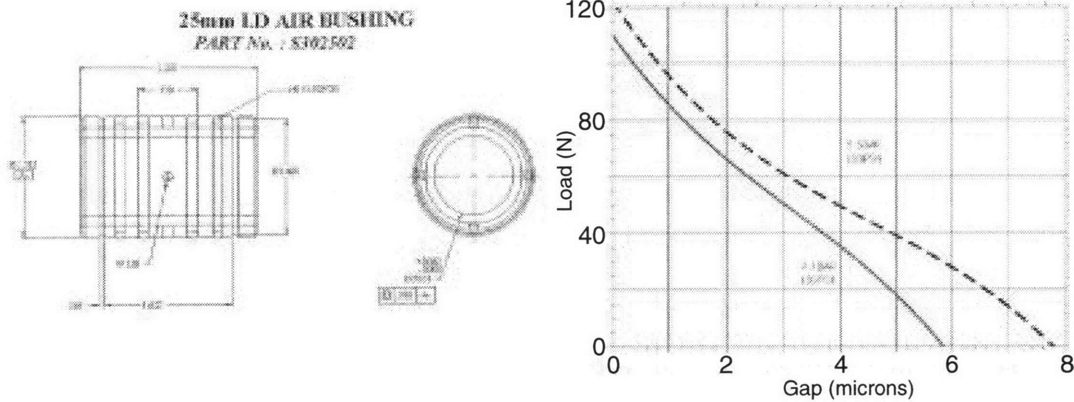

Figure 3-4: Air Linear Bushing and allowable loads. The bearing was operated at 110 psi. From New Way Bearings [9].

3.3 Bearing Selection

Having selected the linear gravity powered ram as the basic design, the next issue became selecting the appropriate components for the system. The bearings on which the sled rides needed particular attention because of the demands imposed on them by the high speed and low friction requirements. Initially the design was supposed to use linear ball bearings [14]. However, it was found that the linear ball bearings develop a slippage problem at speeds exceeding 6 m/s. Since the expected maximum velocity is 10 m/s, linear ball bearings were abandoned in favor of air bushings [9]. Air bushings ride on a thin high pressure cushion of air between the steel guide rail and a ring of porous graphite which is encased in an aluminum tube. The bearings have no sliding contact and generate almost no friction. Air bearings also are inherently self centering, and have $\pm$ 10 μm tolerance for radial and axial misalignment as a result of the air gap on which they ride. A drawing of the bearings as well as permissible loads can be seen in Figure 3-4. The low stiffness of the air bearings was judged not to be a problem, since the radial forces that the bearings experience is minimal due to the vertical configuration of the ram. In addition, the impact forces were expected

to be axial, and consequently have have no detrimental effects on the bearings.

3.4 Spine

Spine of the ram is the main structure which supports all the other components of the system. In this design the spine includes a vertical U-beam attached to a wall by several stand-off spacers, two round guide shafts for the ram to slide on, and the top and bottom clamps that hold the guide shafts at the proper spacing. The use end supports rather than full length rail supports for the guide shafts was dictated by the choice of bearings as well as manufacturing issues. Although the rail supports produce significantly more rigid shaft mounts, the design would require split bearings. The air bearings chosen for the design are not readily suitable for split applications, and thus would need to be custom made. The required modification included shutting down airflow on part of the bearings, significantly reducing their load carrying capacity. In addition, rail supports would have constrained the guide shafts to the spine beam for their entire length. Since the spine beam could not be manufactured to high tolerance, such a constraint would have transferred any straightness errors to the guide shafts themselves. Instead the shafts are constrained only at both ends with highly accurate clamps, and remain straight in their free hanging section due to their vertical orientation. In addition, the bottom clamp is used to tension the shafts and further inhibit undesireable deflection.

The precision ground guide shafts are available from Thomson Industries [14] in solid as well as hollow forms. The hollow shafts were considered for their much greater stiffness to weight ratio. However, since the shafts in the hanging configuration are not deflected by their weight, the additional four-fold cost premium of lighter hollow shafts was judged unnecessary.

The maximum height of the ram spine is limited only by the 4.85 m height of the lab ceiling. Consequently, the spine length was chosen to use the entire height. The one-piece guide shafts also span the entire length. In the design, consideration was given to the fact that the sheer size of workpieces prevented them from being machined

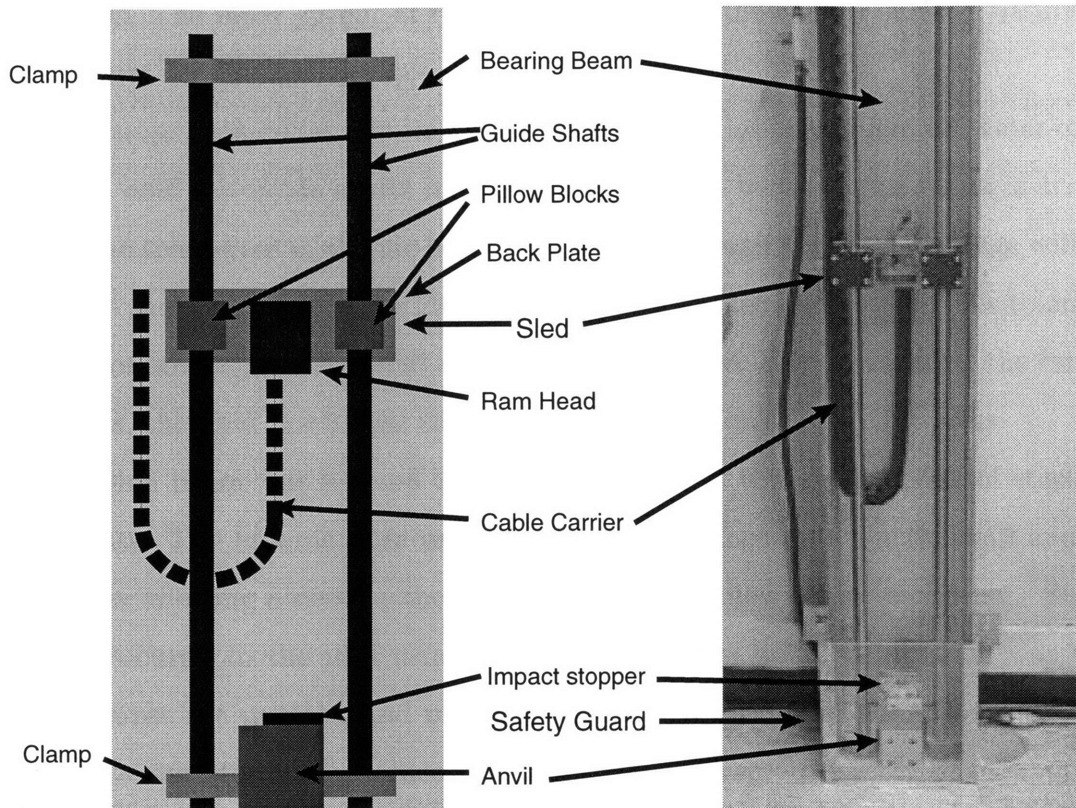

Figure 3-5: The complete layout of the ram as finished. The ram consists of a sled running on air bearings and an anvil that holds the polymer sample and pin array. Also visible is the chain conduit that provides air to the sled. The component nomenclature will be used throughout the rest of this document.

except with the use of portable, and therefore imprecise, tools. This limitation was taken into account by building adjustability into the fixed components by way of increased clearances on mounting holes and the use of small contact patches between parts rather then large surface to surface contacts.

The spine of the ram was purchased from Industrial Aluminum as a single U-beam cut to a specified length. Modifications on the beam were restricted to simple hole drilling with a hand held drill, and ample clearance was left on each mounting hole for final adjustments. Before mounting, the beam was pre-drilled with holes for both the end clamps. In the process the inside back surface of the beam was found

to be convex by about 2mm, justifying the concept of small mounting pads for the end clamps. The inner cutout of the clamps straddles the convex surface, assuring a secure mount for the end clamps.

End clamps themselves require a high tolerance in the spacing and diameter of the holes that hold the guide shafts in place. The spacing between the shafts is critical because the tolerances in the air bearings are tight enough that the bearings will not work if the shafts are more than 20 μm out of parallel - see Figure 3-4. This tolerance is easy to obtain using wire EDM on an aluminum plate. Having satisfied the critical dimensions, the final machining can then be done on a mill or a drill press.

The spine beam was secured to the wall indirectly through a series of stand-off wall mounts. The mounts were used to provide clearance between the wall and the beam, thus allowing access to the back, and also to allow easier mounting. Stand-offs were secured to the wall using concrete expansion bolts. The beam was then placed against the mounts, and mounting holes were drilled in the spine beam and the mounts simultaneously. Once the beam was secured to one set of mounts and adjusted to be completely vertical, the rest of the mounting holes were drilled and secured. Since the top of the beam is about 5 m above the ground, drilling of the topmost holes required protective gear to guard against falls from the ladder. Safety was provided through the use of 30 kN Spectra [1] webbing anchored to expansion bolts sunk in the wall, and secured to the graduate student on the other end.

Once the beam was secured, the end clamps were mounted on the top and bottom. At this point the sled, whose manufacturing is described in Section 3.6, can be slid onto the guide shafts. Guide shafts were then secured on in the top clamp. The bottom clamp was tilted up and then secured around on the shafts. The bolts securing the clamp to the beam were then tightened. In this manner a small degree of additional preload on was achieved, helping to keep guide shafts straight and parallel.

3.5 Air Piping

Once the bearing design was chosen, a way had to be found to supply pressurized air to the bearings with minimum disturbance and friction on the ram. In addition, the system had to be robust enough to withstand repeated impacts, as well as reliable enough not to be subject to snags and possible damage during operation. The pressurized air line was planned to be one of several cables that would have to reach the sled.

The system was designed to connect all the cables to the sled, allow unconstrained linear motion of about 5 meters, and permit speeds up to 10 m/s. Initially a spring loaded spool mounted on the top of of the ram assembly was considered. During the ram operation, the spool would unroll, releasing as much of the cable as required. This concept was quickly abandoned as not robust enough, and too complicated due to multiple rotational couplings required in the spool itself. The second concept considered consisted of air piping built into the ram structure itself. This concept was dismissed due to the complexity of the sliding seal that would be necessary, and also potential difficulties with electrical contacts.

The solution chosen was a chain cable carrier from Igus Corporation [2]. The chain was combined with the Chainflex air hose also from Igus. One end of the cable carrier was hung half way up the spine beam, resulting in a 'hanging J' configuration. Center hanging allows the shortest possible carrier length to be used. In addition, due to space constraint imposed by the minimum bending radius of the air hose, the cable carrier is mounted sideways. This configuration takes up more space than planned, but thanks to the much larger bend radius on the chain also smoothes out the motion by preventing sharp kinks between individual links.

A flexible air hose is routed through the chain and features a flow shut-off valve on the outside of the ram. The chain is kept centered by gravity and slight adjustments of the end points.

Some thought was given to the effect of the chain on sled velocity. The weight of the chain is significant in proportion to the sled. However, at the bottom end of the

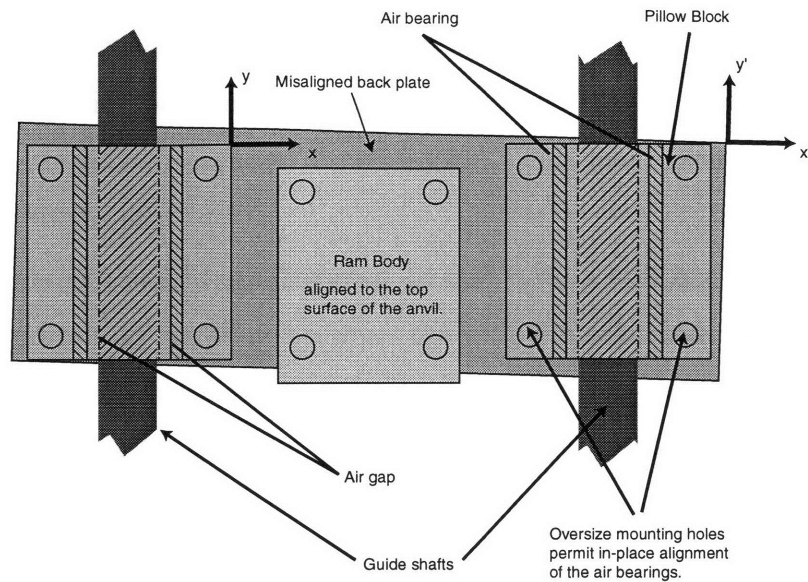

Figure 3-6: Pillow block adjustment on oversized holes prior to bolt tightening allows alignment of the bottom surface of the ram to the anvil. In addition, the alignment process prevents kinematic over-constraining of the sled, even if the backplate is skewed.

sled's travel, little or no chain remains suspended. Because the chain is subject to gravity just like the sled it will fall at the same rate. Because no chain is left suspended on the sled at the bottom of the stoke, it will not contribute to the effective mass or velocity of the sled. See Fig. 3-5 for a view of the chain installation.

3.6 Sled

The sled of the ram drops along the guide shafts and provides energy necessary for the impact shaping process. In addition, the sled is subject to significant impact loads, and therefore must be strong enough to survive these repeated impacts. Since this is a research application and optimizing the sled to survive only the predicted loads is not required, the sled is over-designed in its ability to handle impacts.

The weak point of the sled are the bearings. Air bearings are notoriously fragile, and cannot handle radial impact loads. Care was taken to minimize radial and twisting impact loads on the bearings by placing the impact point and center of gravity

halfway between the two bearing center axes. This directs the impact load axially along the bearing, resulting in sled motion but no radial load on the bearings. If, however, the sled is not completely balanced, some load will be transferred to the bearings and cause their eventual deterioration. This may occur due to post-design modifications to the sled.

Components of the sled are designed to bolt onto a stiff backplate that provides structural rigidity and coupling between the pillow blocks and the ram body itself. The backplate is also used as a manifold for the bearing air supply, significantly reducing the complexity of tubing connections inside the ram body. While an initial design called for fastening the pillow blocks directly to the ram body, that design was abandoned due to kinematic over-constraining that would have potentially resulted in bearing alignment problems. Instead, the body of the ram simply bolts into the backplate like the pillow blocks.

Since mounting the array on the ram sled itself was found to be unsatisfactory (see Section 5.1), the mounting plate was removed and the ram body itself was used as a hammer.

From a manufacturing perspective, the most difficult component of the sled was the ram body itself. The component's initial specifications demanded it to be quite precise and strong, but high aspect ratio of the part and the stainless steel construction made milling the piece problematic. Instead, it was machined from a block of stainless steel on the wire EDM. Initially, a high precision array mount was affixed to the ram body. However, after initial tests this configuration was abandoned in favor of an anvil-mounted case that contained both the sample and the array. The bottom surface of the ram body was then relegated to the role of a hammer.

The ram and the mounting backplate were assembled along with air bearings in their pillow blocks. The bearing pillow blocks were left unsecured until the sled was mounted on the guide shafts and the guide shafts were fastened in their clamps. The cable carrier and air supply hose were mounted to the spine and the sled, and the air hoses are connected to the bearings. At this point, the bearings were activated, and aligned themselves with the guide shafts. Subsequently they could be secured to the

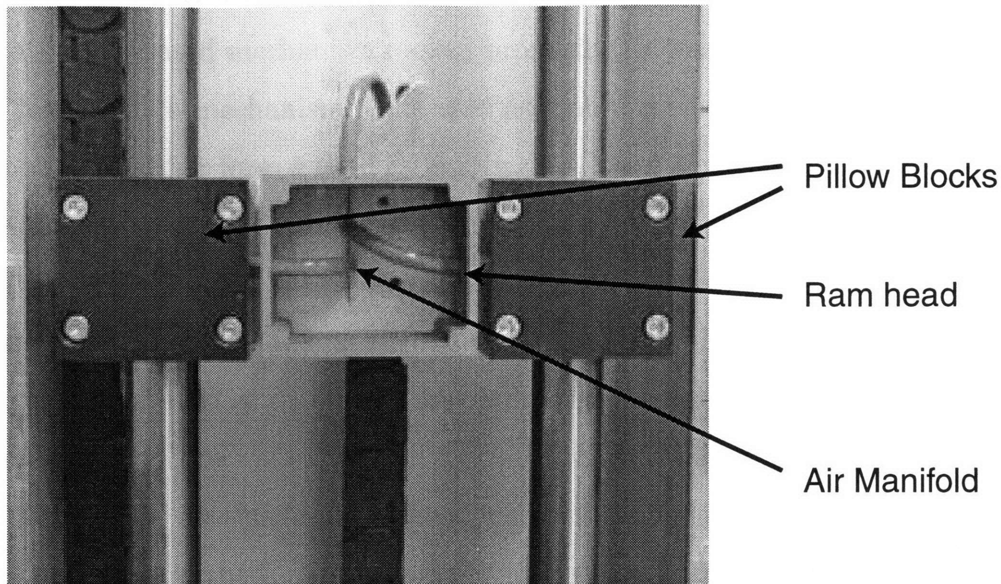

Figure 3-7: The sled of the ram is a bridge between two air-bearing pylons. The back plate contains a built-in compressed air manifold.

sled without misalignment.

3.7 Anvil

Designed to hold the sample in place for impact, the anvil is mounted at the base of ram. The mount consists of two parallel linking bars that are soft enough to allow some vertical travel by the anvil. The 4-bar linkage functionality of the mounting bars was supposed to keep the top surface of the anvil parallel to the ram body for small deflections. Two plates on top of the anvil were used to hold the sample in place.

Tests with high speed camera (see Section 5.1.1) determined that locating the pin array and the plastic target sample on the sled and anvil, respectively, would not produce satisfactory results. The sum of deflections of the parts that separate the two critical components is simply too great. Consequently, another way to constrain the critical components had to be designed.

Several configurations were considered for the enclosed case approach, and then

evaluated on the criteria of stiffness between the pin array and the plastic sample. While a flexure-based mechanism looked promising, it was judged inferior to a simple spring loaded slide mechanism. The said assembly consists of two steel blocks that when bolted together form a rigid assembly. The lower block contains a sample holder and alignment pins, while the upper block contains the rectangular insert slideway as well as a slide and a spring mechanism. A strike pin is used as a push rod to transfer energy from the falling sled to the array itself. Loose coupling between the strike pin and the array facilitates assembly. To ensure that the array is protected during handling of the case and that it is withdrawn after the strike, the strike pin is spring loaded. By alternating the spring constant and the length of the spring used, it is possible to vary the force with which the pins are extracted immediately after an impact. For the occasions when the pins are stuck, a threaded hole in the back of the strike pin facilitates removal of the pin array. A washer may be added onto the top cover to modify the maximum depth to which the pin array extends into the plastic.

The sample itself may either be left unsecured, or be clamped down by a set of four set screws. These screws further prevent any lateral dislocation between the array and the sample. An impact limiter described in Section 3.8 is affixed to the case assembly which then bolts onto the old anvil support. An exploded view of the case assembly can be seen in Figures B-1 thru B-3 on pages 90-92, respectively.

After the redesign following failed impact tests, the anvil assembly became the most complex part of the ram. The base of the anvil rests on a plate of plastic that absorbs some of the shock of impact. This can be easily replaced with a less flexible aluminum or steel version. Two horizontal plastic bars anchor the anvil to the spine, and allow some vertical displacement. The actual case that holds both the sample and the array was made out of stainless steel using a 3-axis milling machine. Stainless steel was chosen for its strength and durability, and also because it was well suited to EDM machining. After the milling was complete, wire EDM was used to machine a precise square hole with corner relief that would be used as the bearing surface for pin arrays. Due to an error in the machining, the guiding hole for the strike pin was machined too large, and needed to be tightened using a metal sleeve. The strike pin

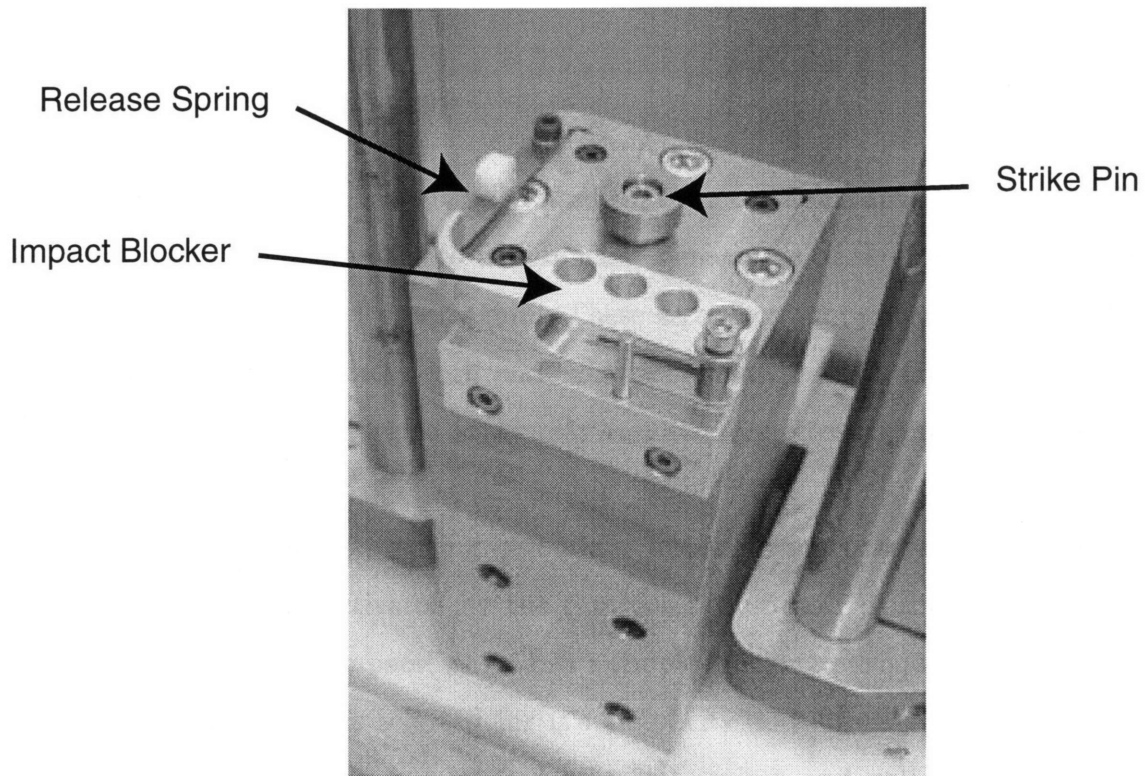

Figure 3-8: The anvil assembly is composed of two solid blocks of stainless steel that house the sample and the array punch. A spring loaded strike pin protrudes from the top block. This strike pin transfers the impact of the falling sled to the array die.

was machined from one solid block of steel on a lathe, and then a wire EDM was used to machine the T-slot for coupling to the array. To allow for easier assembly, the front of the strike pin was tapered. The contour of the cover plate that constitutes the second bearing surface for the strike pin was machined using EDM. The piece was subsequently finished on a milling machine, where the center bearing hole was reamed out to ± 0.01 mm tolerances. All the parts were assembled together according to to the schematic shown in Figure B-2 on page 91.

3.8 Impact Limiter

After initial testing of the ram, it was found that the collisions are quite elastic. The sled bounces back after impact to a significant percentage of the initial height, and then drops back down to impact again. These secondary impacts are undesireable, particularly because the well depth and extrusion characteristics may be altered. A second impact into a pre-formed array may result in unnecessary stresses on the die insert.

Several methods for preventing secondary impacts were considered. These included a one way gate activated by the ram passage upward, spring loaded shocks that would deploy upon impact, as well as a simple blocking mechanism. In the end, a blocking mechanism was selected for it's simplicity and effectiveness. A rotating block actuated by a spring is triggered by a flat spring, and will put itself in the way of following impacts (see Fig. 3-8). The only concern was whether the block would deploy quickly enough when the drop was from relatively low heights. The deployment time is calculated using the following equation:

$$t_{max} = \sqrt{\frac{2J\theta_{max}}{\tau_{spring}}}, \tag{3.1}$$

where J is the rotational moment of inertia of the swing arm, θ_{max} is the desired angle of deflection, τ_{spring} is the average torque imposed by the spring and t_{max} is the deployment time. Note that the stopper does not have to be completely deployed to

fully stop the ram. However, 35 degree deflection was used as a guideline to verify that the deployment was fast enough. τ_{spring} was measured to be 0.04 N·m; the moment of inertia J was calculated from a solid model of the swing arm in the Pro/Engineer package, and found to be 8.04×10^{-5} kg·m^2. Given that the observed 'bounce' height of the ram head was found to be about 20% of the initial drop height, solving

$$h_{min} = \frac{5}{8} t_{max}^2 g \tag{3.2}$$

for h_{min} will produce the minimum drop height. Using Equations 3.1 and 3.2, the minimum drop height is found to be 4 mm, much less than realistically needed for a drop.

The impact limiter consists of only three manufactured components and a single standard spring shelf spring, as well as some fasteners. For simplicity of manufacture, the swing arm was cut out of an aluminum sheet on the wire EDM, and then finished on a mill and a drill press. The block holding the swing arm was manufactured on a milling machine, with enough clearance left on the mounting holes to allow final positioning when attached to the head case. Modifications on the head case were kept to a minimum, and were restricted to three drilled and tapped holes. The hardened spring used to trigger the deployment of the ram was found too hard to cut or drill using conventional methods. Consequently, it was cut out on the wire EDM, which handles the 0.6 mm hardened spring steel stock with aplomb. A polyoxymethylene (Delrin) block is glued on with a flexible glue to to the top of the spring. The block pushes down on the spring when the sled drops, triggering the limiter deployment. See Figure 3-8 for a photo of an assembled impact limiter.

Chapter 4

Pin Arrays

4.1 Functional Requirements

Functional requirements for the pin arrays are constructed from the impact process and ram designs that have been discussed in the previous sections. The bulk shape of the array is determined by its interface to the rest of the kinetic ram. In this case, the array is in the form of an insert whose outside surfaces are used for bearings. The pins themselves need to be of suitable shape and size, which in turn depend on metal properties as well as the polymer to be tested. Consideration must be given to the limits of the manufacturing methods used to manufacture these arrays. In this case, the arrays are made using a wire EDM, and their final shape is limited by what that process can achieve. As such, the arrays constitute a multi-dimensional optimization problem where tradeoff decisions are made depending on the performance of actual produced arrays. This feedback design mechanism introduces a time consideration into the design. Array inserts needed to be easy to produce so that multiple variants could be tested.

The original specification of the array design calls for manufacturing of well or channel arrays with well counts well in excess of 10,000. However, during initial research it was found that machining of array dies with 100×100 pin dimensions, while quite possible, is extremely time consuming - up to 30 hours for a steel array. In addition, arrays of that size introduce a new problems in tool holding and ram

design. Instead, the tests were conducted using much smaller 100 pin arrays. The pin materials and shapes are identical in the small arrays as they would have been in their large versions, and the test results will be valid when scaled up to full scale production arrays.

4.2 Stress Analysis

In the design if the most recent version of the ram, great emphasis was placed on eliminating lateral loads on the pin array. Therefore, the analysis that follows considers an impact load that acts primarily along the axis of motion of the inserts, parallel to the array pins. Under these conditions, significant lateral bending of pins is unlikely to occur, and buckling becomes the primary expected mode of failure. Micron-level lateral displacements that are necessary for buckling to occur still exist and are considered impossible to eliminate. Since all the pins in an array are identical and have identical spacing from their neighbors, a single pin may be used as a model for the rest of the pins in the array.

The following model treats a pin as a beam rigidly supported at the base, and completely free to move at the other end. This clamped-free model is primarily supported by experimental observation of the mode of buckling of pins in plastics tested. A clamped-hinged model may be more appropriate in harder plastics. An example of the clamped-free specific buckling mode can be seen in Fig. 4-1.

Closed form solutions for buckling loads are available for simple, constant cross-section beams with various end support conditions. However, since the pins may be tapered in shape, a standard rectangular beam analysis is not adequate. For example, a tapered beam 0.9 mm length, 0.2 mm base with a 3 degree taper will have a buckling load greater than an inscribed simple beam, but less than a circumscribing simple beam. Even for this small taper, the bucking loads differ by a factor of twelve. Since the critical load on the tapered beam may be anywhere between these two bounds, it is necessary to find a way to better approximate this load. Unfortunately, no closed form solutions for tapered beams are readily available, and no critical load coefficients

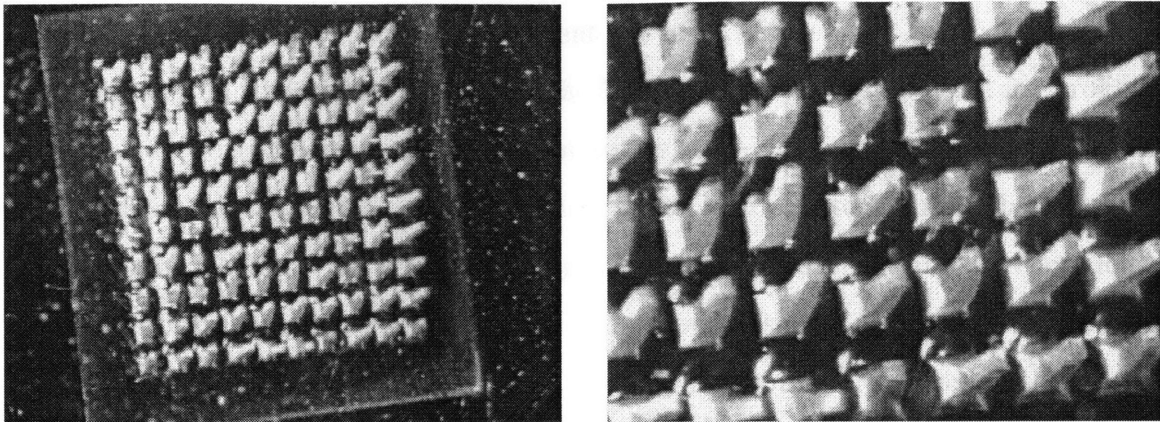

Figure 4-1: Imprints of buckled pins demonstrate the clamped-free specific mode of failure. Here a stainless steel insert was used in polycarbonate.

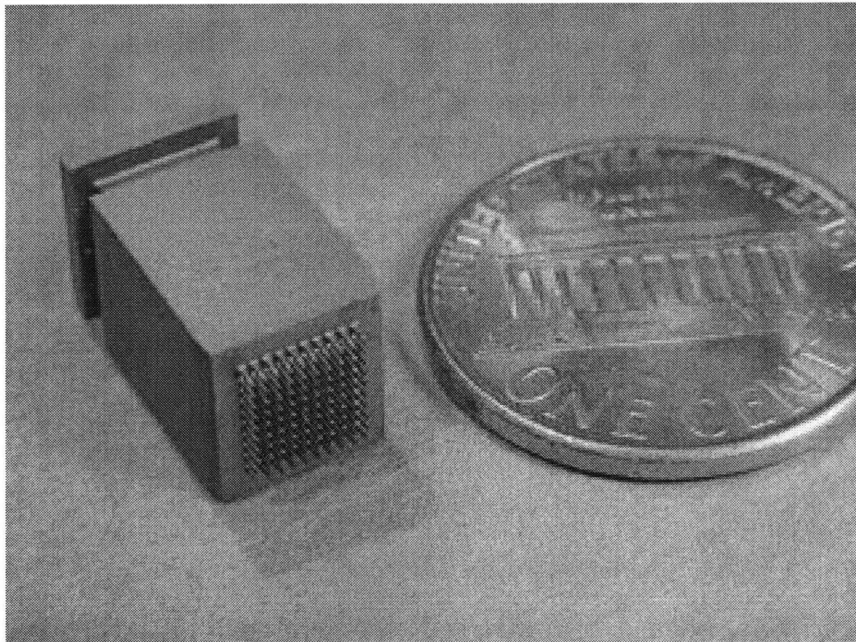

Figure 4-2: The final version of an array die insert. This particular insert was made from hardened steel.

are tabulated.

It is possible to circumvent the lack of tabulated critical values by realizing that buckling behavior of a beam is dependent on its lateral spring constant, which in turn depends on its bending stiffness. The beam's inherent spring constant provides the restoring force that allows the beam to resist being pushed sideways by small disturbances. A tapered beam with end stiffness identical to a simple beam of the same length will have the same buckling load as that simple beam. Critical loads for simple beams can be thus correlated to a tapered shape or for that matter any possible beam shape, and finding critical loading is simplified to finding a solution to the beam bending equation.

For a tapered beam, the beam bending equation may be solved by re-integrating the general differential equation for an elastic curve [18] for a beam subject to an applied moment M

$$EI\frac{\partial^2 v}{\partial x^2} = M, \tag{4.1}$$

where the v is the deflection from the centerline of the beam. In the case of the tapered beam, the moment of inertia I also becomes a function of the beam location x, and must be taken into the integration. The cross-sectional dimension of the tapered beam

$$l(x) = l_0 + x\sin(\theta) \tag{4.2}$$

can then be used to find the moment of inertia

$$I(x) = \frac{1}{12}l(x)^4 \tag{4.3}$$

of the tapered beam. The moment of inertia can then be substituted back into Equation 4.1, where the mechanical moment M has been replaced by the equivalent product of force P at a distance x. This results in the equation

$$E\frac{d^2v}{dx^2} = -12\,\frac{Px}{\left(l_0 + x\sin(\theta)\right)^4}, \tag{4.4}$$

where l_0 is the tip size of the pin and θ is the taper angle. Equation 4.4 needs to be integrated twice, using the limits imposed by geometry, with respect to x to obtain the desired deflection $v(x)$. Since the integration was intractable by hand, Maple [4] was employed to help evaluation. However, the closed form solution was found to contain singularities at θ=0, limiting its usefulness.

Instead, several pins were modeled in the ProEngineer [10] solid modeling package, and analyzed in the ProMechanica [10] finite element modeling package for deflections due to small forces. The results from simple beams were compared to analytic solutions, and were found to be in excellent agreement. Next, the desired tapered pin was analyzed in a similar manner, using a small test load P_{test} to create a deflection δ_{test}. This δ_{test} was used to calculate the moment of inertia

$$I_{eqiv} = \frac{P_{test}h^3}{3\delta_{test}E} \tag{4.5}$$

of the equivalent simple beam with the length h equal to the tapered beam's. In the final step the critical load

$$P_{crit} = \frac{\pi^2 E I_{eqiv}}{4h^2} \tag{4.6}$$

of the tapered beam was calculated using the standard beam buckling formula for a simply supported beam. The resulting critical loads were found to be almost exactly the average of the inscribed and circumscribing beams' critical loads. This numerical approach through a solid modeling package has the advantage that it potentially can scale to arbitrary beam cross sections and is more robust than an analytical approach. In addition, it does not require simplification in pin shape.

4.3 Material Selection

As shown in the buckling analysis in Equation 4.6, the buckling load of the pins is proportional to the Young's modulus of the metal, and should have no relation to its yield strength. Consequently, a selection was made to use a material with the highest possible modulus that could be machined into the desired shape. The EDM process used for manufacturing these arrays allows machining of conductive materials regardless of their hardness. The hardest widely available material is tungsten carbide, which was purchased from Leech Carbide [3]. The LC-115 variety is formulated to have impact resistance suitable for die applications. The exact material properties vary depending on the percentage contents of the binder as well as the grain size of the initial carbide powder. Tungsten carbide used in this experiment has a modulus of 540 GPa and compressive strength of 5.3 GPa, both of which are several times higher than any steel. However, the material is brittle, and it's performance in tension is much worse than that of any tool steel.

During initial testing, lateral displacements and shock loads were found to break a large percentage of pins on each array. This pattern continued with the new setup, and could not be rectified by tightening of slide fitting tolerances. Examination of the broken arrays revealed that while carbide pins penetrated into the plastic, they broke off at some later point in the impact. Remedy was sought by the use of high tensile stainless and tool steels instead.

Steel has a modulus of 203 GPa. The tensile strength differs depending on the particular kind of steel, as well as the type of heat treatment applied to the steel. Stainless steel was chosen initially over tool steel because of ready availability and because stainless steel did not rust in the EDM tank. The oxidation was thought to weaken the fine pin structure and leave undesired residue on plastic arrays. Finally, since the modulus of stainless and tool steel is identical, the former was chosen for the experiments. Once the first steel arrays were made, it was also found that the EDM machining time for steel was approximately 40% less than that of carbide (see Section 4.5.3). After several tests revealed the need for a stronger material, the

stronger tool steel was adopted. Heat treatment of tool steel had to be done before EDM machining took place. The heat treatment process changed the dimensions of the insert and rendered it useless if performed after EDM machining. In one example, a critical dimension on an insert increased by 0.2% after heat treatment.

For a production application, wear rates of the different materials would need to be considered along with other material properties. However, since the arrays inserts used so far have been strictly single use, the wear issue is not crucial. If wear does become and issue, it is possible to treat the surface of the array with titanium nitride or a similar hard coating.

4.4 Pin Array Design

4.4.1 Pin Design

The wire EDM method as later described in Section 4.5.1 required that the pins have a rectangular cross section. Also, no sharp internal corners were possible, necessitating that the pin bases be rounded. The pins were to be easily removable after impact, therefore it was necessary to minimize the time that they spent in contact with the plastic after the impact was complete. This requirement was fulfilled by tapering the pins in a manner similar to relief angles on injection molding dies, ensuring easy separation. In addition, tapered pins exert pressure on the walls of the holes during the entire impact, potentially reducing surface roughness of the finished product. However, the pin taper was limited by the desired well or channel aspect ratio. Especially in the manufacture of channels, the bottom cross section area of the hole needed to be kept similar to the top, preferably no smaller than about 100 μm $\times$ 100 μm for yeast based assays. Consequently, a taper needed to be determined separately for each particular application, depending on material thickness.

4.4.2 Array Design

The spacing and layout of the pins was again in large part determined by the EDM machining process. The layout of the array had to be rectangular. For simplicity the array was kept square in shape. In order to facilitate assembly, a 1 mm space was left on either side of the pin array. This space was necessary to avoid damage to pins during assembly into the ram. A chamfer on the edges of the array face was also meant to simplify assembly.

4.4.3 Tool Holding

Tool holding refers to interfacing of the array insert to the ram itself. In the first ram prototype, the array was positioned by the means of a taper, and held in place using a simple sliding lock. Since that design was abandoned, the tool holding problem has changed. The objective of the next holding system was to allow exclusively single axis motion while transmitting an impact force from the ram to the array. The holder also had to accommodate pulling forces that were necessary to extract the array from a sample after a test. The coupling chosen for this tool holding task was a T-type interconnect. A 'T' shaped mushroom machined into one end of the array coupled with a 'T' shaped slot machined into the strike pin. A built in clearance of 0.5 mm de-coupled the array from small angular and lateral motions of the strike pin, and facilitated assembly. The array fit into the rectangular slot in the head case of the ram anvil assembly. The slot was precision machined on the EDM to have exact dimensions of 7.100 mm, squared. However, the actual dimension were found to be several microns larger in both directions . Careful fitting of machined arrays determined that to achieve optimum fit, array inserts needed to be manufactured with cross sectional square dimensions of 7.103 mm on each side. Repeating this dimension to the limit of measurable accuracy ($\pm$ 0.001 μm with a digital micrometer) was found to be within the capabilities of the temperature-controlled wire EDM, but care had to be taken because even a change in the type of steel resulted in slightly different fit qualities.

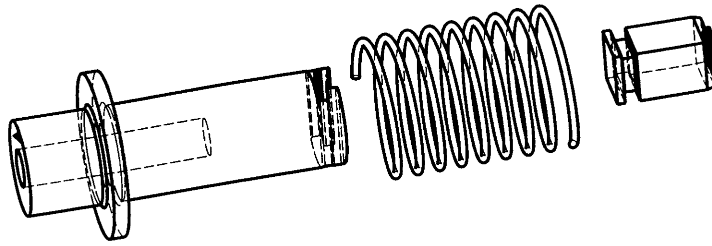

Figure 4-3: The 'T' shaped mushroom on the array interlocks with a mating slot on the strike pin. A spring slides over the assembly. See Appendix B-3 for more drawings.

4.5 Pin Array Manufacturing

4.5.1 EDM Wire Method

Wire EDM imposes a limit on the minimum inside corner radius that can be machined using a given wire diameter. This limitation arises from the need to perform multiple skim cuts in addition to the initial rough cut. The skim cuts improve geometry and surface finish, but also remove a significant amount or material. The smallest radius that can me machined using a 100 μm diameter wire is approximately 85 μm, with the exact value depending on the workpiece thickness. Consequently, the narrowest slot that can be machined using that particular wire is about 170 μm. Figure 4-4 demonstrates this limitation, which applied to both array die inserts as well as EDM electrodes that will be discussed in more detail in Section 6.3 on page 65.

Pin arrays were manufactured out of various materials ranging from tungsten carbide to hardened steel. Usually the array insert was machined from a slightly oversized billet of virgin stock. The billet was held in a System3R [13] indexing tool holder while the first cut was made. After the cut was finished, the tool holder was rotated by 90 degrees, and the operation was repeated. While the tool holder was claimed repeatable down to a micron or better, the actual variation was somewhat larger due to oxidation on the reference element surfaces. However, since the dimensions of the die walls only needed to be accurate with respect to one another, the produced results were adequate. The produced arrays were measured to have a better than ± 1 μm

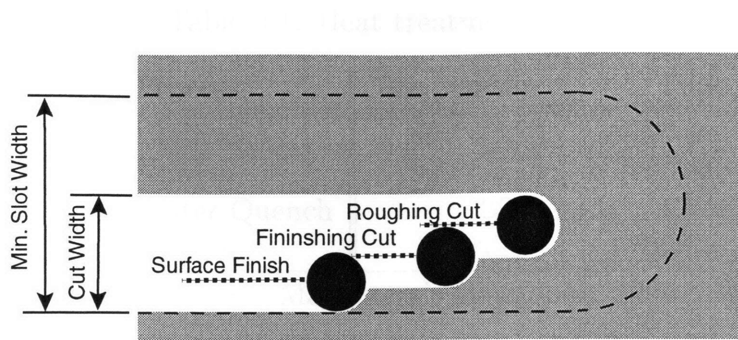

Figure 4-4: Minimum slot width on the wire EDM is limited by the thickness of the wire as well as the need to perform multiple sequential cuts. These 'skim' cuts are required for an acceptable surface finish.

repeatability, which was also the limit of the (Mitutoyo digital) micrometer used in the measurements.

4.5.2 Heat Treatment

While a few of the materials used for array inserts, such as carbide and stainless steel, could be machined in supplied form, a tool steel used for the final batch of arrays required heat treatment to obtain the desired strength and toughness properties. D2 tool steel 12.7 mm round stock was purchased from MSC [8], and the desired heat treatment process as shown in Table 4.1 was selected from the Machinery's Handbook [26]. A Lindberg/Blue tube oven with a nitrogen atmosphere was used for the heat treatment. The steel was heated, quenched and tempered to a Rockwell C Hardness of approximately 58. This value was chosen as a tradeoff between toughness and hardness, and proved adequate in later tests.

Since the neutral atmosphere in the oven prevented oxidation and assured good surface finish, the first set of heat treating was completed on finished array inserts. Unfortunately, it was found that the heat treatment process significantly affected overall dimensions of the processed metal, in this case increasing dimensions by 0.2%. For all subsequent inserts, heat treatment preceded machining, resulting in accus-

Table 4.1: Heat treatment of D-2 steel

Process	Temperature	Time
Preheat	$800^oC \pm 15$	2700 sec
Harden	$1000^oC \pm 15$	2700 sec
Water Quench	25^oC	30sec
Temper	$370^oC \pm 5$	> 7200min

*Source:*Machinery's Handbook, 1996.

tomed accuracy of the finished product. One interesting detail to note is that while the raw D-2 steel was prone to oxidation in the EDM tank, the heat treated version of the stock seemed to be quite immune to oxidation. It exhibits no traces of rust even after extended time in the EDM water tank. The resistance to oxidation may be due to the change of crystal structure of the metal from annealed to the more stable martensitic.

4.5.3 Machining Time Estimates

Machining time of the arrays bears a direct relationship to the ultimate cost of the tools. While in this case the cost was of little importance, it would have to be considered for a high volume production situation. For identical array inserts the overall machining time varied from 170 minutes for both types of steels to about 240 minutes for tungsten carbide arrays. These times can be reduced by roughly 60% by using high-precision stock with exact outside dimensions. Array pins are the only features that need to be manufactured on the EDM. For the 100 pin arrays used in the experiments, the machining cost, assuming a standard shop rate of $45/hour rate, is between $130 and $230, depending on the material type.

Chapter 5

Impact Forming Results

5.1 Initial Ram Results

5.1.1 High Speed Photography

After initial unsuccessful tests, a high speed camera from Kodak (Ektapro RO), capable of imaging 1000 frames/second, was employed to examine the collision. The camera had a resolution of 384 by 512 pixels in monochrome, adequate for the purposes of this study. The motion of the falling ram was first recorded and used to calculate the bounce height. The bounce height was found to be on the order of 16-20% of the initial drop height. Also, the speed of the ram was verified to be within 20% of expected speed, but due to the blurring in the individual frames and the low resolution the exact velocity could not be calculated. Photos of the ram are shown in Fig. 5-1.

The impact itself was found to significantly move the anvil. The downward motion of the anvil was was on the order of several millimeters, depending on the height of the drop. In addition, the sled itself exhibited a rocking motion observable even on the low resolution video camera. The displacements were judged more than sufficient to break off the brittle pins by either shear or bending. A final movie was taken to find the the exact instant at which the pins are broken and examine the role of secondary impacts. Fig. 5-2 shows that all the pins were in fact broken on the first

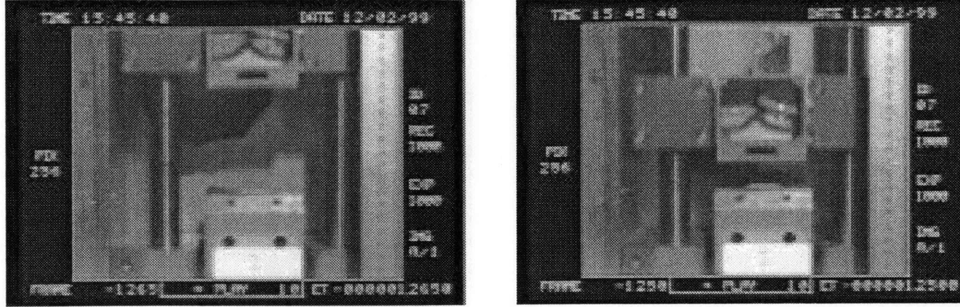

Figure 5-1: Two frames from the high speed camera show the first version of the ram. The sled is falling and about to impact on the anvil. Lateral movement of the anvil was judged responsible for pin breakage.

impact, and the secondary impacts likely could not contribute any more damage.

5.1.2 Failure Analysis

Through the use of the high speed camera and subsequent analysis of the structure of the ram itself, the failure was traced back to lack of rigidity between the sled-mounted array and the anvil-mounted sample. The mounting of the anvil, while designed to have a small amount of compliance vertically to provide damping, was shown to have unexpected lateral deflections upon impact. High speed filming demonstrated that a more closely coupled sample and die holder were required. This second design was described in detail in Section 3.7.

5.2 Results for Revised Ram

The second version of the ram was initially tested using arrays made from tungsten carbide, the same material as used on the first version of the ram. While the initial results with the tungsten carbide arrays were more promising than previously recorded, most of the pins still broke upon impact, with only about 15% of the pins surviving, the remaining pins usually located in the center. The failure mode was identified as brittle fracture at the bases of the pins. At that point a tougher material was sought.

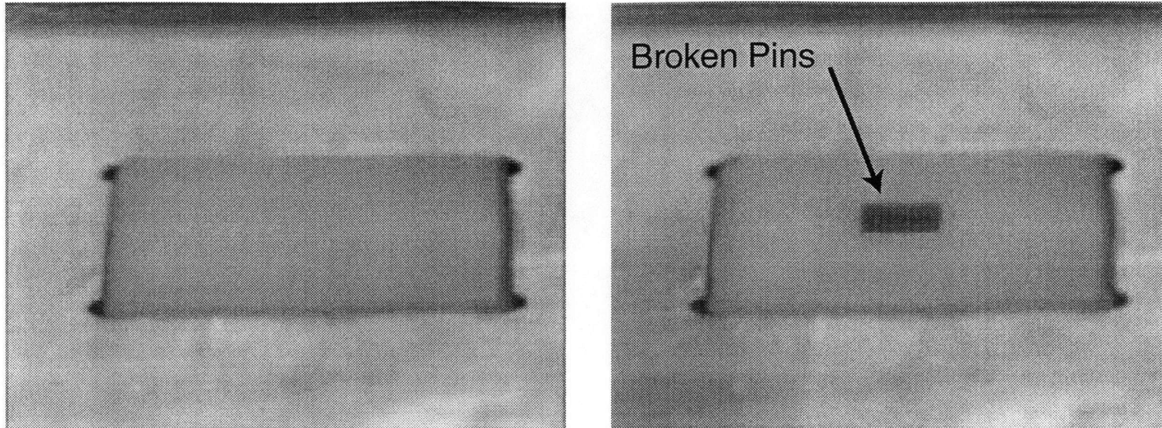

Figure 5-2: Two images taken by the high speed camera, immediately before and after the first impact. The second image shows a dark set of broken pins embedded in the plastic. Low resolution due to camera limitations.

As described in the following section, two types of steel were tried, and eventually success was achieved with hardened steel.

5.2.1 Failure modes

Breaking

Carbide pins consistently broke at the their base. Since carbide is a brittle material, it was reasonable to assume that these pins were subject to a significant lateral shock load. While tungsten carbide was selected for its high hardness and high modulus, it is a material whose tensile strength is low. Consequently, the decision was made to switch to softer but tougher stainless steel as the array material.

Buckling

406 type stainless steel inserts were manufactured using the same setup as used for tungsten carbide. The steel was found to be significantly more ductile, and no pins were broken is subsequent impact tests. However, while a single impact did not break off any of the steel pins, the metal would buckle and deform during the impact, producing skewed holes and permanently bent pins. Polycarbonate well arrays produced

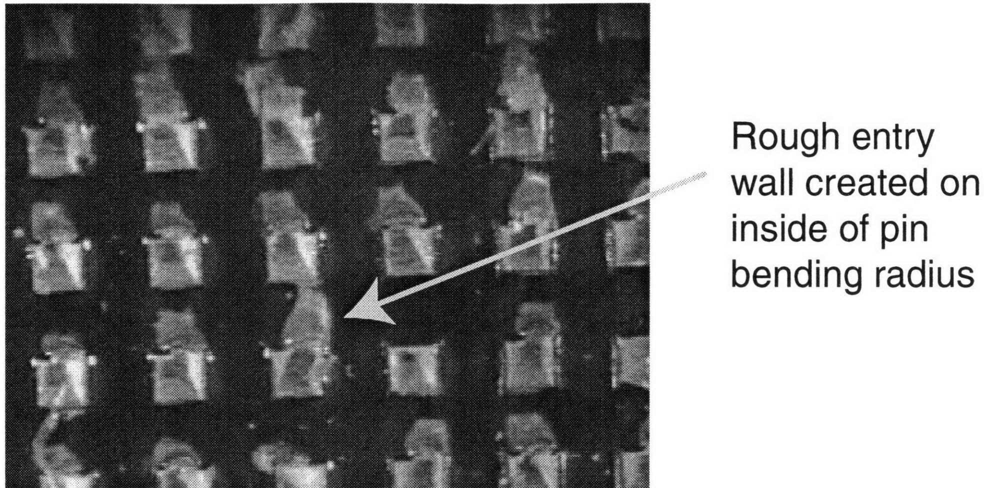

Figure 5-3: Bending pins produced a distinctive melt artifact on one of their entry hole, always formed on the side towards which the pin was bending.

with this method exhibited melt and scoring features (see Fig. 5-3) on the edges along the interior bending radius of the pins. The stainless steel, even though it could be used for a single impact array, was not a suitable metal.

According to the buckling Equation 4.6, the only material property important to the buckling load of a column is the Young's modulus. While the modulus of carbide is three times higher than that of stainless steel, there are few readily available materials stronger than steel but tougher than tungsten carbide. However, at this point it was assumed that the poor performance of the steel dies was due to premature yielding. The buckling strength relies on the beam to be able to re-center itself after it is displaced, as may occur during the impact. A material with a low yield stress will plastically deform much earlier than a high yield stress material, even though it may have the same modulus. Consequently, array inserts were made from hardened D2 tool steel, with the hardening process described in Section 4.5.2.

Bending

A first impact of the hardened steel array into polycarbonate produced excellent results. While the array embedded itself into the plastic and had to be removed

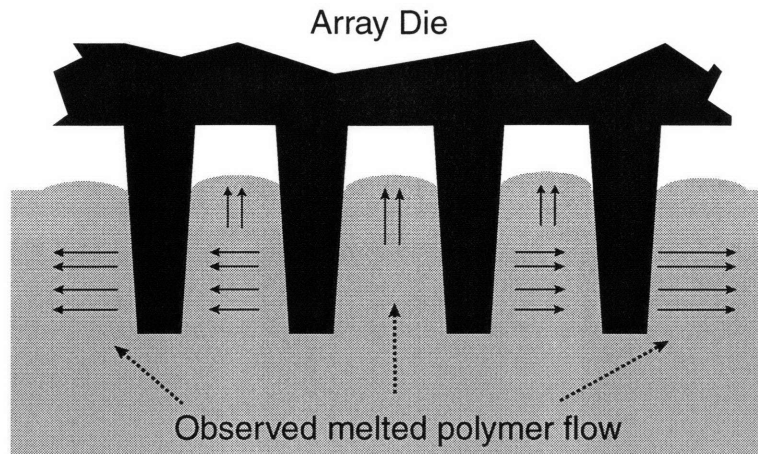

Figure 5-4: An impacting array of pins extrudes the polycarbonate sample upward and radially outward. This phenomenon is responsible for breakage of outermost pins in an array.

manually, it was reasonably easy to extract. Under a microscope, the polycarbonate wells were straight and even, exhibiting no burn or melt markings on any of the edges. This experiment was followed by a subsequent experiment to determine the durability of the array. The results of that experiment are shown in Fig. 5-5. While the buckling of the pins and the impact breakage problems were solved, another problem surfaced with lateral displacement of the plastic. When the pins are driven into a sample, the displaced polymer flows not only up, as shown in Fig 5-4, but also radially outward from the center, causing permanent bending of the pins. This slight bend in pins then results in significantly higher forces in subsequent impact cycles, quickly causing failure, with the outermost pins breaking first. A possible solution to this may be to only partially plunge the pins into the plastic, leaving a greater length of the pin to flex and absorb the lateral displacement without permanent deformation. However, this approach was tried by impacting an array to half the pin depth. While the array lasted for six cycles instead of one, pin breakage still eventually occurred.

The lateral displacement phenomenon is more pronounced in softer plastics, especially PTFE. A test drop into thin PTFE sheet produced extreme pin displacement on the test die insert. A photo of this array is shown in Fig. 5-6.

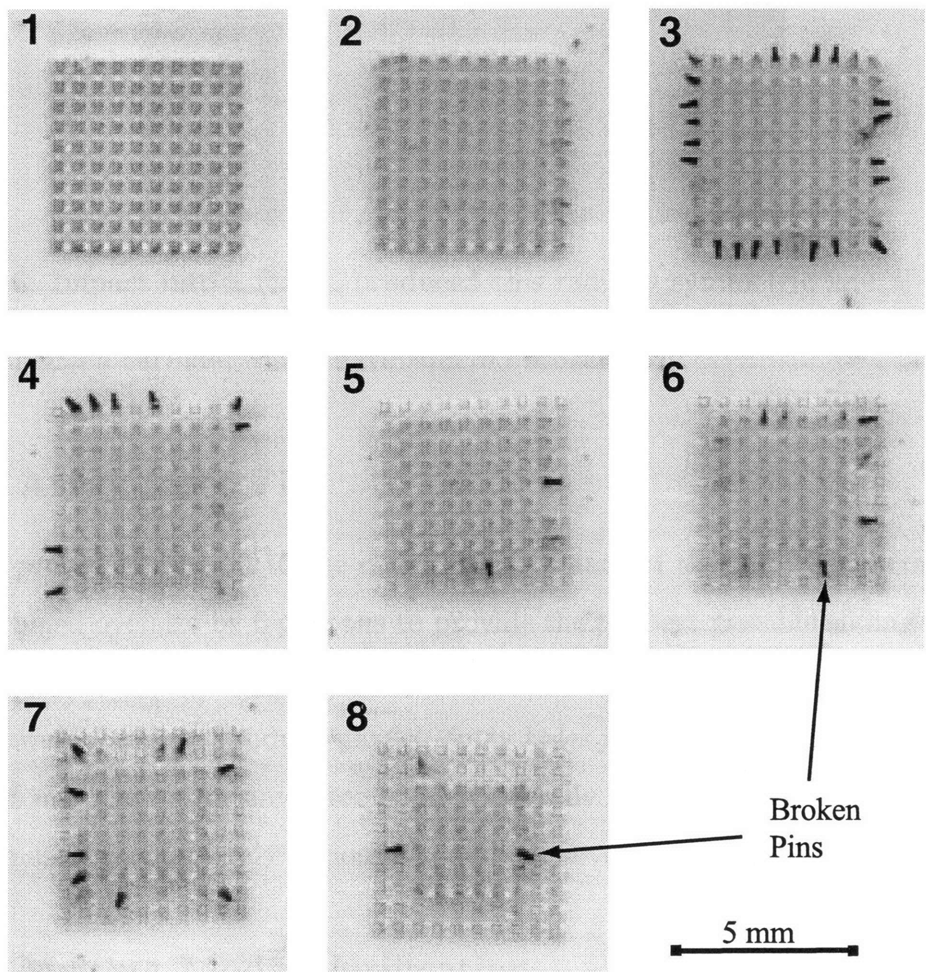

Figure 5-5: A series of eight polycarbonate samples that were impacted using a single D2 hardened steel array. Outer pins break as early as the second impact, whereas the innermost pins remain untouched through the sequence of eight impacts.

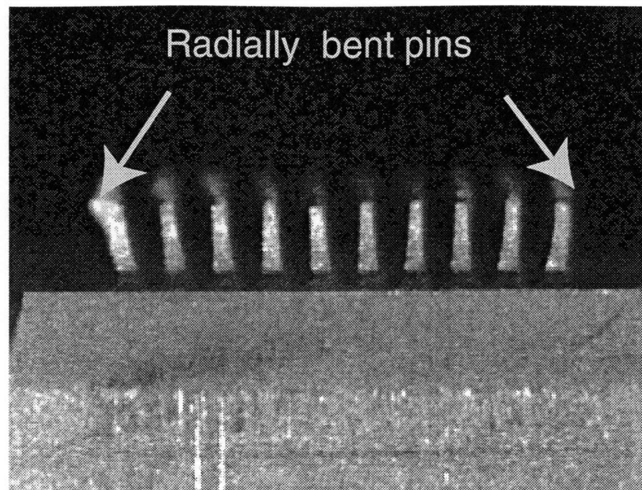

Figure 5-6: Impact into a PTFE produced this radially symmetric lateral displacement pattern into a a stainless steel pin array. An die made of more rigid material, such as tungsten carbide, would have suffered broken pins.

5.2.2 Array Inset Fit

Array fit proved important to the overall performance of the ram. The array inserts were machined oversize by 6 microns to provide the tightest possible sliding fit in the guide slot. Arrays that were not machined oversize exhibited a significant amount of slop, and were found to produce uneven entry holes into the plastic. The strength of the pins is much lower for any force applied laterally, this possible source of problems was eliminated as completely as possible, and only oversized arrays were used in tests.

5.2.3 Melting Model Verification

As discussed in Section 2.1.1, the two possible modes of polymer displacement involve either ejection or more widespread melting and lateral motion. If the first case is true, remainders of ejected plastic could be expected to be observed on the surface after the impact. Since the thickness of such would be rather small, the expected shape of this ejecta was a bundle of thin ribbons, similar to a machining burr. In the initial tests, the pins were driven to full depth, and any such burr would have been driven back into the plastic once the die bottomed out. However, an experiment was set up to

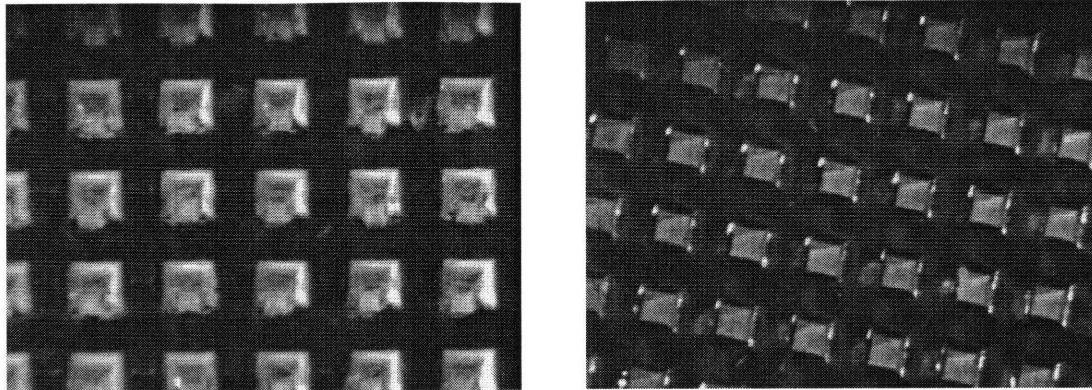

Figure 5-7: A microscope image of a polycarbonate sample reveals a perfectly punched set of wells.

limit the depth of the array by placing a washer under the sacrificial cap on top of the strike pin. This effectively limited the depth of the wells to half the pin length. After several experiments, no ejected material was observed. Consequently, the ejection model of displacement can be eliminated, at least for the velocities encountered in this experiment. In addition, the overall increase in the height of the walls between individual wells suggests that the widespread melting model is more correct.

5.3 Polymer Selection

Of all the polymers, polycarbonate was found to the material best suited for impact forming. The good ductility of the material prevented shattering, while good strength keeps the radial flow down to reasonable levels, allowing at least a few good arrays to be manufactured before replacement of the die becomes necessary. This radial flow was the main problem of PTFE, which uniformly produced a radial bending pattern with any insert. Nylon and Delrin were found to have forming qualities similar to polycarbonate, although the holes in both materials usually filled with debris. This debris was found to come from plastic that melted and solidified on the pins, and was stripped away as the pins were withdrawn. However, since these materials are hygroscopic, their use as well arrays is limited. An interesting result was produced

with PMMA. This brittle material, with many properties similar to polycarbonate, caused extreme pin buckling and flattening, and was found completely unsuitable for impact forming, though the reasons are not completely understood.

Chapter 6

Silicon EDM Machining

Machining of silicon using electrical discharge machining (EDM) was investigated concurrently with the impact shaping process. EDM machining of silicon is a newly emerging method that takes advantage of the precision machining methods developed for the die and tool making industry. The method was found more than sufficiently accurate for the purposes of making micro-channel arrays, and may be suited for further miniaturization. Since silicon was one of the target materials for array manufacture, the EDM method was compared the current lithography methods that are used in Micro Electro Mechanical Systems (MEMS) manufacturing, and that were the other option for manufacturing arrays in silicon.

6.1 Traditional Silicon Machining Processes

Thanks to demand by the electronics and MEMS industries, multiple methods for sub-micron and sub-nanometer level machining of silicon have been under development. These methods usually involve photolithography and any of a number of chemical etching processes. Depending on the type of process used the etch rate and the maximum and minimum feature sizes will vary. This section provides a brief overview of these traditional silicon etching methods, compares them to EDM machining, and evaluates each process' in light of silicon array manufacturing.

Photolithography is used in all of the etching techniques described below and, by

the means of x-rays, in the LIGA process (the acronym comes from the German name Lithographie, Galvanoformung, Abformung). Photolithography is the basic process which defines a shape on the silicon substrate. An image of the desired shape is created by projecting UV light through a mask, usually chromium on a glass plate, onto an oxidized wafer coated with polymer sensitive to UV. The exposed polymer is then developed, leaving a resist pattern on the silicon wafer. Photoresist can be positive or negative, depending on whether it is strengthened or weakened by the UV light. This will determine whether the remaining pattern is positive or negative. The resist mask is then used as a pattern for etching the oxide layer underneath. Finally, the resist can be removed, and leave an oxide pattern on the wafer .

6.1.1 Wet Etching

Wet etching generally encompasses any method where the wafer is placed in a liquid etchant bath. Usually, the etchant reacts and removes pure silicon much more quickly than the oxide layer. The etchant may be either isotropic or anisotropic. Isotropic etchants, such as hydroflouric acid, etch at the same rate in all directiions, meaning that they will usually etch under the oxide layer and create a cavity with semi-circular cross section. Anisotropic etch compounds, such as potassium hydroxide (KOH), have a preferential etching direction depending on the orientation of the silicon crystal planes. These etchants may be used to create basic structures into a the silicon. Doping compounds such as boron can slow or stop the etching, allowing for preservation of desired areas. Etching rates of 120 μm/hr are possible, but the method depends on the anisotropy of the material for direction control.

6.1.2 Dry Etching Processes

Dry etching processes use a vacuum chamber filled with reactive ion etchant (RIE). The ions are accelerated by an electric field and impact the wafer surface, etching away the sections not protected by an oxide or resist layer. The process it directional, and not limited to the crystal planes of the silicon.

A versatile process using RIE and a passivating polymer coating was patented by Robert Bosch AG [11], and is used under license by several companies in the USA. A deposited layer of passivating polymer , usually PTFE, is used to coat the wafer. The polymer shields surfaces parallel to the ion stream, but wears away quickly on suface perpendicular to the ion stream. As a result process is anisotropic, and can achieve features with aspect ratios of 250:1 or better, and etch rates of up to 10 μm/min.

Another method often used for creating microstructures is LIGA. LIGA uses X-rays to expose thick layers of photoresist. The structres thus created are then electroplated with metal. The metal can be the final product, or it can be used as a mold to produce a complementary structure in another material, such as plastic. LIGA can produce features up to 1mm in size, but requires an expensive synchrotron x-ray source to work properly.

6.2 EDM Machining Method

While the photolithography methods described in Section 6.1 are powerful and can produce the desired arrays of wells, they share a few drawbacks. Photolithography is generally expensive and equipment-intensive. In addition, with etch rates on the order of 1-10 μm/min, with repeated resist coatings necessary, the process is time consuming when it comes to etching features hundreds of microns deep. Finally, micro-channel arrays used for high throughput scanning do not necessarily need the sub-micron level of precision and small features available through lithography-based methods. EDM is an attractive alternative because it is accurate down to micron level, anisotropic, and has achieved erosion rates over 600 μm/min, significantly faster than any etching methods.

6.2.1 Overview

EDM machining relies on electrical discharges to melt or vaporize small amounts of the surface of the material that is being cut. Silicon happens to to have a combination of properties that make it attractive to EDM machining. For a given material, the

EDM machining coefficient can be expressed as a function of the thermal conductivity, heat capacity, and the melting point. The lower the coefficient, the more effective electrical discharges are at wearing away on the surface. Literature [27] suggests that equation 6.1 be used to compute the EDM machining coefficient C_m, which is a function of thermal conductivity k, specific heat c, and melting temperature T_m.

$$C_m = kcT_m^2. \tag{6.1}$$

While this equation is obviously simplistic, and omits important factors like heat of fusion, it does seem be adequate for first order prediction of a materials resistance to EDM wear. While electrode materials such as tungsten and copper have an index of about 3, and steel has an index of about 0.25, silicon is much lower at 0.0075 [27]. The Table 6.1 compares several materials often used in EDM to silicon. Silicon has an extremely low coefficient and should be quite easy to machine. Silicon is also attractive from the point of bio-compatibility. The metal is non-toxic, and has been successfully used in the growth of bacterial colonies. In addition, it is reasonably inert towards most compounds likely to be used in pharmaceutical screening.

Table 6.1: Erosion Resistance Index C_m

Material	C_m
Copper	2.79
Tungsten	2.99
Steel	0.23
Silicon	0.0075

Adapted from: Reynaerts et. al, 1997. [27]

Many varieties of silicon wafers of various are available because of the demand from the electronics industry. Commercially available silicon wafers with surfaces polished to to nanometer-level smoothness constitute the perfect base material for array manufacture. More importantly, silicon is available with various impurities that change its electrical properties. For the EDM experiments, boron doped, 625 μm thick silicon wafers with conductivity of 0.00008 to 0.0002 Ω·m were purchased from

TYGH Silicon, Inc. [15]. Higher conductivity silicon is available, with resistivities as low as 0.001 $\Omega \cdot$m. These should be considered for future machining.

6.3 Electrode Manufacture

Cutting electrodes for machining silicon arrays was accomplished on a wire EDM machine. A specialized low-power set of machining parameters, also called a technology file, was created specifically for this task. The arrays of pins were cut in a manner identical to the inserts for the ram, with the sole exception that a finished array was left attached to the indexing holder. The holders, manufactured by System3R, are common between the wire EDM and the die sinking EDM , allowing precise indexing of the finished electrode onto the head of the sinker EDM. While the advertised repeatability of the reference elements on the electrode holders is on the order of one micron, the actual accuracy suffers due to corrosion of the reference elements during the wire EDM machining process. Wire EDM machining sometimes lasted up to 24 hours, exposing a simple hardened steel reference element to a harsh environment in the presence of a copper electrode. While some of the rust could be removed and prevented by judicious use of protective machine oil, the lifetime of the reference elements is limited to a few cycles, and the accuracy is at best adequate. Electrode removal for cleaning during machining was found impractical, as the pins would not return to their previous positions. In-situ cleaning was necessary. A stainless steel reference element in a dedicated wire EDM fixturing system may be needed in the future for electrode cutting applications.

The workpiece of for manufacturing the electrode was always slightly oversized to provide adequate space for reference flats to be machined - see Fig. 6-1. These flats serve to align the electrode with respect to the silicon on the sinker EDM machine. Initially, the pins themselves were used for alignment, but they were found to be so fragile that the electrode measurement touches caused them to bend, thus damaging the electrode.

Just like the inserts for the ram, the pin density of the electrodes is limited by the

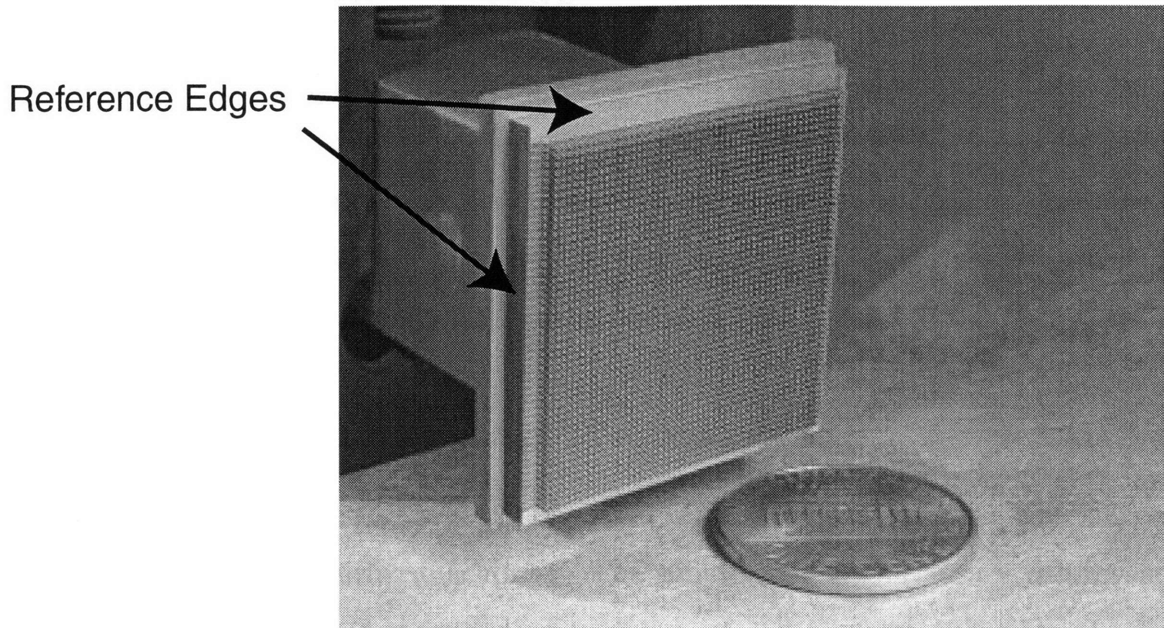

Figure 6-1: A 2500 pin die sinking electrode. This electrode requires 10 hours of manufacturing and can be used up to 12 times, depending on the desired accuracy of the holes.

wire diameter and minimum cut thickness as described in Section 4.5.1. The electrode cutting was done with 100 μm wire, which is the smallest wire still available with round diamond wire guides, making it significantly easier to use. With a minimum slit width of approximately 240 μm and a pin width of 90 μm, the best achievable pitch was approximately 3 pins/mm or 9 pins/mm^2. This pitch may be improved by the use of a thinner wire, available in diameters as small as 30 μm. However, thinner wire represents a significant, order-of-magnitude decrease in machining speed and robustness. As a result, increased density was judged to not be a sufficient tradeoff for speed and convenience.

Because it was desired to localize the maximum wear in the frontal section of the electrode, the electrode pins incorporate no taper. Consequently, while the details of the frontal section of the pins are eroded away, the rest of the pin remains untouched, and is ready to be used for fine finishing of the interior of the the channel or well. In a manner similar to wire EDM, the sinker EDM requires finishing passes to obtain the best surface finish.

6.4 Experimental Setup

For most of the experiments, the EDM was used without any physical modifications. A silicon rectangle blank was cut out on the wire EDM using the silicon power settings, and carefully clamped into a precision vise. The electrode was aligned an positioned over the center of the array. A steady stream of oil from a side nozzle provided flushing to clear particulate matter from the erosion area.

6.4.1 Oil Based Machining

The standard machine utilizes a carbon based oil in a dielectric bath. The silicon blank was submerged during machining. The submersion was necessary to prevent the volatile vapor created during decomposition of the oil from being ignited by EDM sparks. The oil itself was kept at a constant temperature and filtered to remove suspended particulate matter.

The electrode was regulated at 80 volts potential with respect to the work piece, igniting sparks that wear away the silicon. At the lowest setting of 0.5 A, this translates to a current density of 2×10^4 to 1.25×10^5 A/m^2. This is significantly below the maximum of 1×10^7 A/m^2 possible with copper electrodes, and is not a limiting factor.

In choosing a material for the electrodes, a series of trade-offs must be made. While graphite has higher possible current density and lower wear than copper, it is too brittle to be machined into the small high aspect ratio pins. Copper is easy to machine and does not break, but the softness of the material produced problems with higher density arrays, where pin bending was a problem. Copper-tungsten is an alloy stronger than copper and more resistant to EDM wear. While the material successfully resisted bending when used in small electrodes, a small percentage of pins broke off completely during the manufacturing process. During testing, 70 μm square electrodes with an 18:1 aspect ratio exhibited 1-3% breakage rate, which was judged unacceptable. If conventional materials are to be used, the apparent limit on electrode pin size is about 10 μm, with an aspect ratio of $\sim$ 13:1.

Electrode size itself is limited by maximum external dimensions by the time vs. reliability tradeoff. While a 10,000 pin array has been manufactured, the process took upwards of 30 hours. The long manufacturing time was dictated by the the necessity to keep the cutting speed lower than maximum to prevent wire breakage. The practical thickness of the electrode stock for a 100 μm wire has been experimentally found to lie in the 30 mm range. On average, a 25×25 mm, 2,500 pin electrode will require 10 hours of machining on the wire EDM. Using a grid sinking pattern described later in this chapter, the electrode can then be used to machine 10,000 channel arrays at the rate of about 1 array / 3 hours.

6.4.2 Erosion Patterns

Given the limitations in electrode size and density, two separate approaches were used to obtain a ten thousand channel array. The first method uses a smaller electrode with the desired final density of pins. The electrode is sunk sequentially in a grid pattern, as shown in Figure 6-2. This approach overcomes the limitation of electrode size, but is still subject to the density limitation as discussed in Section 6.3. This method does have the advantage that the electrical resistance from the pins through the silicon is identical for each sinking operation, and thus the machining speed is identical for each of the grid rectangles.

A second, more interesting method overcomes both the bulk size as well as the density limitations of the electrode. The method uses a 70 μm beam electrode combined with a superposed sinking pattern as shown in Figure 6-3. The method effectively quadruples the density of the channel array, and at first glance appears to be the perfect solution to the electrode density problem. However, an unexpected problem with silicon resistance was found to hamper this approach.

6.4.3 Silicon Resistance

During the first EDM cycle, the resistivity encountered through the silicon wafer may be modeled as a resistivity between a small cylindrical source and the edges of a round

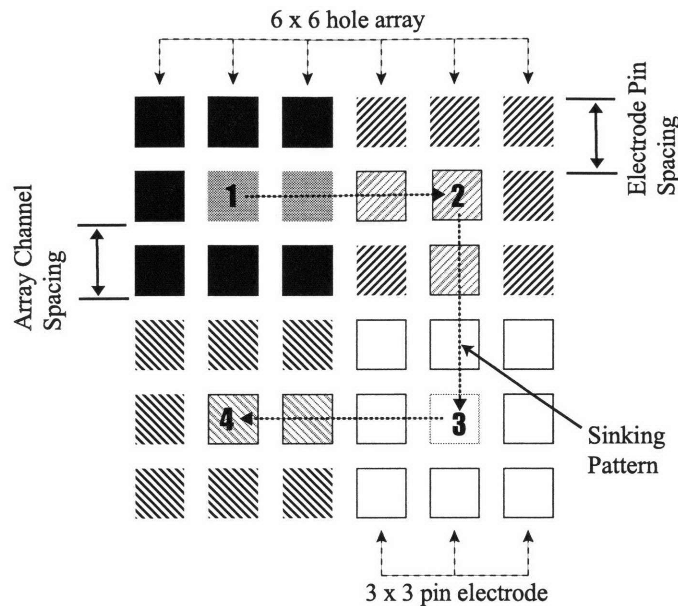

Figure 6-2: One simple solution to manufacturing large size electrodes is to use the same electrode in a grid pattern to create an array four times the size. The hole density of the array is the same as the electrode's pin density.

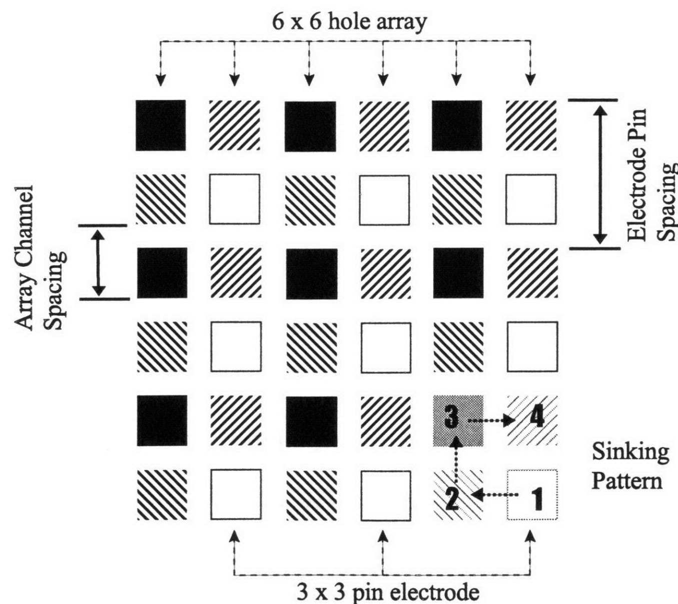

Figure 6-3: The limitation in the density of the electrode pin array (See Section 4.5.1) may be bypassed bt superposing several machining cycles with a slight offset. In this pattern the hole density is increased by a factor of four.

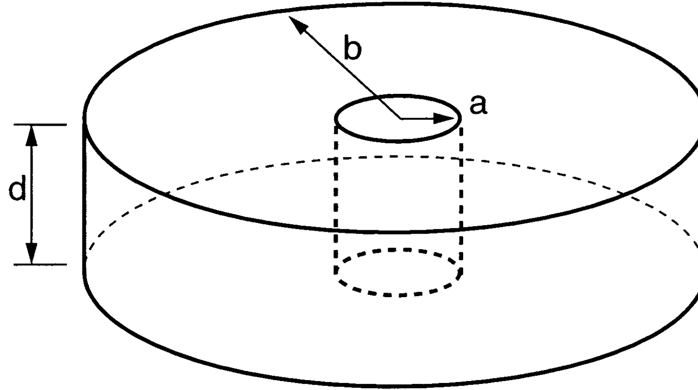

Figure 6-4: For a continuous model of the silicon wafer the resistance may be found by integration.

plate of finite thickness. By integrating the electric field in the plate, we obtain the expression for the resistance

$$R = \frac{\rho * ln\left(\frac{b}{a}\right)}{2\pi d}, \tag{6.2}$$

where ρ is the resistivity of silicon in ohmΩ·m, d is the thickness of the wafer, and a and b are the inner and outer radius of the of the wafer, as shown in Figure 6-4. The inner radius is assumed to be of approximately the same diameter as the pins, or 0.1 mm, while the outer radius is the longest distance to the edge of the array, or 15 mm.

However, once a set of channels has been sunk into the silicon, the subsequent resistance will be dependent on the resistance of a large set of silicon beams that form a resistive network. This network will have a higher resistance than the solid silicon wafer, and thus negatively affect machining performance. If all the beams are identical, and voltage is applied to an arbitrary location in the grid, the voltages of individual nodes may be determined by a simple Laplace numerical method. Voltage of each node in the network

$$v_s = \frac{1}{4}(v_1 + v_2 + v_3 + v_4) \tag{6.3}$$

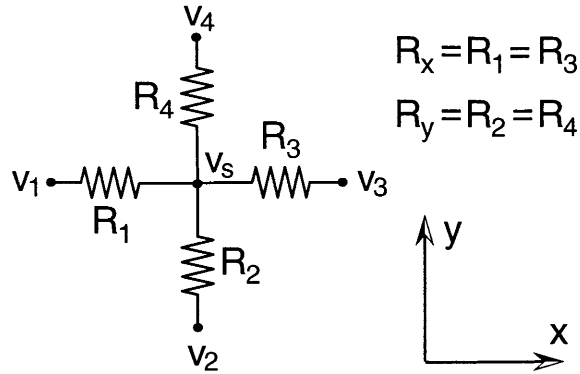

Figure 6-5: A resistor network element in a Laplacian numerical simulation model for a silicon array.

is the average of voltages v_i that are shown in Figure 6-5.

These voltages translate into a matrix $\mathcal{L}$ that may be used in a Matlab program that repetively convolves it with a 50×50 matrix $\mathbf{M}$ to create

$$\mathbf{M_{new}} = \mathcal{L} \otimes \mathbf{M_{old}}, \tag{6.4}$$

where $\mathbf{M_{new}}$ converges on a solution to the voltages in the resistance network. The variable a in

$$\mathcal{L} = \begin{vmatrix} 0 & a/4 & 0 \\ a/4 & (1-a) & a/4 \\ 0 & a/4 & 0 \end{vmatrix} \tag{6.5}$$

controls the rate of convergence of the solution. Once the matrix $\mathbf{M}$ converges, the center node and the surrounding four nodes are evaluated to find the current flow from the center node. Since the voltage difference between the source v_s and the sink v_{ref} as well as the individual resistances are known, the resistance of the network

$$R_{network} = \frac{v_s - v_{ref}}{\sum_{i=1}^{4} \frac{v_s - v_i}{R_i}} \tag{6.6}$$

can be computed. Unfortunately, the resistances are not always identical and the

resistance in the x direction may be different from the resistance in the y direction. In that case the simple model in Eqn. 6.3 must be expanded to the following:

$$v_s = \frac{R_x}{2(R_x + R_y)}(v_2 + v_4) + \frac{R_y}{2(R_x + R_y)}(v_1 + v_3). \tag{6.7}$$

This results in a change to the Laplace matrix $\mathcal{L}$ in the Matlab evaluation program, which now reflects the changes in resistance.

$$\mathcal{L} = \begin{vmatrix} 0 & \frac{R_y}{2(R_x+R_y)} & 0 \\ \frac{R_x}{2(R_x+R_y)} & (1-a) & \frac{R_x}{2(R_x+R_y)} \\ 0 & \frac{R_y}{2(R_x+R_y)} & 0 \end{vmatrix}, \tag{6.8}$$

where the resistances R_x and R_y are related to R_i as shown in Fig. 6-5. The final evaluation of resistance is calculated using Eqn. 6.6. For a sample 100×100 array with .25 mm pitch and 140 μm channels, the resistance estimates are shown in Fig. 6-6. For this particular case, the resistance increases by at least a factor of two, despite the rather wide (110 μm) wall thickness used in this array. The results of this resistance increase on available power and machining performance are shown in Fig. 6-7.

6.4.4 Silicon Fluid Based Machining

While carbon-based oil works reasonably well for machining dense silicon arrays, the carbon deposits that form on the electrodes and the array itself encourage stray discharges that erode the silicon in places that the electrode does not even touch.

In order to reduce silicon array damage from stray discharges, a dielectric fluid was sought that would not form a carbon layer after decomposition. Silicon based transformer fluid from Dow was selected as a possible candidate. The silicon fluid contains long chains of silicon instead of carbon like the normal oil-based EDM liquid. Consequently, it was hoped that its decomposition by EDM sparks would be cleaner.

The Roboform 30 EDM had to be modified to machine using a silicon liquid. The oil circulation and the associated interlocks were temporarily disabled, and a temporary tank with an integral filtering and flushing system was installed on the

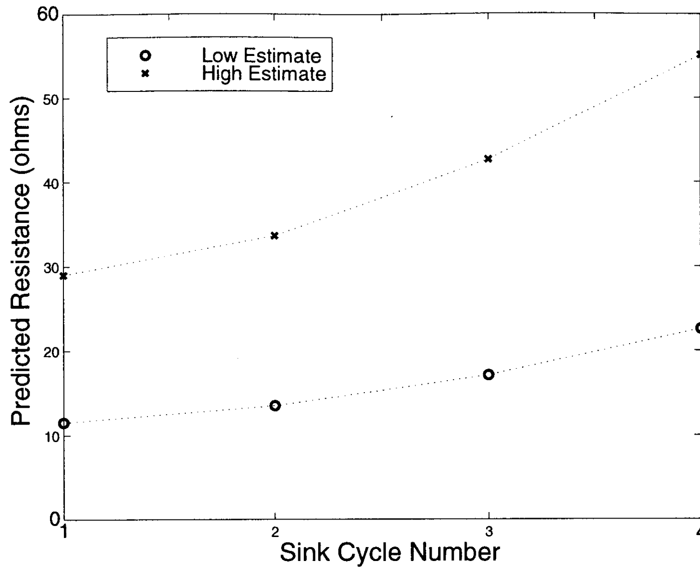

Figure 6-6: Electrical resistance encountered by the EDM machining process increases in successive steps of the superposition machining pattern. The two curves represent the lowest and highest resistances possible with the boron doped silicon used in machining.

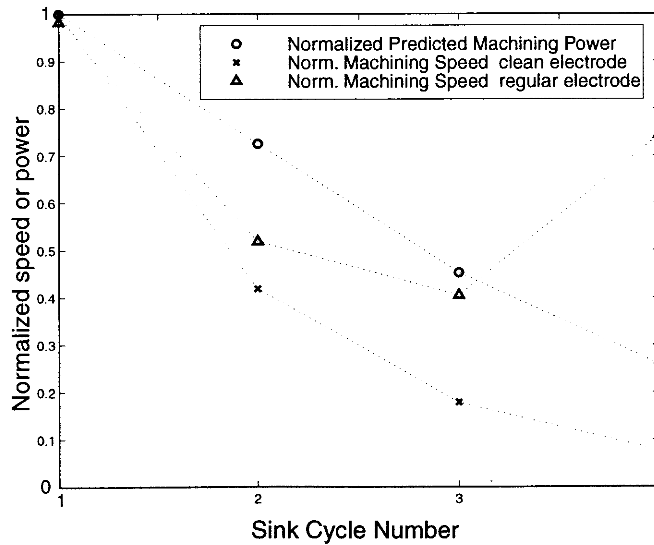

Figure 6-7: The theoretical power drop as a result of resistance increase (described in Fig. 6-6) as compared to the machining speed of the silicon array. All results were normalized for better comparison. Note that the last die sinking cycle was almost always faulty due to carbon fouling.

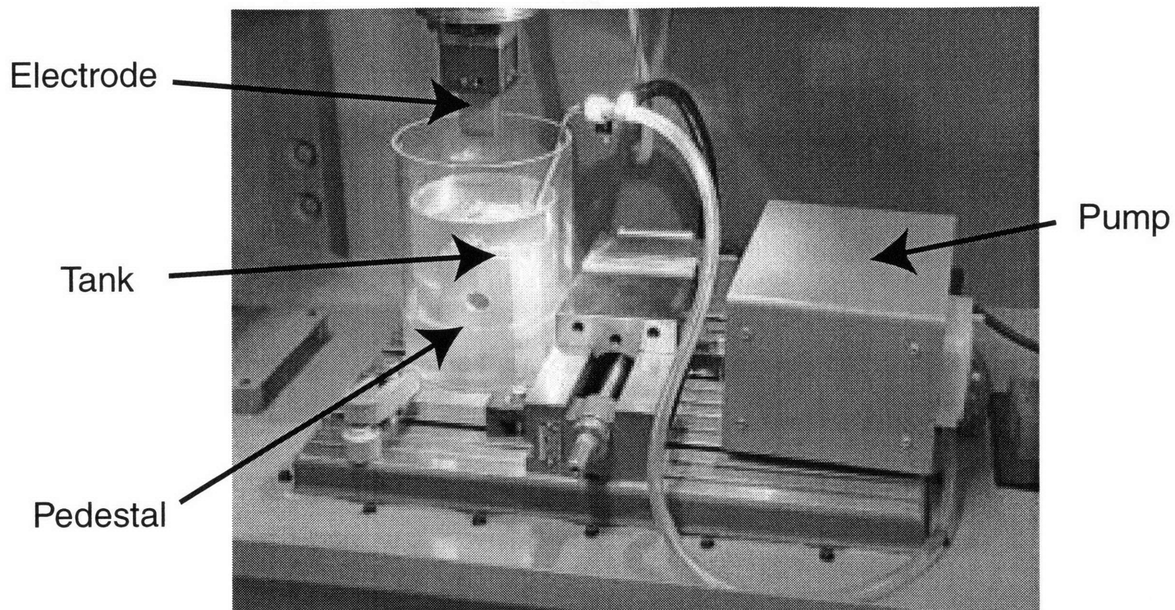

Figure 6-8: A self contained tank in the sinker EDM was used to test machining in silicon dielectic and water. The container features a tank-within-a-tank construction that allows level control and a closed fluid flow with only one pump. In line pump and filter element clean the dielectric. An aluminum post holds the array.

work surface. The setup can be seen in Fig. 6-8. The pump circulated the dielectric and provided a flow for flushing debris from the machining area. An 0.45 μm in-line filter was used initially, but abandoned due to severe restrictions in flow volume.

The setup proved functional and allowed for limited machining in silicon. However, a dark carbon deposit still formed around the wells as with the standard machining techniques. In addition, the viscosity of the silicon dielectric was higher than that of the regular oil. This is reflected in reduction of machining speed as the well depth increased. The debris of machining remained in the hole, and halted machining at the depth of approximately 300 μm. Surface finish, as seen in Fig. 7-3, was worse than usual. Cleaning of the carbon and silicon residue also proved difficult.

A much lower viscosity dielectric liquid combined with high pressure cleaning nozzles may contribute to better machining results.

6.4.5 Water Based Machining

Water is used as a dielectric in the wire EDM with excellent results and is recommended by several sources [21][28] as the best dielectric for sinker EDM machining. Excellent thermal conductivity, low viscosity, and a lack of by-products of decomposition make water ideal as a dielectric for machining silicon. Water based machining was attempted on a setup identical to the one used with silicon oil, except that the wire EDM's filtered and deionized water supply was used for a dielectric. Unfortunately, the collision sensor on the Roboform machine is sensitive enough to detect the small conductivity of water, and interpret it as a collision. To counter this problem, highly pure Milipore water with low conductivity was substituted for standard deionized water. Although the problem was somewhat mitigated, it persisted and made machining impossible, eliminating this promising method from this investigation. Interestingly, Panasonic Corporation has been working on creating machines specifically for micro EDM machining of silicon, and water seems to be their dielectric of choice. For further work on high density arrays, the acquisition or building of such specialized machine may be required.

Chapter 7

EDM Manufacturing Results

Oil-based EDM machining is the most commonly used method for sinker EDM applications. Consequently, it was the first method tried for machining silicon arrays. While a number of good 10,000 channel arrays were created using this method, with densities ranging from 4 wells/mm^2 to 36 wells/mm^2 (see Fig. 7-1). Despite the successes, problems related to carbon deposition hamper this method (see Fig. 7-2). Silicon-based dielectic fluid was tried in hopes to reduce carbon buildup. The high viscosity of the fluid prevented successful machining of the small wells due to flushing difficulties. Water-based EDM was evaluated on the wire EDM machine and found to produce excellent results. However, application of water in the sinker was thwarted by electronic hardware incompatibility.

7.1 Erosion Rates

The maximum erosion rate measured in silicon was 600 μm/min while machining with a 400 pin copper array. However, with the array size increased to 2,500 pins and smaller pin sizes the erosion rates dropped to approximately 13 μm/min in the average. The worst performance was recorded in in silicon based fluid, where the machining speed was measured at less then 1 μm/min before the program was stopped.

One possible reason for those slow machining speeds may have been the silicon wafers themselves. As was shown in Fig. 6-7, the machining speed is related to the

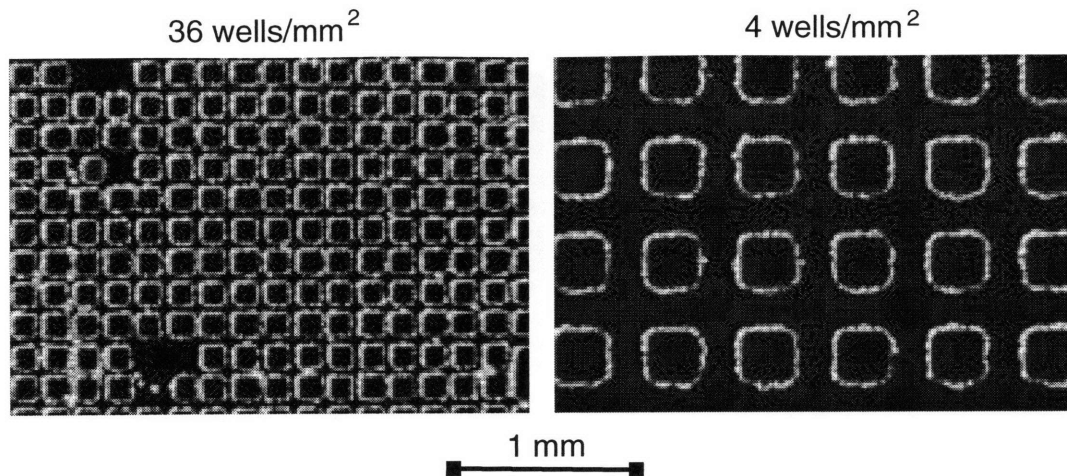

Figure 7-1: Microscope images of finished silicon arrays. The low density array was produced using a grid process, while the high density array required the much slower superposition. Both photos are taken at the same magnification. Flaws in the array on the left are caused by broken pins in the electrode.

available power. Since the power depends on the resistance of the workpiece, a lower resistance silicon may produce much higher erosion rates.

7.2 Surface Finish

Using the profilometer, the best suface finish measured for a surface machined in oil was 3 μm RMS . On the wire EDM, where the machining was done in water, the best surface finish obtained was 1.7 μm RMS. Rough surface finish in water had a surface roughness on of approximately 2.2 μm RMS. A sequence of several machining cycles, each with a lower power lever, was necessary to provide a smoother finish. While the wire EDM was quite capable of achieving good surface finishes, achieving a good surface finish on the sinker EDM proved problematic because of the necessary enlargement of the channels bored into the silicon. A minimum 20 μm skim cut, necessary for removing the heat affected zone (HAZ), created oversized channels,

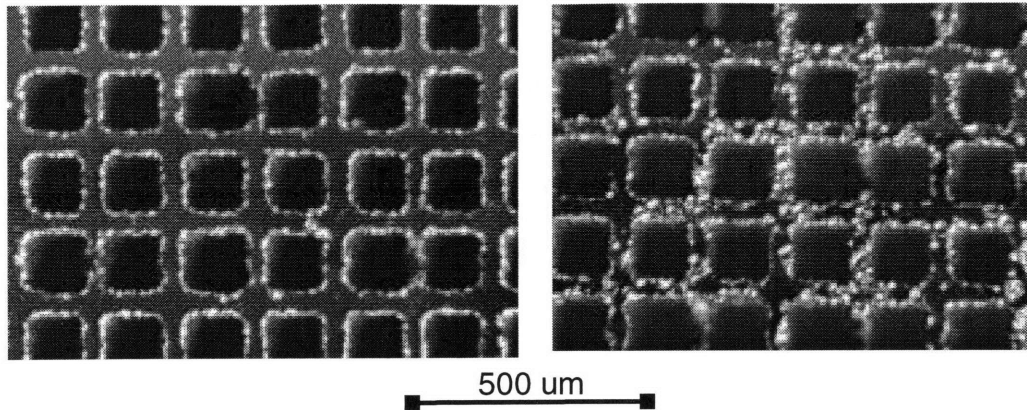

Figure 7-2: Two microscope image of the same 36 wells/mm^2 silicon array. The rough finish the horizontal surfaces of the right was created by parasitic discharges, which most likely form due to short-circuits through carbon residue deposits. Left photo shows a section where better flushing kept carbon deposits low.

reduced wall width, and resulted in increased electrode wear. For example, finishing channels resulted in a 100 μm electrode producing a 140 μm square channel. In order to obtain 100 μm wells it was necessary to reduce electrode size to 70 μm, at which point pin breakage and bending became a problem. The heat affected zone was reduced by reducing spark duration and increasing time between sparks, but this tradeoff resulted in slower machining. While literature [34], [32] suggests that much improved surface finish may be obtained by using a suspended powder in the EDM oil, the method was not tried due to anticipated problems with filtering. Since the particulates are suspended in the oil to begin with, it becomes impossible to keep the fluid clean after a brief machining period.

7.3 Electrode Wear

Electrode wear measures the ratio of material removed from the electrode with respect to the the material removed from the work piece, in this case a silicon wafer. Ideally, both the electrode and the work piece would be weighed before and after

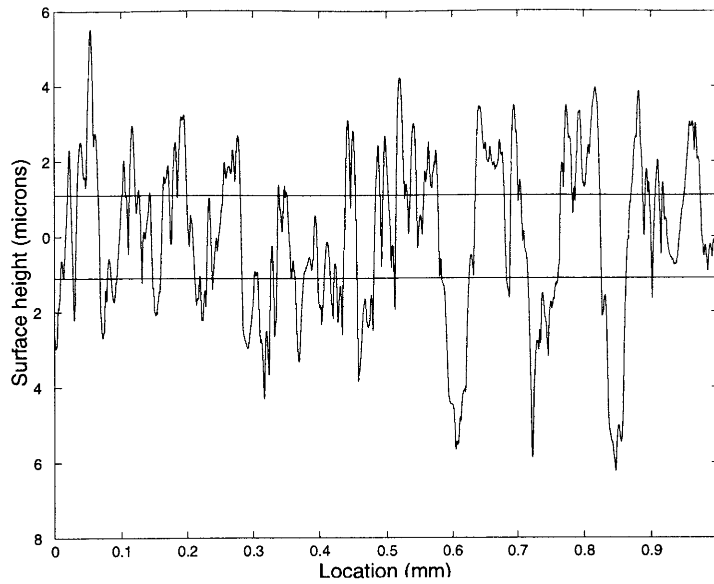

Figure 7-3: A surface profilometer image of an EDM machined silicon surface. Also shown are the RMS roughness bounding bars.

the experiment, and the ratio of lost masses would have determined the wear ratio. Unfortunately, the electrodes used in EDM are too heavy to be weighed on high precision scales, and carbon deposits between pins would have rendered any such mass measurement meaningless. Instead, the length of the pins of an electrode was measured before and after machining. Taking into account the thickness of material that was removed using the array, the wear rate was calculated to be approximately 0.5%. However, while this particular rough cutting wear rate of silicon compares favorably to that of steel, the actual wear rates will vary widely depending on factors such as the power settings and wave forms employed, electrode material and work piece material. Tabulation of these values is beyond the scope of this paper.

Another type of electrode wear was the bending of pins. When machining with a high density copper electrode, physical contact between the electrode and the pins would take place. In copper, these mini-collisions caused slight to extreme bending of the pins and erosion in wrong location. When copper-tungsten, a much stiffer electrode material was employed, the pins simply broke instead. This problem only occurred with the 70 μm pins, and may be solved with a machine more sensitive to

small short-circuits.

7.4 Silicon Array Cleaning

After the machining was complete, a carbon residue and a coating of oil covered all the surfaces of the array. The oil and carbon were undesireable contaminants for biological experiments. In addition the contaminants prevented any secondary operations to change the hydrophobicity of the finished array. Several cleaning processes were tried, ranging from simple flushing using methanol to ultrasonic cleaning in acetone or other organic solvents. While it was initially feared that an ultrasonically agitated bath might shatter the brittle silicon arrays, that cleaning process proved to be the effective. Oil residue and carbon dissolved readily in either methanol or acetone. Several sequential 'baths' were necessary to completely dilute the oil and retain little residue on the surfaces. Between baths, the solvent inside the channels is removed using compressed air. A more efficient method may involve continuously flushing the array inside a filtered utrasonic bath. However, for the purposes of this project an optimized cleaning solution was judged unnecessary.

Silicon based liquid produced significantly smaller amounts of carbon residue. However, the silicon liquid proved extremely tenacious, and difficult to clean with the previously described technique. Repeated rinsing produced adequate results, but overall silicon dielectric fluid required significantly more cleanup effort.

A final cleaning step may be necessary to remove carbon deposits from inside the wells. A sulfuric acid treatment was reported successful in etching away all remainders of oil and carbon deposits with no effect on the silicon itself.

Electrode cleaning was investigated as a way to improve surface finish and machining efficiency. In breaks during machining, the copper or copper tungsten electrode was submerged in an ultrasonically agitated cleaning solution. Arrays themselves were wiped clean with a soft tissue. Carbon deposits were successfully removed using this method, and frequency of secondary discharges was reduced, but not eliminated.

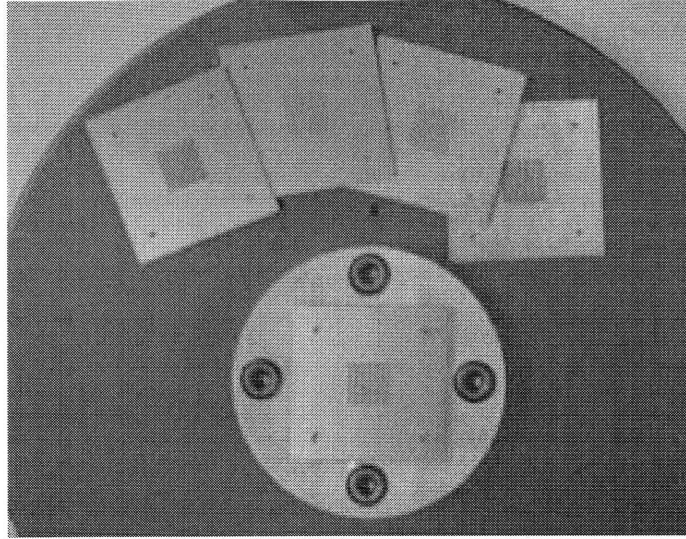

Figure 7-4: The silicon arrays and an alignment jig. Once the arrays are stacked on top of an alignment jig, the fluid inside the holes mixes and reactions take place. This setup is to be mounted directly on an optical system for examination, and is used in flourescence detection. From Kanigan et. al [23]

7.5 Applications

The silicon arrays found an immediate application in research at the BioInstrumentation Laboratory at MIT. The first batch of 10×10 channel test arrays was modified and machined with the addition of four alignment holes. A jig was produced to facilitate the alignment of the arrays by stacking. The tolerance on the alignment hole position is 10 μm and therefore the maximum possible misalignment is 14 μm in any direction. Since the wall thickness of the silicon between the channels is 0.25 mm, no cross-contamination between the should occur. In fact, after the array surfaces are oxidized to make them hydrophobic, no cross talk occurs, but the contents of stacked wells do mix. This setup, combined with an optical system, has been successfully used in flourescence experiments [23], and validates the idea behind the construction of the larger arrays. Photos of the alignment jig are shown in Figures 7-4 and 7-5.

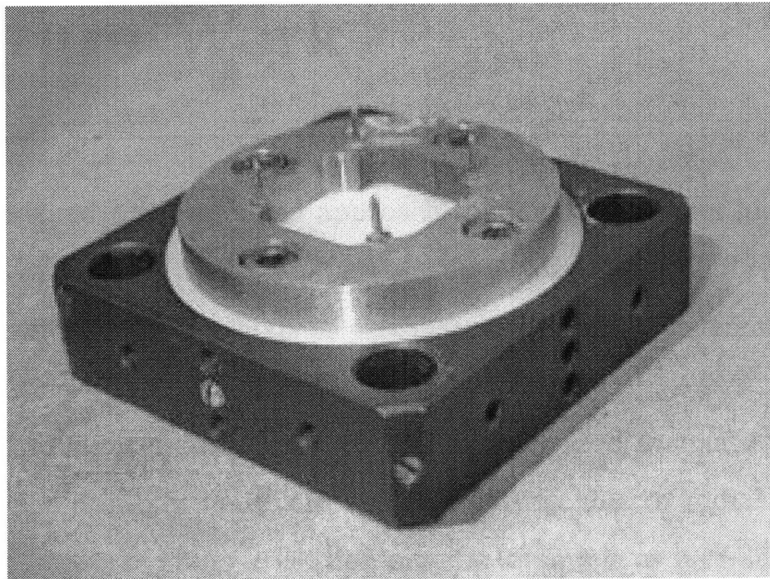

Figure 7-5: The alignment jig has four pins to for alignment of up to three layers of arrays.

Chapter 8

Conclusions and Recommendations for Future Work

This thesis presented a two pronged approach to manufacturing of high density well and channel arrays to be used for pharmaceutical scanning. While the end use of the arrays is identical, the methods of productions are vastly different, yet both are promising.

The impact forming method has been successfully used in creation of small well arrays. While the durability problem with the inserts, due to radial flow of plastic still remains to be worked out, a solution may be as simple as increasing the impact velocity by an order of magnitude or laterally pre-compressing the plastic during impact to force upward displacement. Also, rigid wedge shaped edge blades could be installed on the inserts to push plastic inward during impact, balancing the outward expansion, and preserving the pins. The impact method is viable and has the potential to be much less expensive than injection molding for machining of sub-millimeter sized features.

Silicon EDM machining was a success in that a several completely functional 10,000 well arrays were created. Increasing the density from 4 wells/mm^2 to 36 wells/mm^2 did not produce perfect arrays, but did show the capability of the process to machine such small features. Based on the experience gained with this method, any further work designed to increase the density of the silicon well arrays should take

into serious consideration the use of water as a dielectric, combined with a machine specifically designed for low-power cutting.

Both processes show promise for the manufacture of high density arrays for high throughput screening systems, although the silicon EDM approach seems much closer to the goal than impact formed arrays.

Appendix A

Plastics

Most of the polymer properties presented in the table below are taken from literature sources such available on the particular plastics. However, since there is a large variability in the commercially available polymers, and because the available sources on the plastic properties differ by a factors of up to three or four, certain tests were conducted in house. These tests were used to calculate the exact heat of fusion and specific heat using the PE differential scanning calorimeter (DSC), or a thermogravimetric analyzer. Table A.1 includes a compilation of the data that was used in the calculations during the course of this thesis. (DSC) data with the associated values highlighted is available in Figure A-3.

Table A.1: Material properties of selected polymers

Property	Acetal	Nylon 6	Polycarbonate	PTFE
Density ($\frac{kg}{m^3}$)	1410	1140	1200	2200
Tensile strength ($10^7 Pa$)	6.07	8.14	6.2	2.76
Compressive strength ($10^7 Pa$)	3.58	8.96	8.62	2.76
Young's modulus ($10^9 Pa$)	3.58	1.21	2.59	4.83
Specific heat($\frac{kJ}{kg \cdot K}$)	1.46	1.67	1.26	1.05
Melting point($Celsius$)	165	216	154	327
Heat of fusion($\frac{kJ}{kg}$)	140	58	N/A	N/A
Thermal diffusivity ($\alpha \times 10^5$)	8.46	8.28	6.66	14.4
Thermal conductivity ($\frac{W}{m \cdot K}$)	0.26	0.2	0.18	0.28

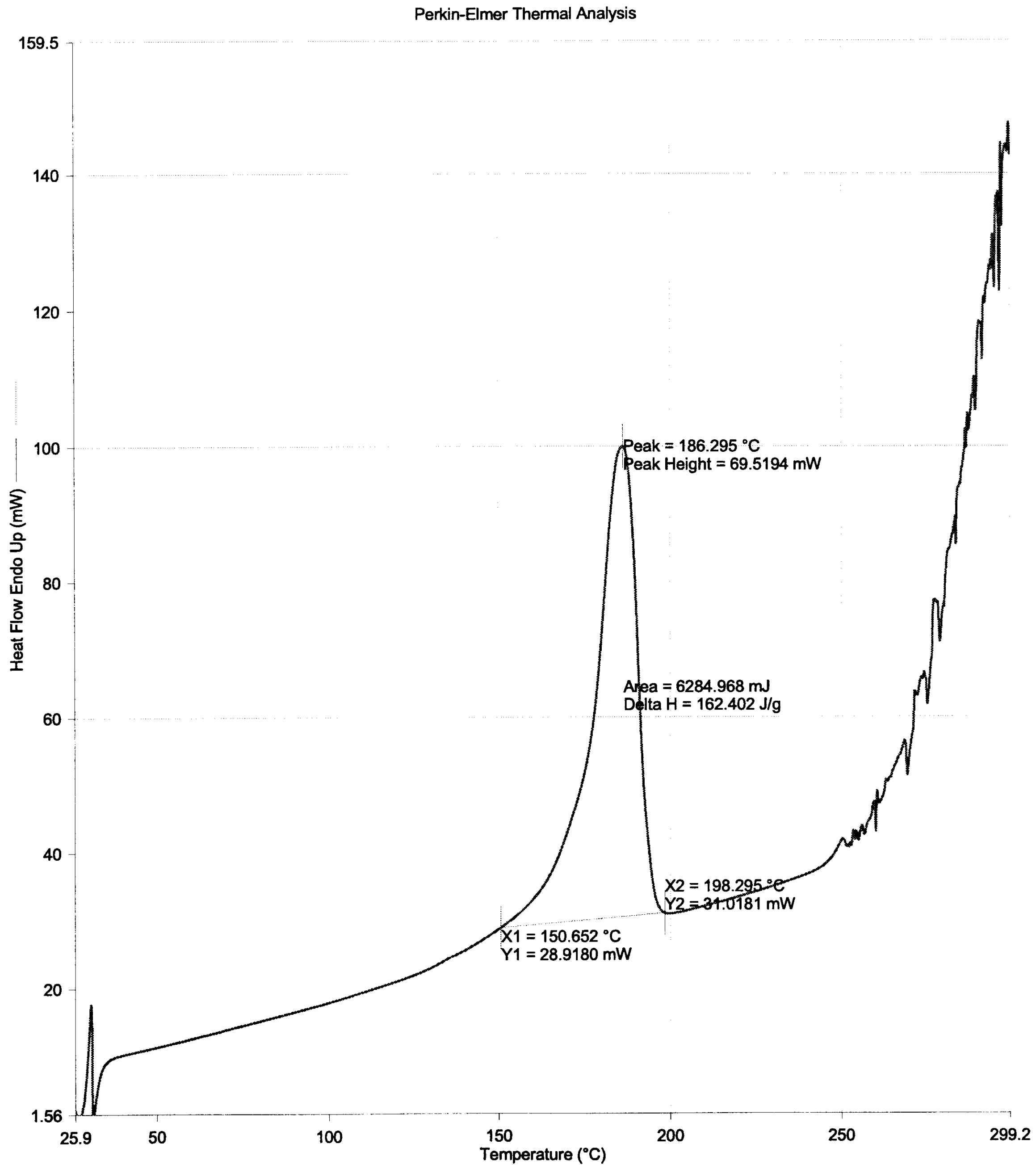

Figure A-1: Polymer data from the PE Differential Scanning Calorimeter (DSC).

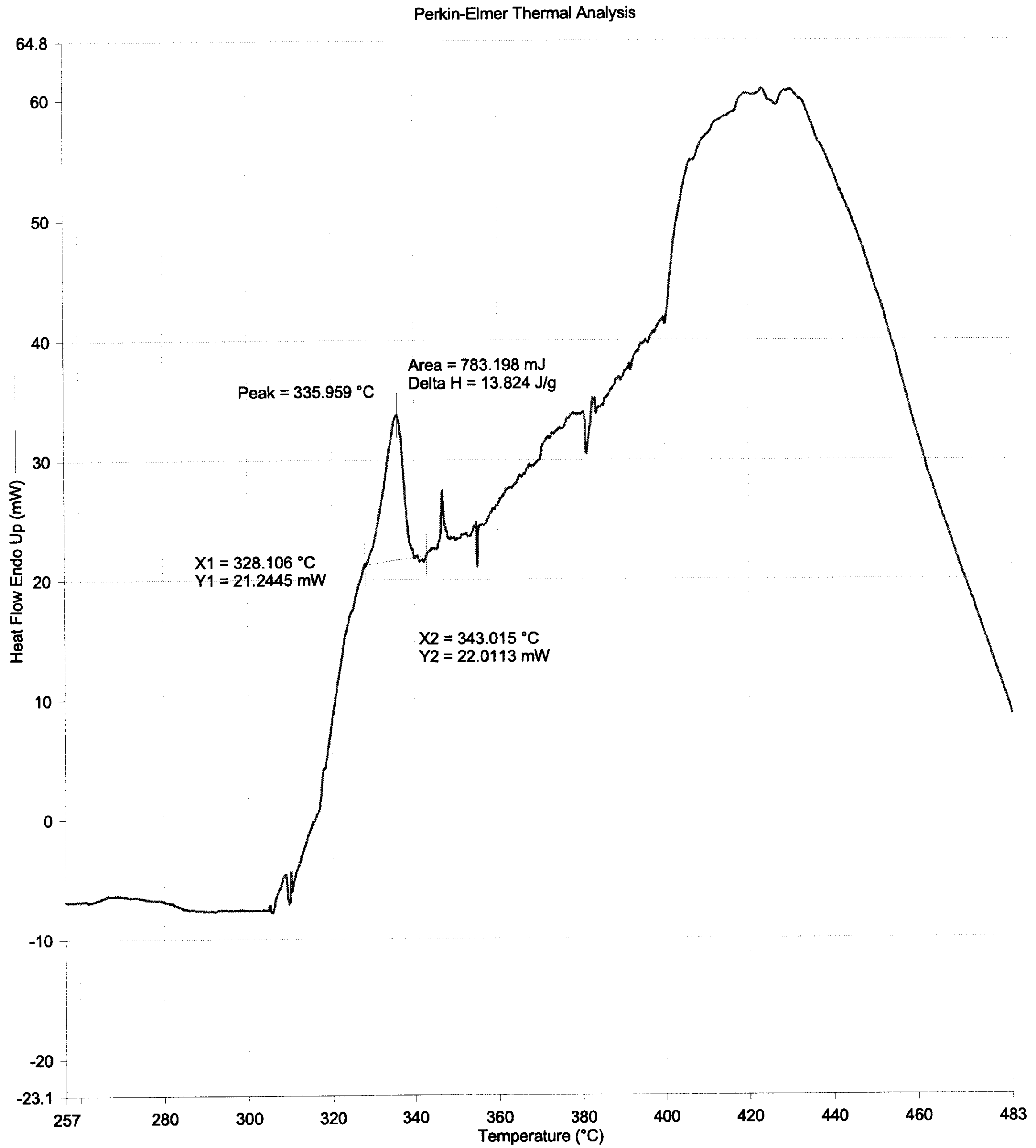

Figure A-2: Polymer data from the PE Differential Scanning Calorimeter (DSC).

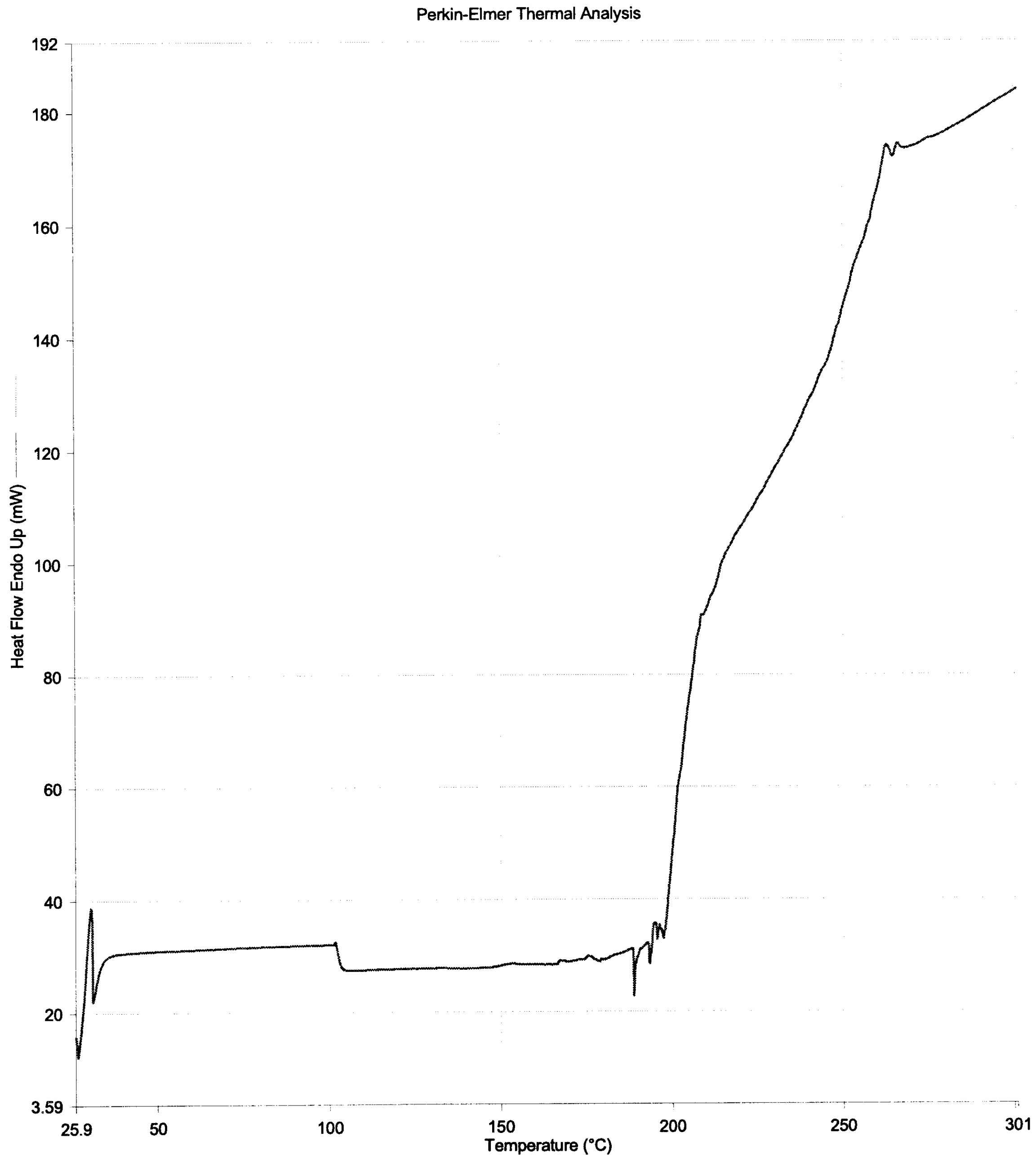

Figure A-3: Polymer data from the PE Differential Scanning Calorimeter (DSC). Note the absence of a melting point in polycarbonate - the polymer simply softens in glass transition.

Appendix B

CAD Drawings

B.1 Ram Final Version - All Drawings

This section contains the drawings of all the parts used to create the kinetic ram.

B.1.1 Ram Head Assembly Drawings

The ram heads needs to be assembled before each test. A new array need to be inserted at the end of the strike pin. The tapered shape of the front of the array facilitates the assembly process. Bolts are not shown as part of the assembly to keep down drawing complexity. For bolt sizes please refer to individual part drawings.

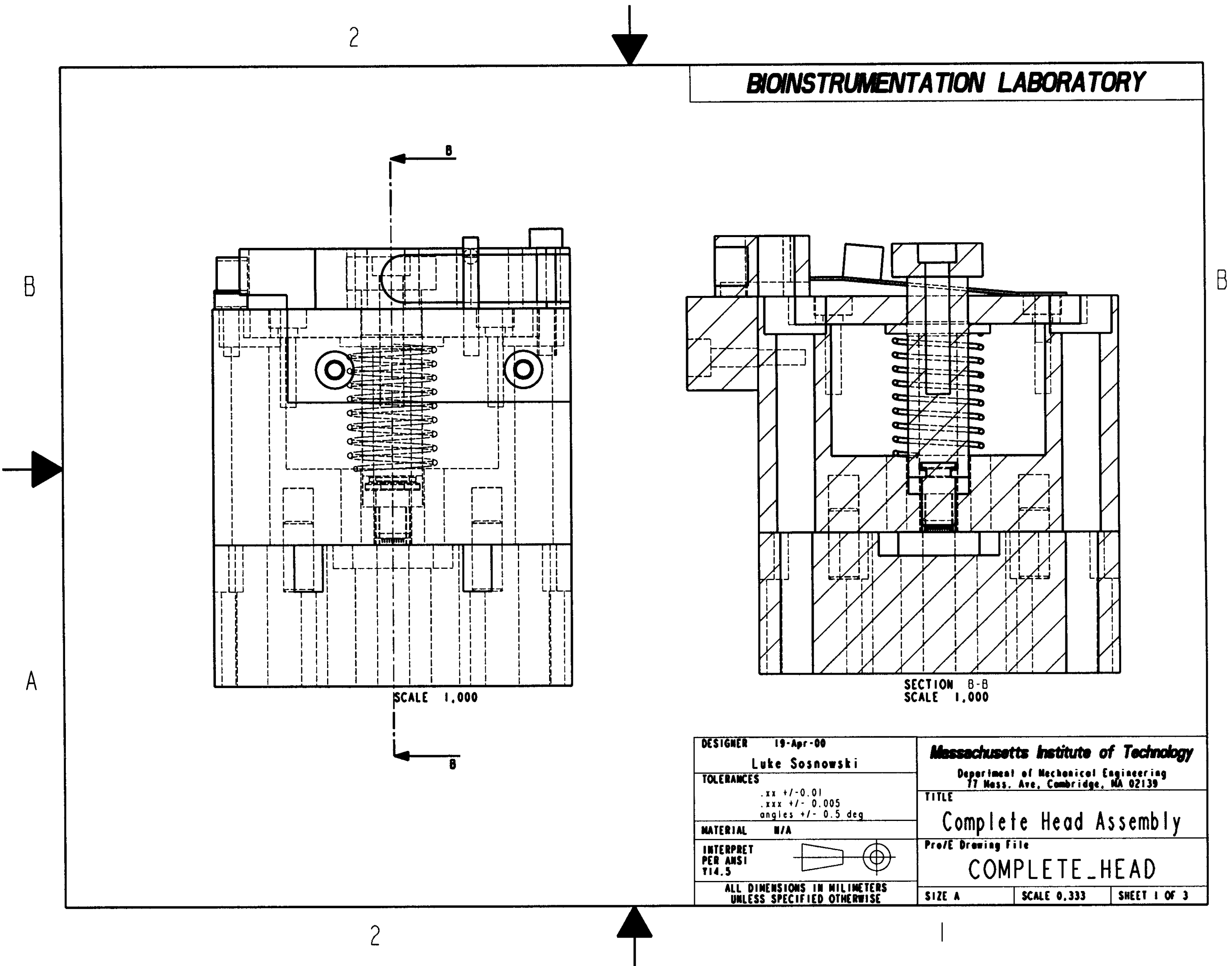

Figure B-1: Complete Ram Head Assembly

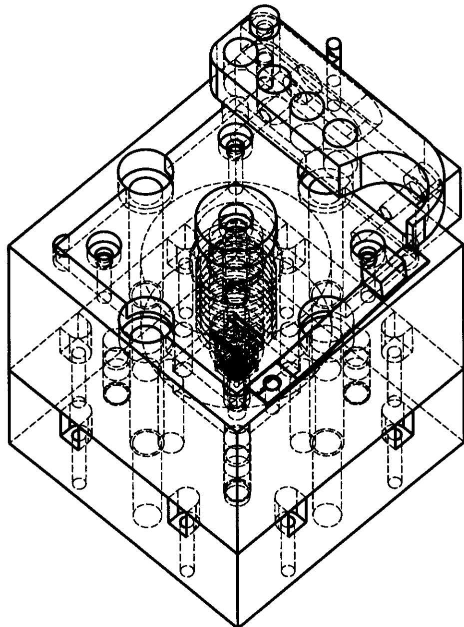

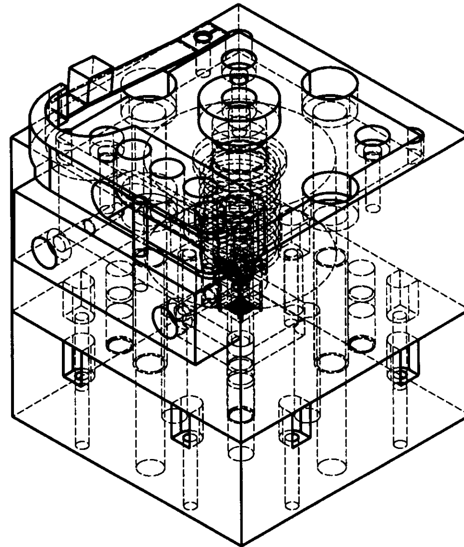

Figure B-2: Complete Ram Head Assembly

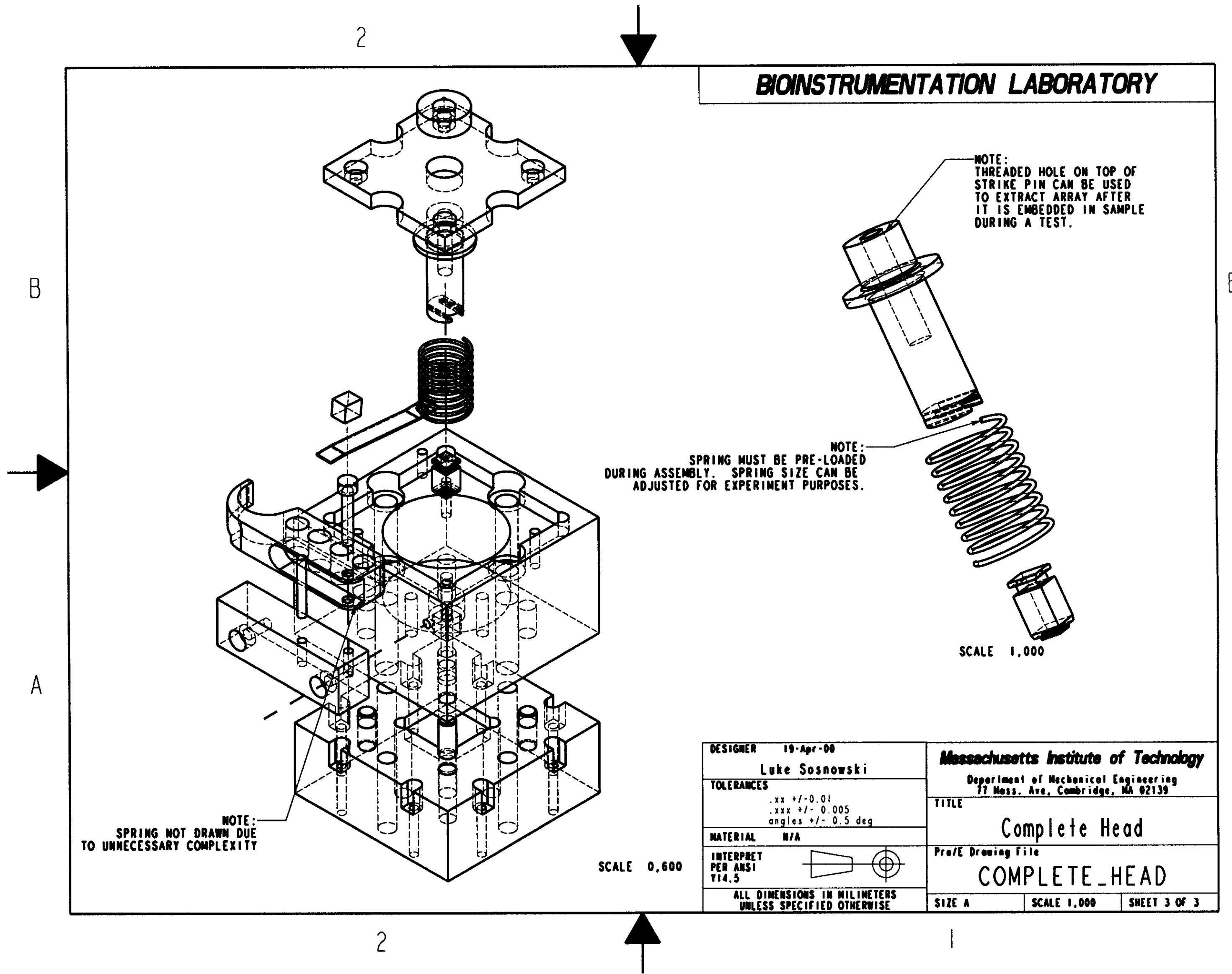

Figure B-3: Complete Ram Head Assembly

B.1.2 Ram Head Part Drawings

These drawings are meant as a deference in case the parts need to be reproduced. In many cases the original manufacturing method is noted, but it should be construed as a suggestion only. Refer to files included with thesis for G codes necessary for creating some of the more complex parts.

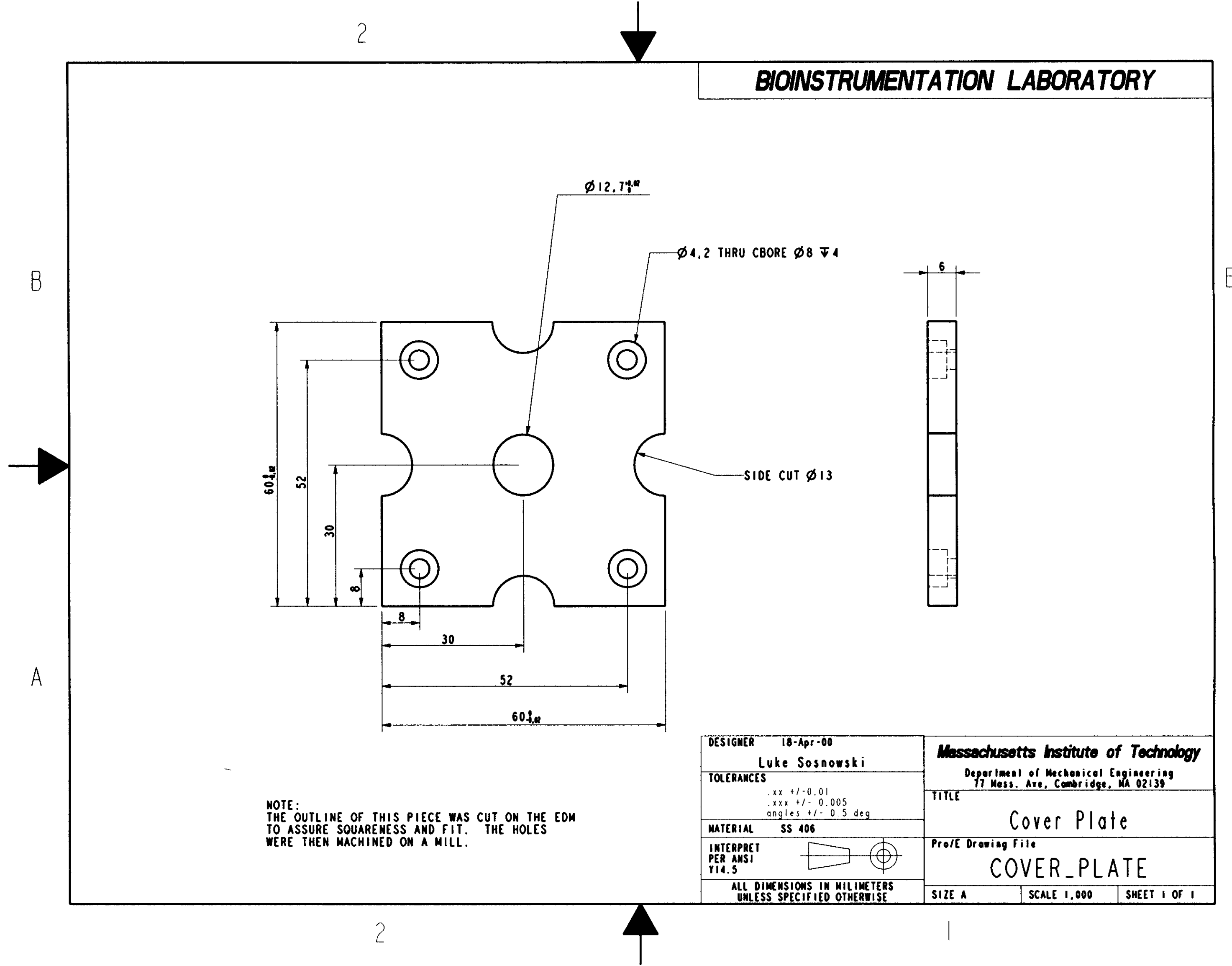

Figure B-4: Cover Plate

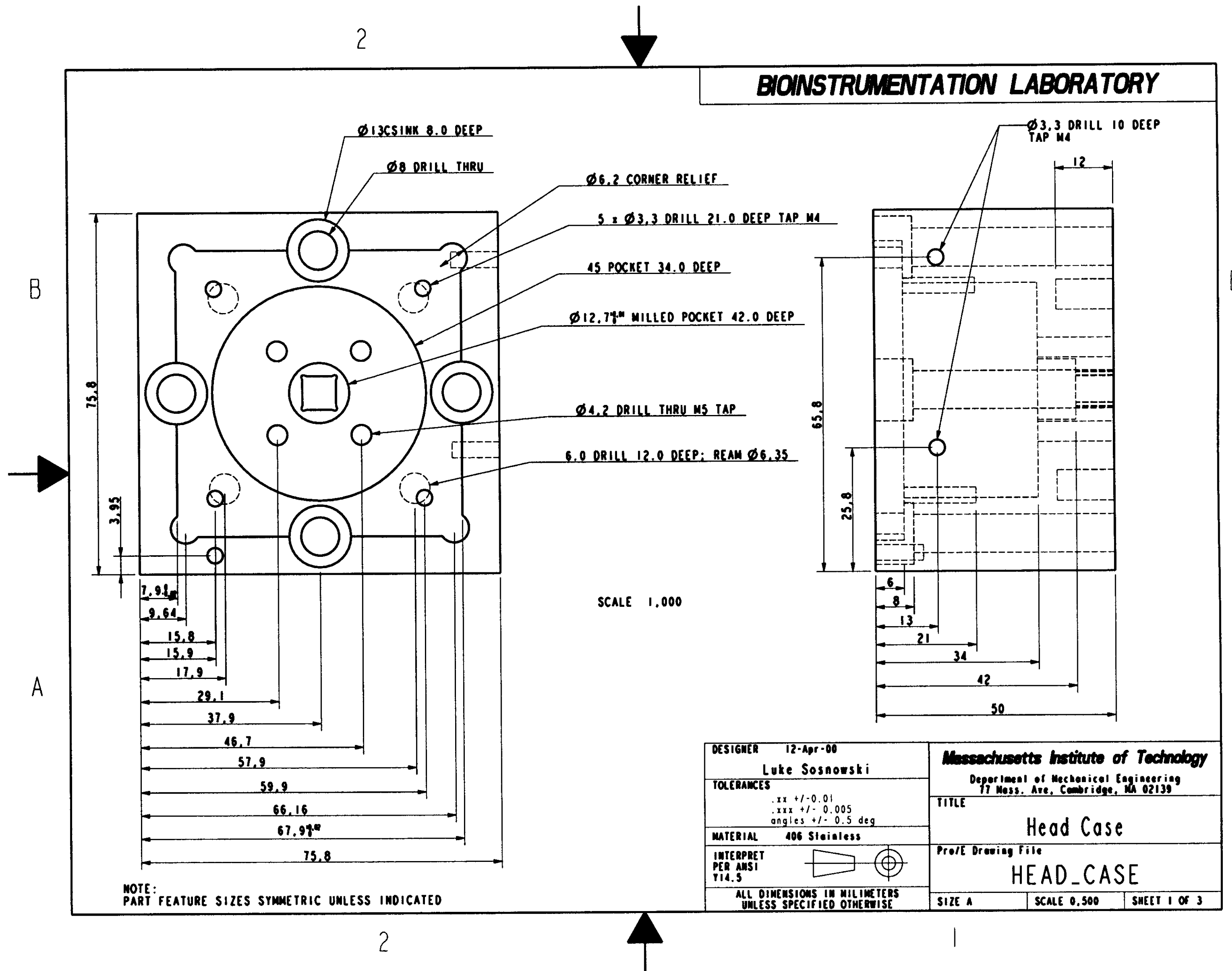

Figure B-5: Ram Head Case

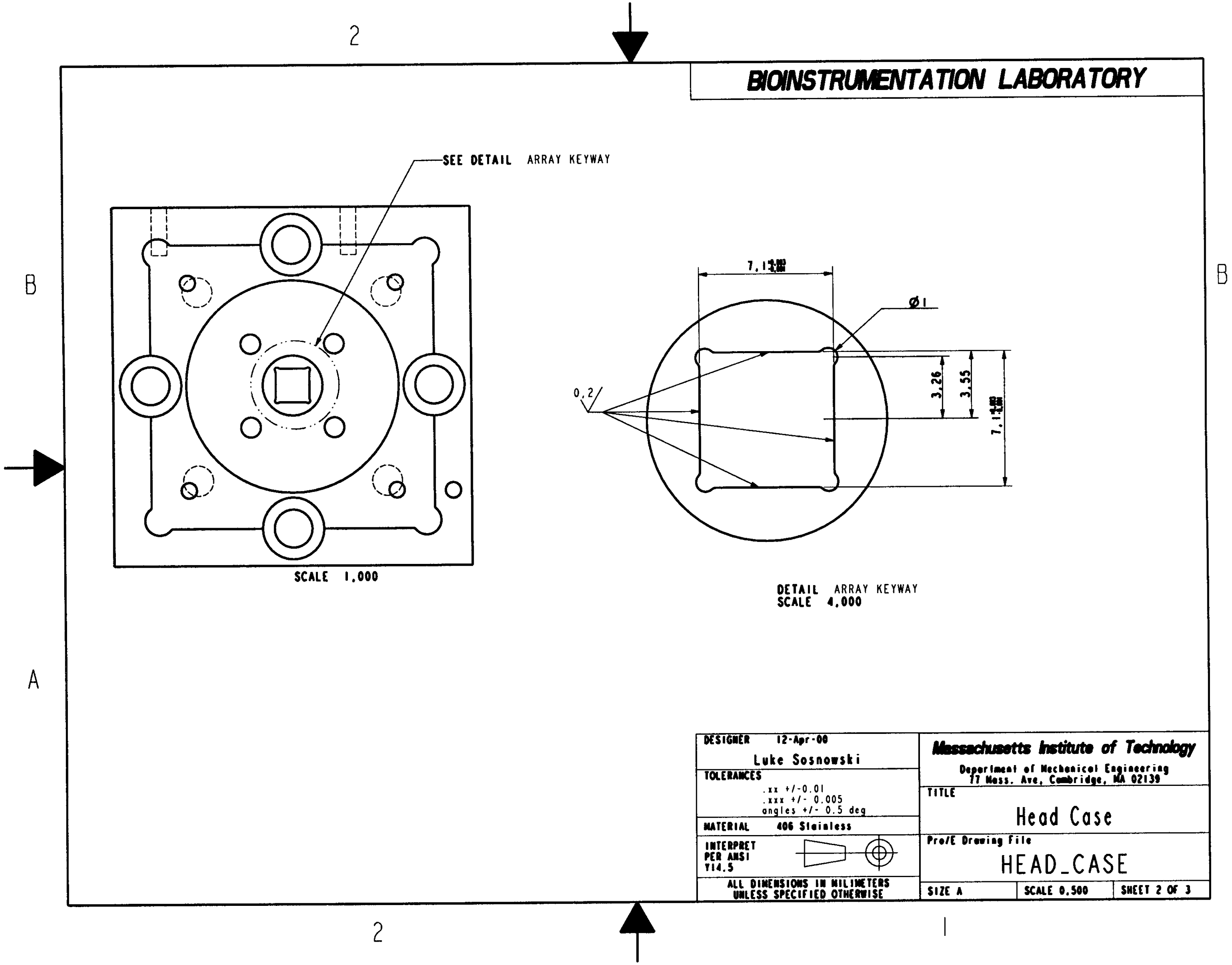

Figure B-6: Ram Head Case

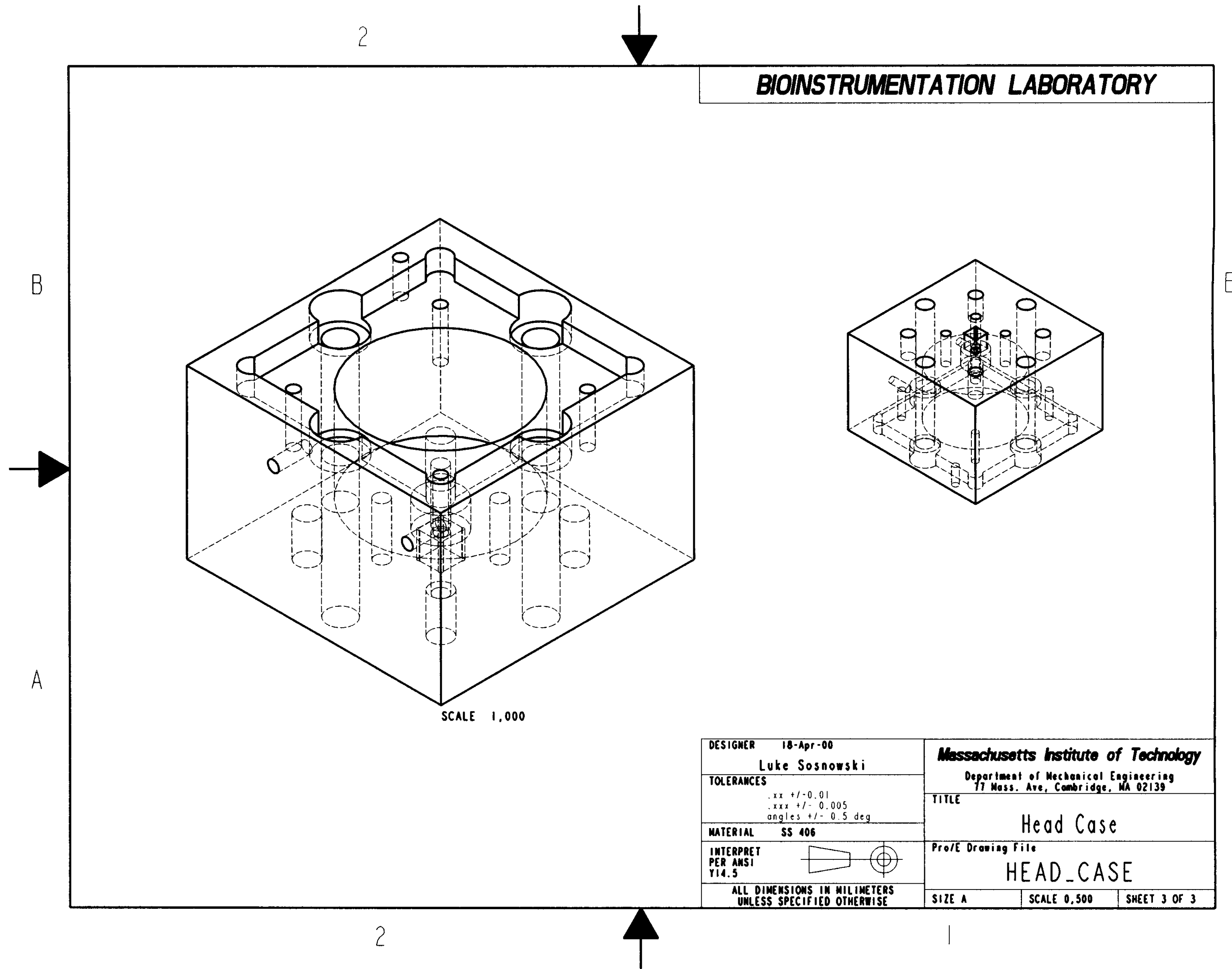

Figure B-7: Ram Head Case

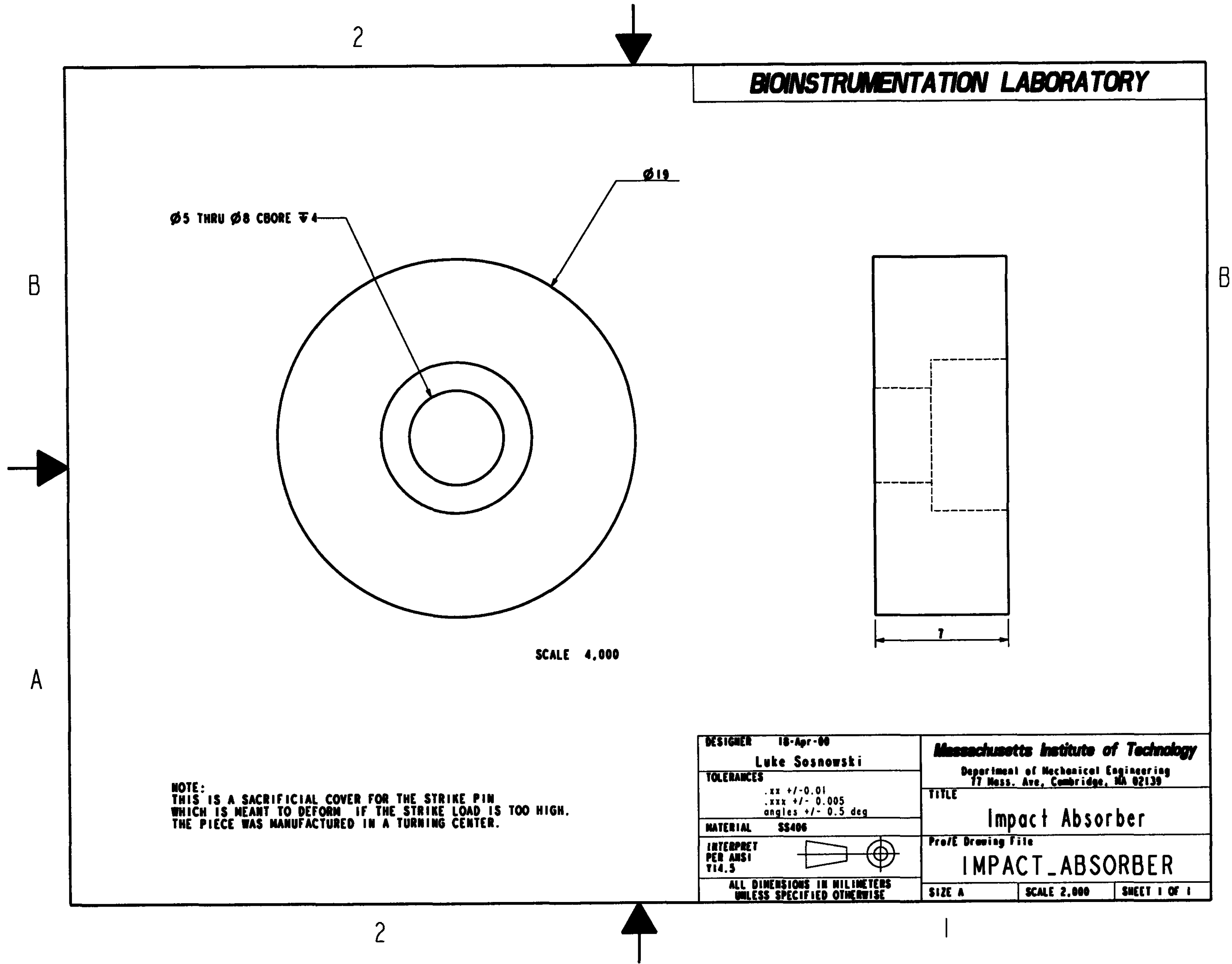

Figure B-8: Impact Absorber - Sacrificial Anvil

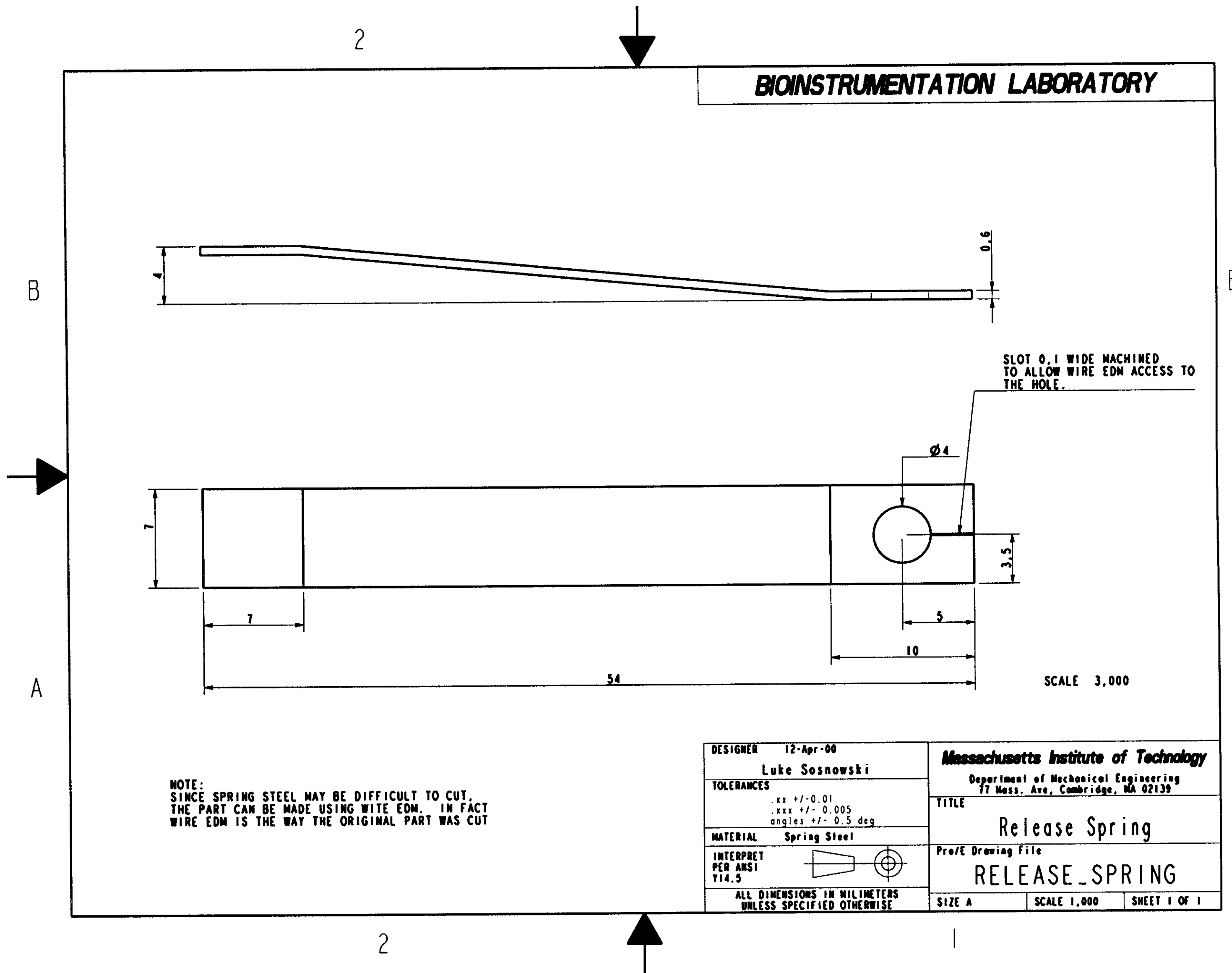

Figure B-9: Release Spring of Stopper Swing Arm

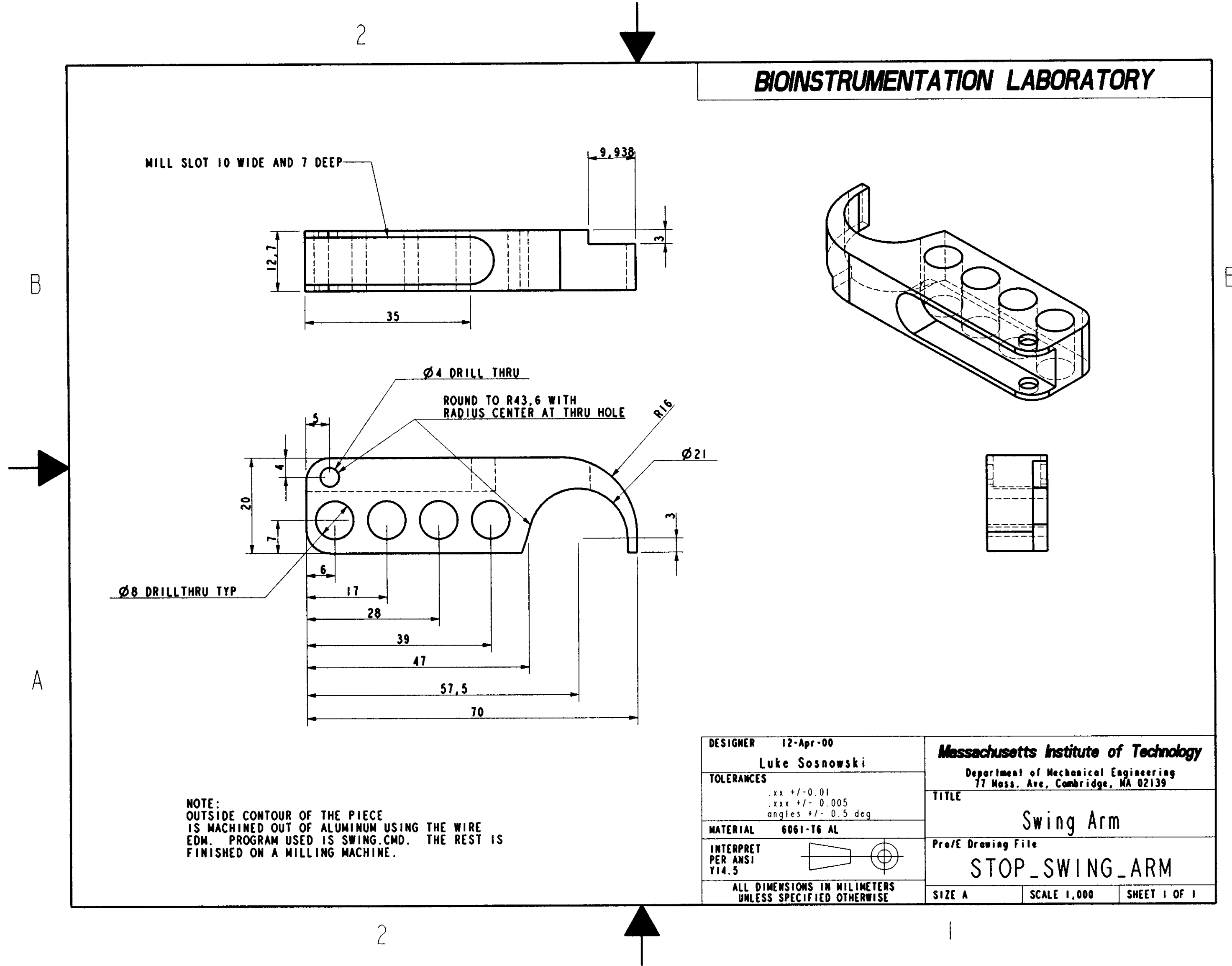

Figure B-10: Multi-Impact Preventing Stopper Swing Arm

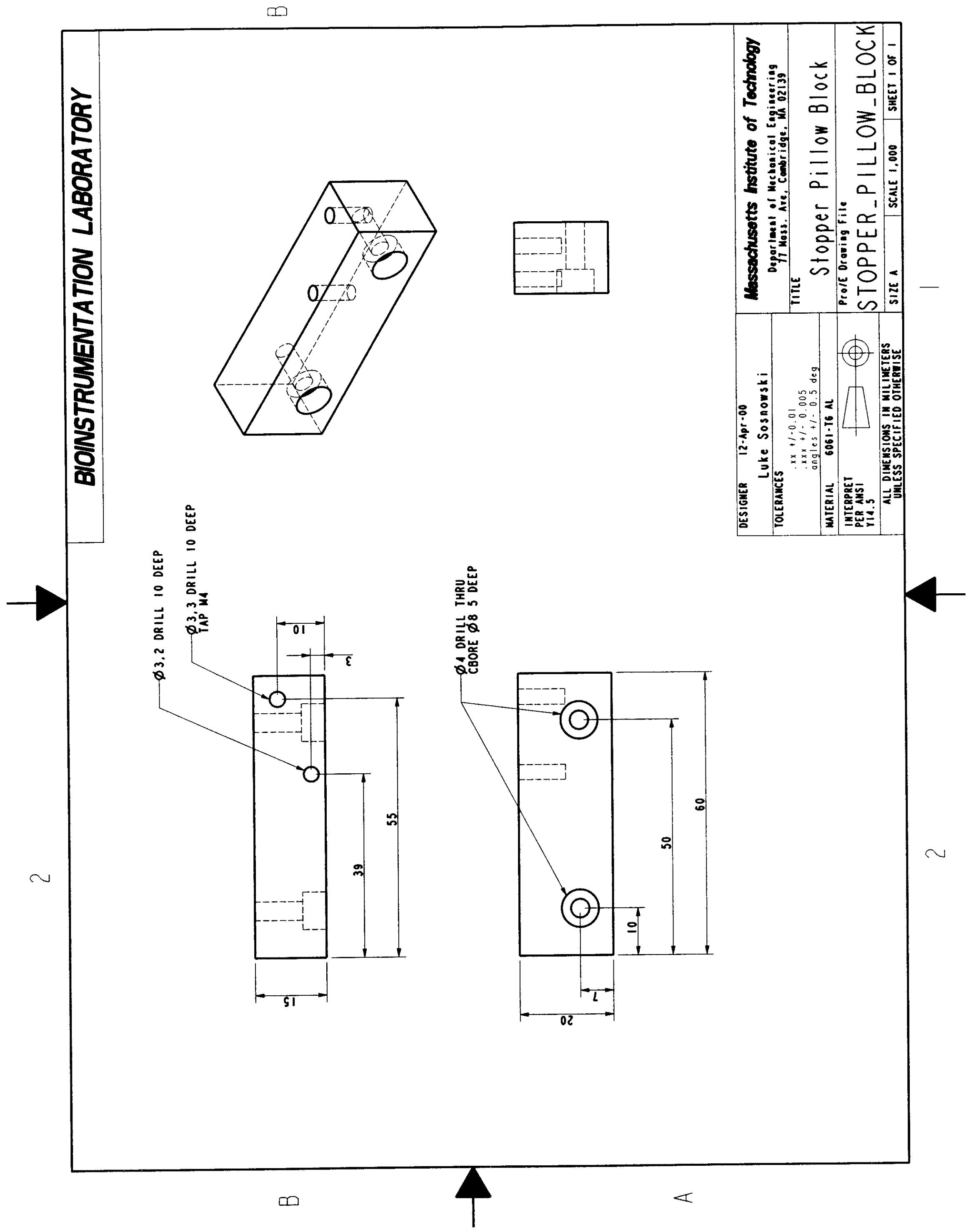

Figure B-11: Stopper Pillow Block

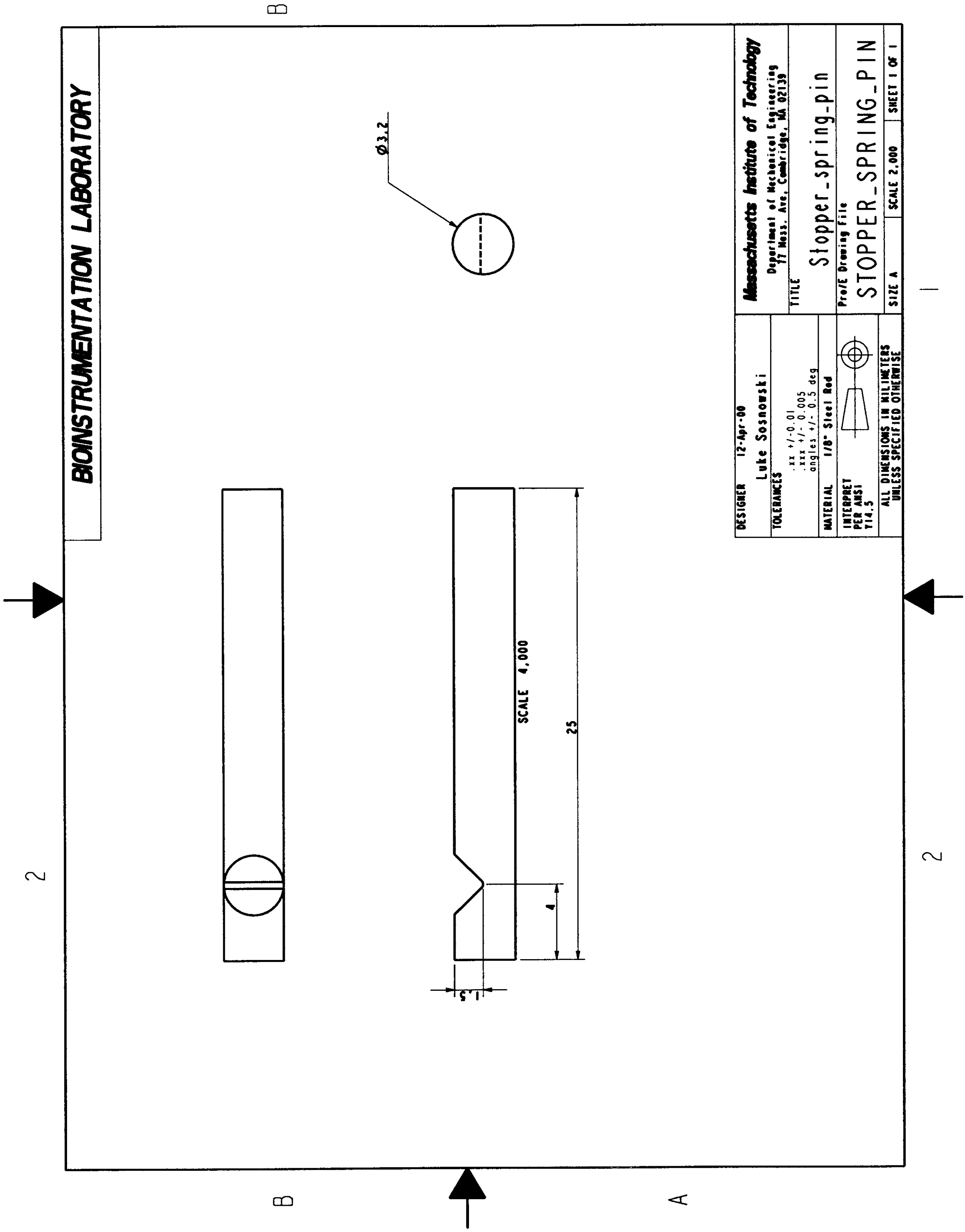

Figure B-12: Stopper Spring Retaining Pin

BIOINSTRUMENTATION LABORATORY

Ø5 DRILL M6 TAP

Ø12,7

Ø22

SCALE 2,000

SEE DETAIL COUPLING_SLOT

R0,5 BOTH SIDES

25

10

12

42,5

1,5

1,5

5,2

8

R0,3 TYP

NOTE:
&VIEW_NAME WAS CUT ON THE
EDM USING 0.25 MM WIRE.
REMAINING FEATURES WERE TURNED.

DETAIL COUPLING_SLOT
SCALE 4,000

DESIGNER 18-Apr-00 Luke Sosnowski	Massachusetts Institute of Technology Department of Mechanical Engineering 77 Mass. Ave, Cambridge, MA 02139		
TOLERANCES .xx +/-0.01 .xxx +/- 0.005 angles +/- 0.5 deg	TITLE Strike Pin		
MATERIAL SS 406			
INTERPRET PER ANSI Y14.5	Pro/E Drawing File STRIKE_PIN		
ALL DIMENSIONS IN MILIMETERS UNLESS SPECIFIED OTHERWISE	SIZE A	SCALE 1,000	SHEET 1 OF 1

Figure B-13: Ram Strike Pin

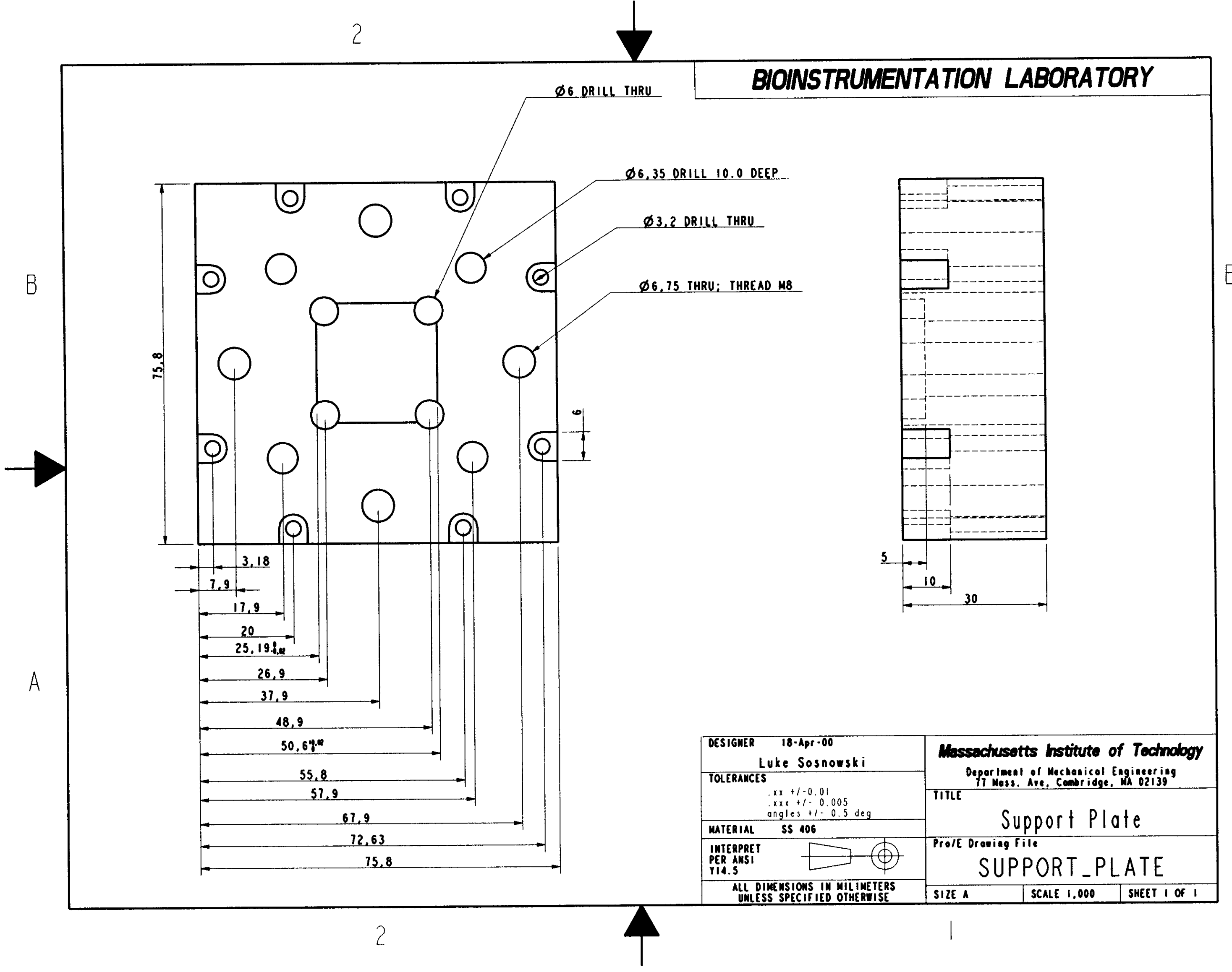

Figure B-14: Test Sample Support Plate

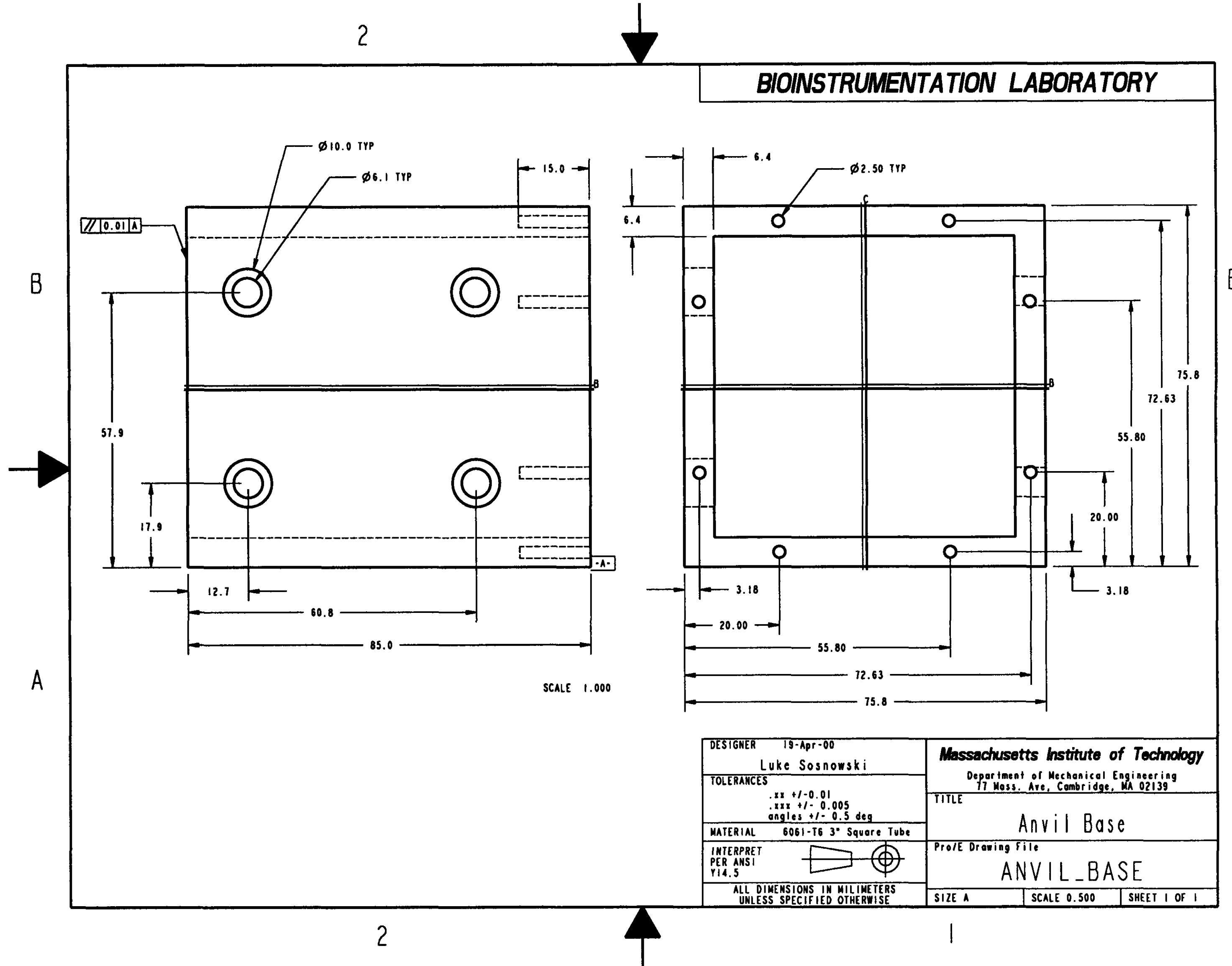

Figure B-15: Anvil Base

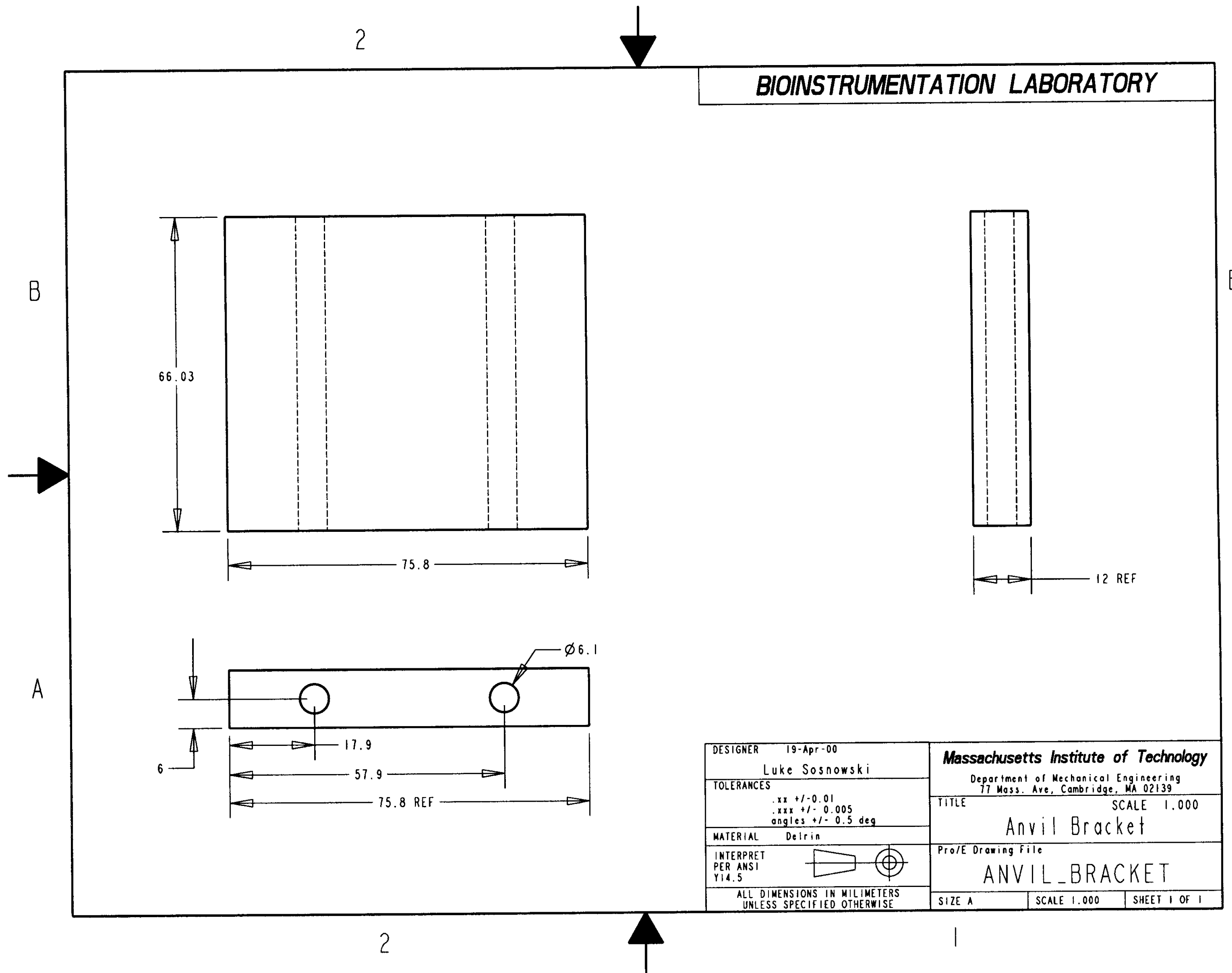

Figure B-16: Anvil Bracket

B.1.3 Ram Structure Part Drawings

This section includes the pasts of the ram other than the high precision head that contains the array die and plastic sample pieces.

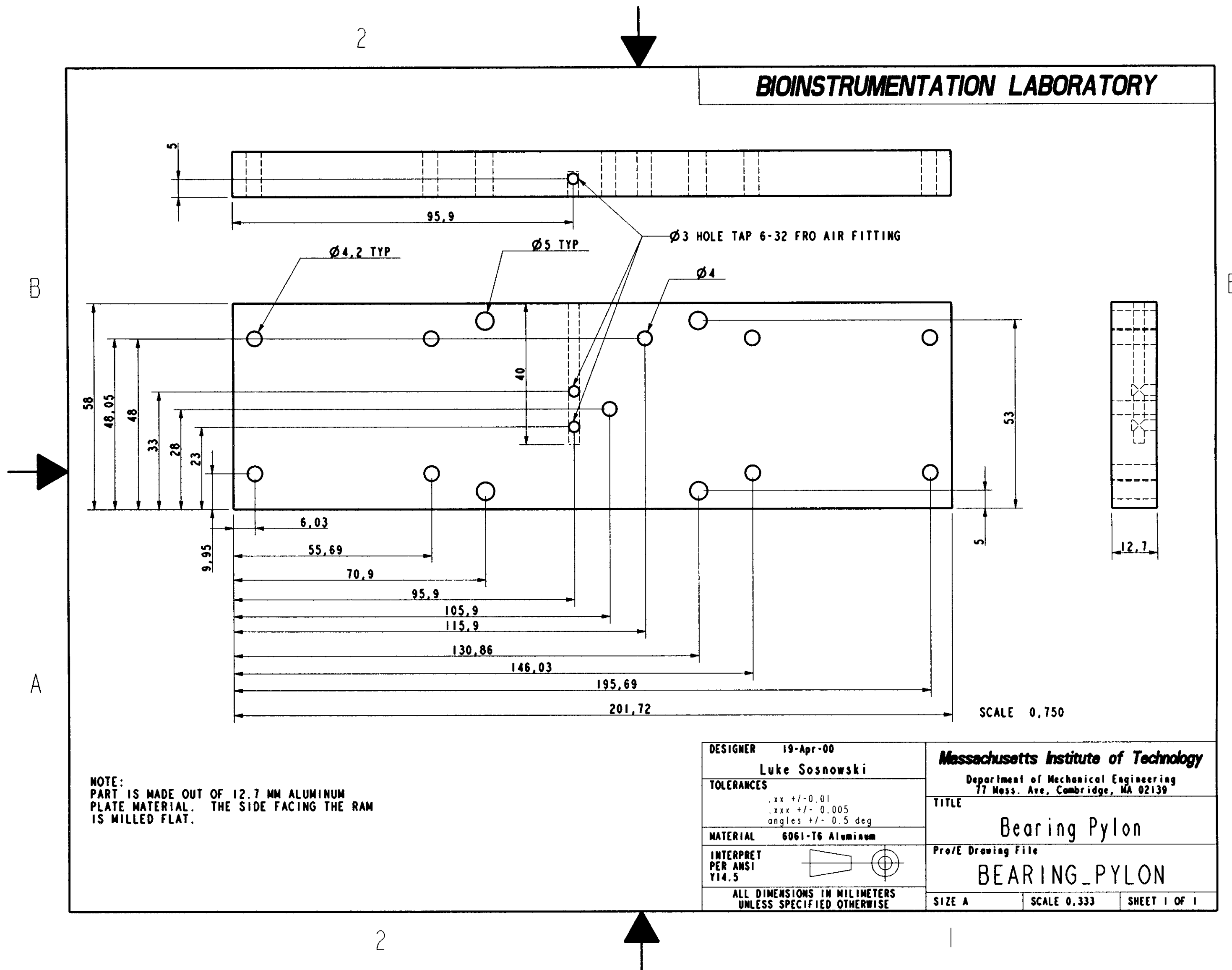

Figure B-17: Ram/Bearing Pylon

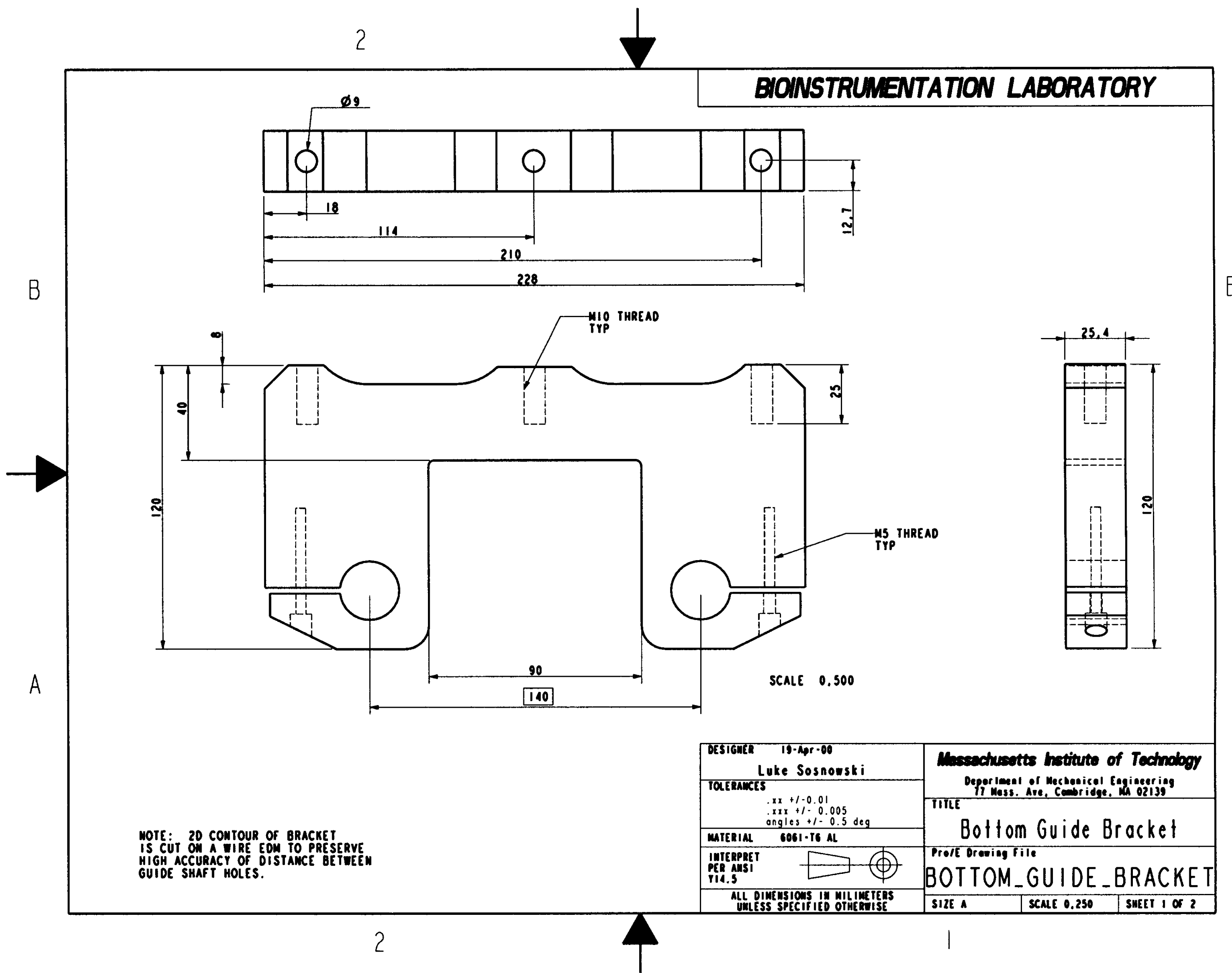

Figure B-18: Bottom Guide Bracket

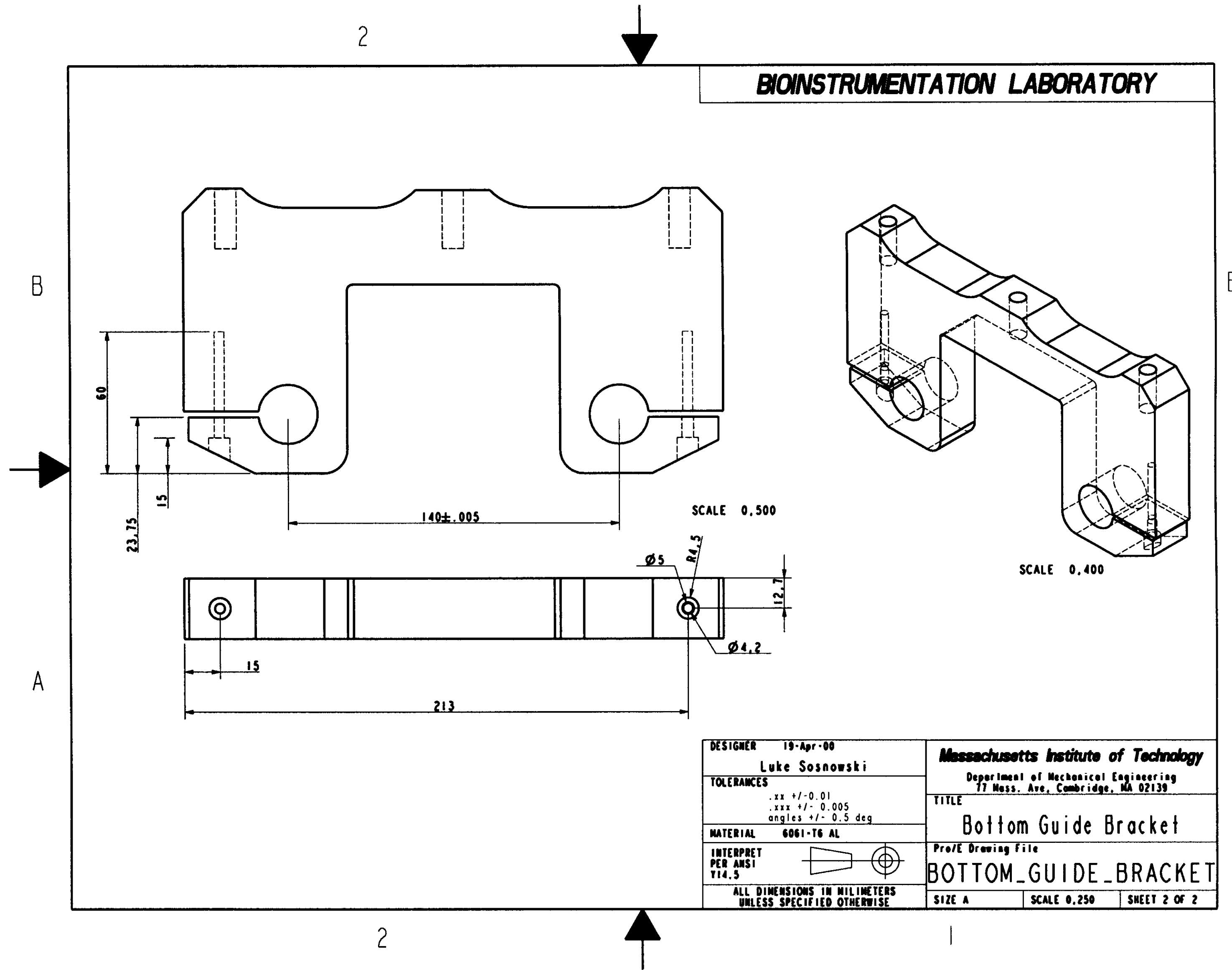

Figure B-19: Bottom Guide Bracket

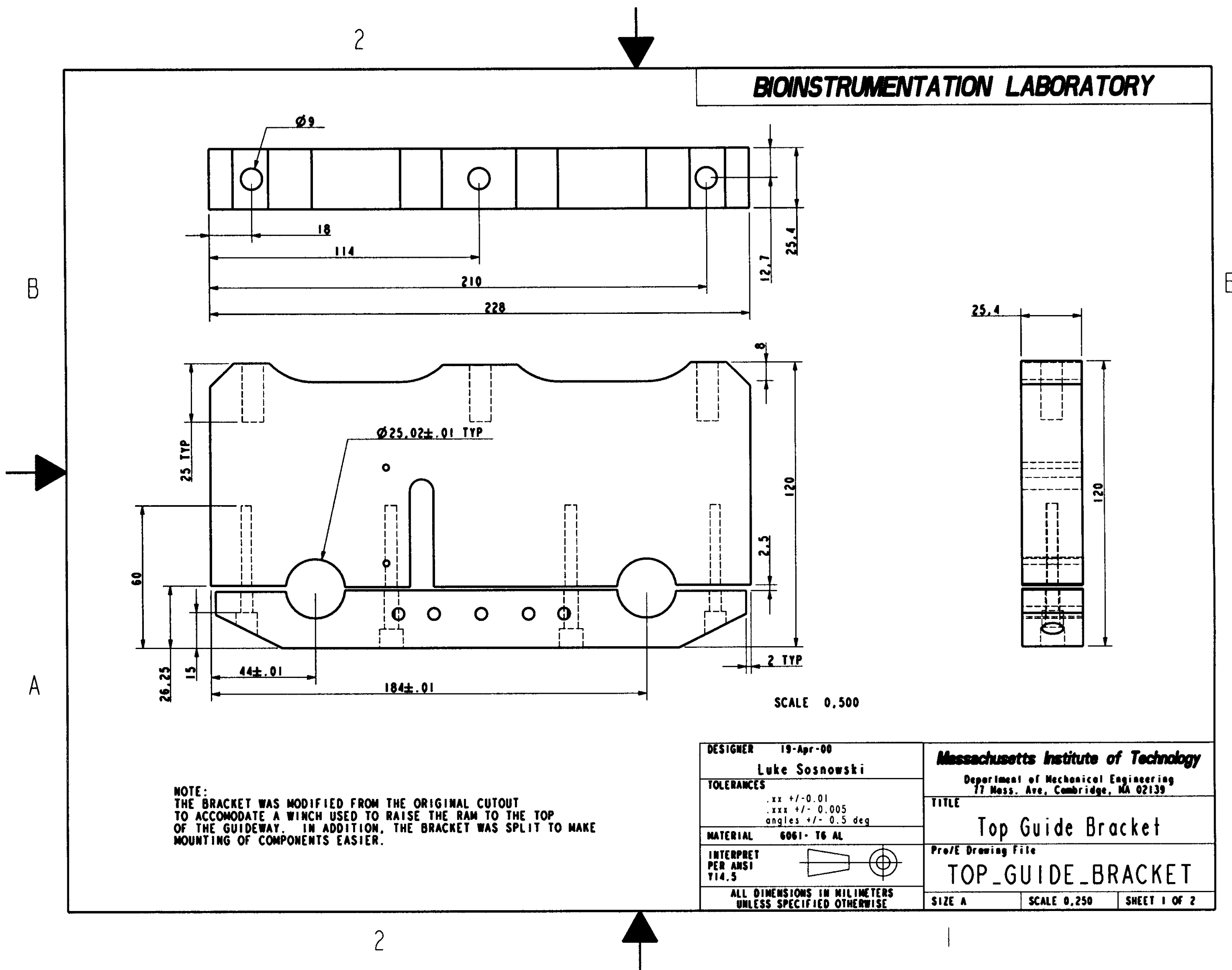

Figure B-20: Top Guide Bracket

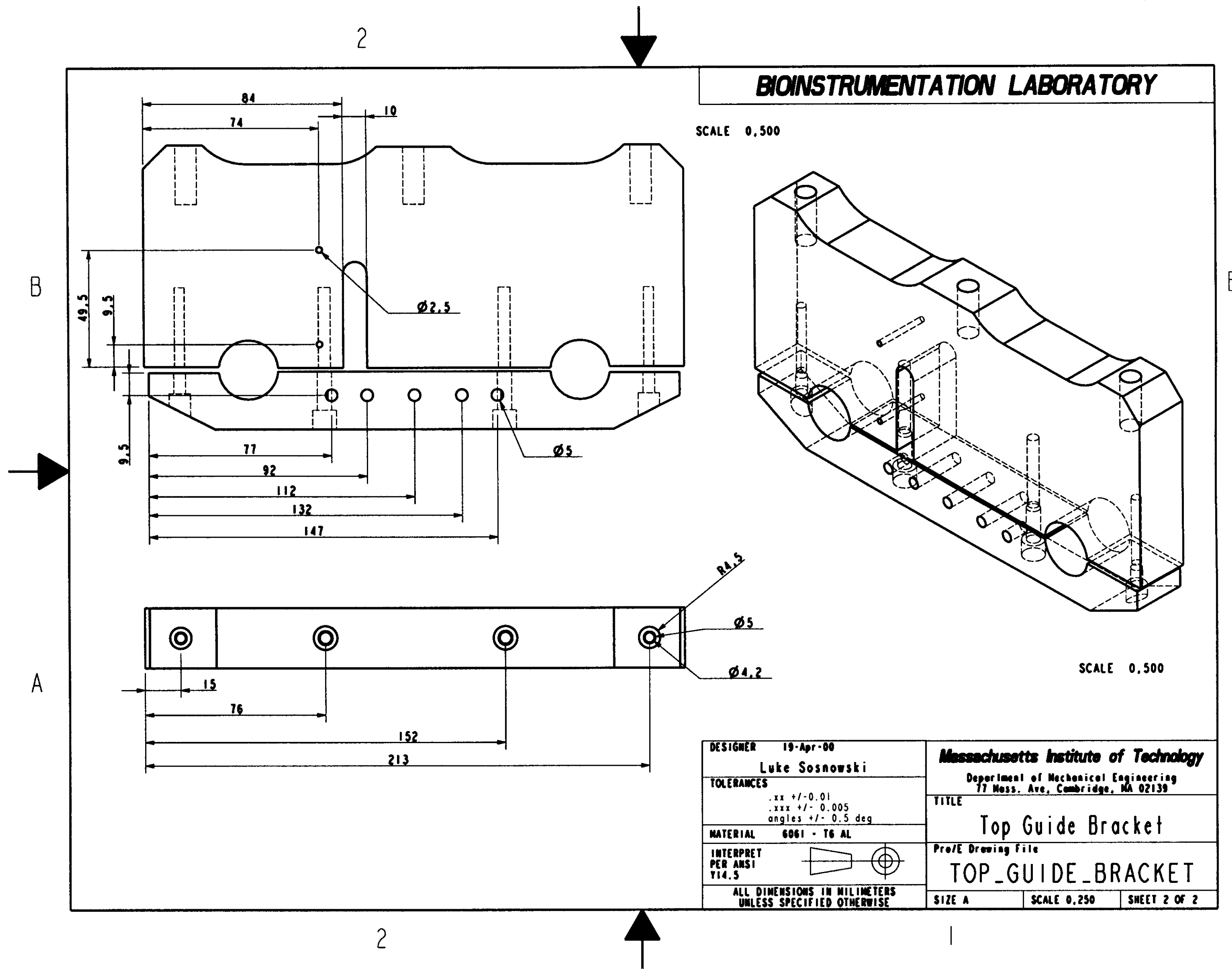

Figure B-21: Top Guide Bracket

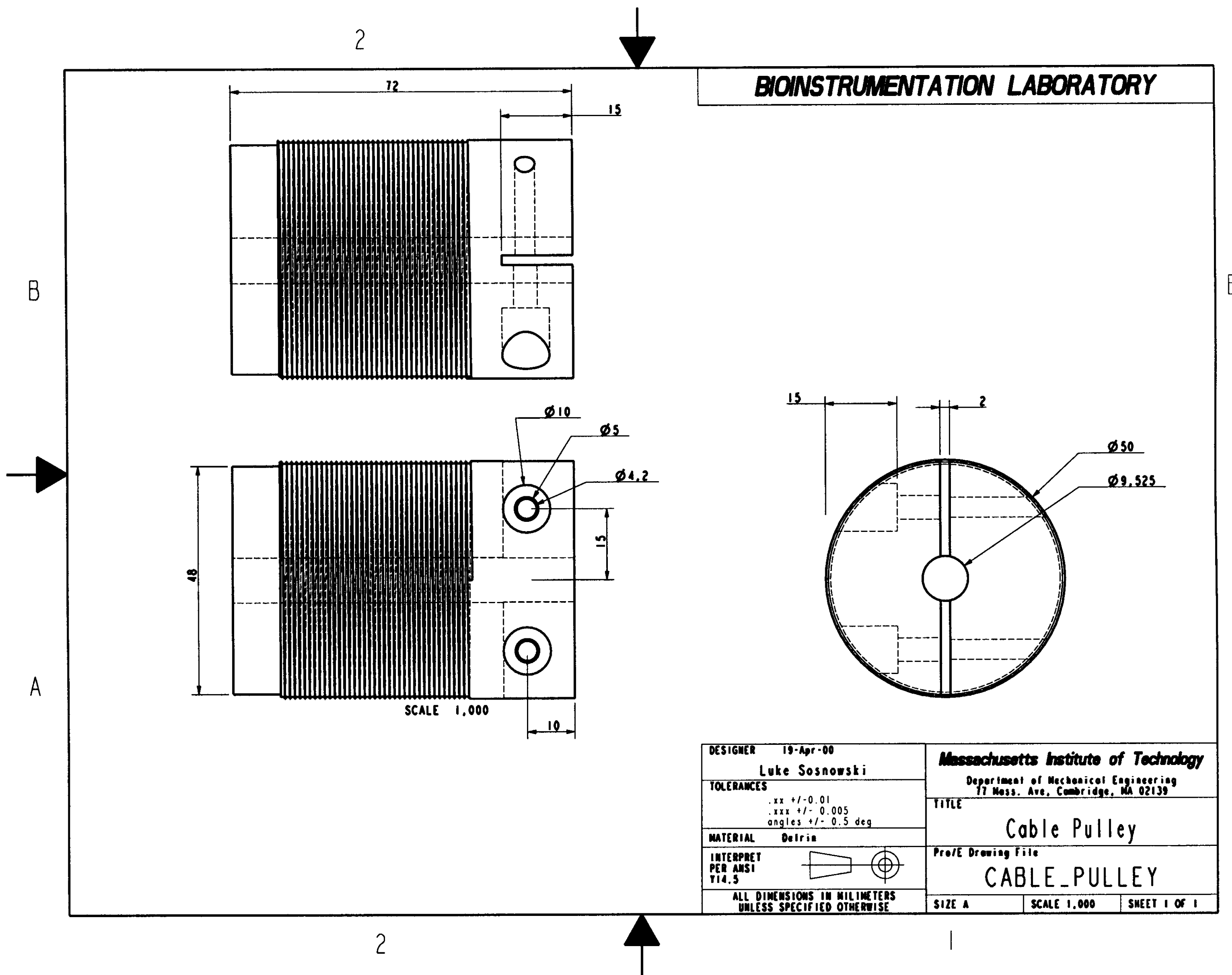

Figure B-22: Cable Pulley

B.1.4 Array Inserts

Array inserts are made out of either tungsten carbide or steel. The drawings reflect different pin configurations that were tested. Please refer to included G-codes for machine specific programs for creating these arrays.

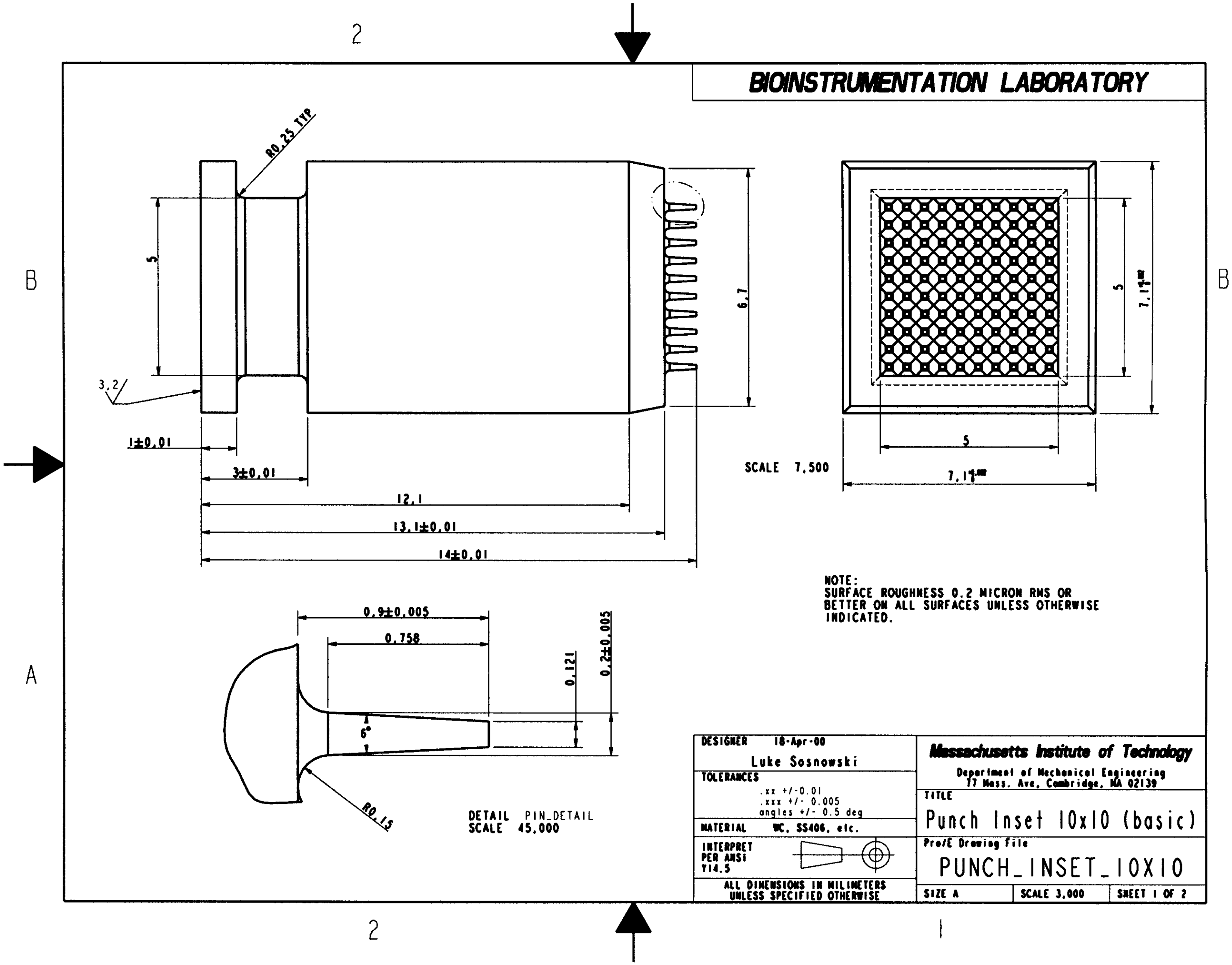

Figure B-23: Punch Inset - 10×10 Array - 0.9 mm Pins

2

BIOINSTRUMENTATION LABORATORY

B

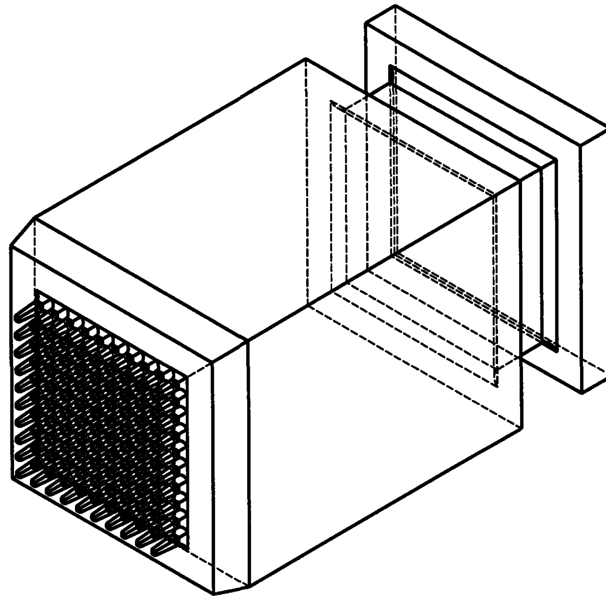

A

SCALE 7.500

DESIGNER 19-Apr-00 Luke Sosnowski	**Massachusetts Institute of Technology** Department of Mechanical Engineering 77 Mass. Ave, Cambridge, MA 02139		
TOLERANCES .xx +/-0.01 .xxx +/- 0.005 angles +/- 0.5 deg	TITLE Punch Inset 10x10 (basic)		
MATERIAL Carbide, SS406, etc.			
INTERPRET PER ANSI Y14.5	Pro/E Drawing File PUNCH_INSET_10X10		
ALL DIMENSIONS IN MILIMETERS UNLESS SPECIFIED OTHERWISE	SIZE A	SCALE 3.000	SHEET 2 OF 2

2 1

Figure B-24: Punch Inset - 10×10 Array - 0.9 mm Pins

B.2 EDM Array Components

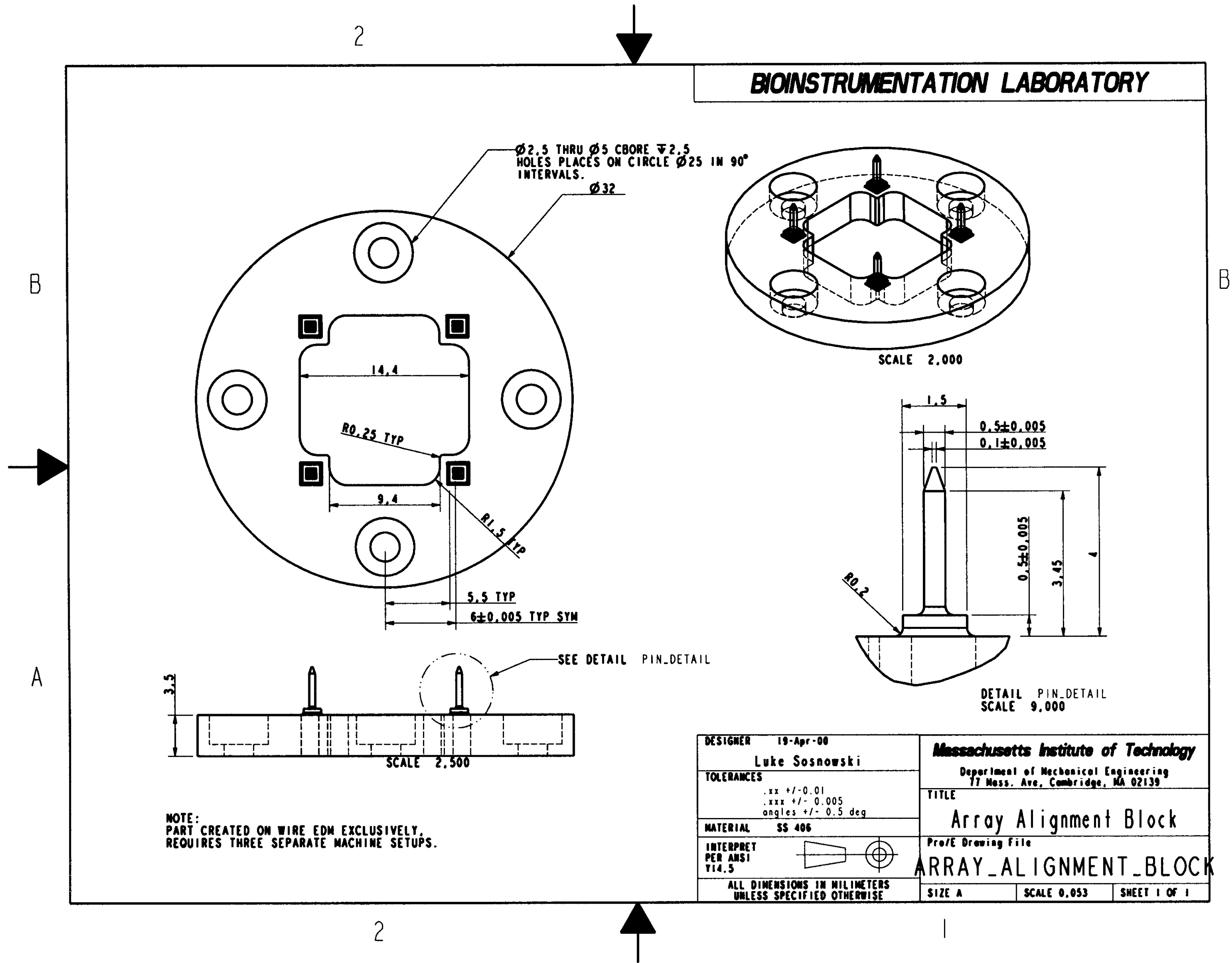

Figure B-25: 100 Hole Silicon Array Alignment Block

Appendix C

Programs

C.1 Matalab

The following Matlab code was useful in performing some of the calculations whose results are presented in this thesis.

```
% Resistor network simulation
%
% Uses Laplacian approximation to find equivalent resistance
% of a network of resistore, as for example a silicon array
% in various stages or machining.
%
% Luke Sosnowski, May, 2000
% Based on Laplacian approximation code by Peter Madden.
%
alpha = 1;

iterations = -1;

accuracy = .0001;

rows = 50;
cols = 50;

% set center

x = 25;
y = 25;

M = zeros(rows, cols);

% set external boundaries

B = ones(rows, cols);
B(2:rows-1,2:cols-1) = zeros(rows-2, cols-2);

% set initial conditions

M(x,y) = 1;
B(x,y) = 1;

figure(1);
surf(M);

figure(2);
surf(B);

U = LaplaceAC(alpha, iterations, accuracy, M, B)

figure(3);
surf(U);

% Resistance calculations

% Uncomment the code below for standard Lapla

%R_beam = 72.7 % ohms
%R_total = 1/(((1-U(x+1,y))+(1-U(x-1,y))+(1-U(
1)))/R_beam)

% Uncomment the code below for non-isotropic

R_1 = 72.7 % ohms
R_2 = 44.4 % ohms
R_total = 1/(((1-U(x+1,y))+(1-U(x-1,y)))/R_1+((
1)))/R_2)
```

```
function U = LaplaceAC(alpha, iterations, accuracy, M, B)

% Laplace(alpha, iterations, accuracy, M, B)
%
% Returns an approximation to the solution of the laplace equation.
% Initial conditions must be specified in M along all the outside edges
% and whatever interior points that need to be specified.
% If boundary conditions need to be specified, set the balue of B to 1
% at the point where value needs to be set.

% Alpha must be between 0 and 2. High values mean faster convergence
% but also greater instability.

% The numer of iterations determines how many tines the program will
loop
% before returning a solution. If the number of iterations is -1, then the
% the accuracy criterion is used instead.

% accuracy is the maximum possible change in values of the solution
matrix
% between iterations.

% Based on code by Peter Madden 5/9/00
% Revised to include

count=0; % set iteration counter
[n1,n2]=size(M); % find array size
error = accuracy + 1; % initialize error variable
M_old = zeros(n1,n2); % initialized M memory matrix

if iterations == -1 % solve fiven accuracy costraint
  while error > accuracy,
    M = LaplaceIterate(alpha, M, B);
    error = abs(max(max(M-M_old))); % find max error
    M_old = M;
    count=count+1;
  end
  U = M;
elseif iterations > 0 % solve with iteration constra
     for i = 1:iterations
      M = LaplaceIterate(alpha, M, B);
    end
    U = M;
else % error message
  (['Wrong iteration number'])
  U = M;
end

(['total iterations:'])
count
```

```
function U = LaplaceIterate(alpha, M, B)

% LaplaceIterate(alpha, M, B)

% Alpha is the convergence rate factor that must be set between 0 and 2.
% alpha is a tradeoff between convergence rate and stability.

% M is the matrix of the matrix of the solution which should include
% boundary values on all the boundaries as well as any interior points that
are specified.

% matrix B must be the same size as M and is Boolean.  The value of B
should be set to one
% wherever a point is to have a constant value.

% Luke Sosnowski, May 9, 2000
% Based on Peter Madden, May 8, 2000
% Based on Gershenfeld, "The Nature of Mathematical Modeling",
%       Cambridge University Press, 1999.

a = alpha;

% Set the method matrix that will be stepped over the matrix M using
convolution.

% Uncomment the code below for standard Laplacian approximation

%Conv= [ 0   a/4       0
%  a/4 (1-a)      a/4
%  0      a/4    0];

% Uncomment the code below for non-isotropic Laplacian approximation

Conv=  [ 0   .18977*a      0
  .31023*a (1-a)      .31023*a
  0      .18977* a      0];

U = conv2(M, Conv, 'same'); % returns only part
U = U.*(1-B) + M.*B; % rocovers the boundary

% repeat as necessary
```

```
% this program loads in a data file from the
% profilometer (headings must be stripped!),
% 'levels' the data, and then finds the RMS
% roughness in microns.
%
% Luke Sosnowski, 5/17/00

% load values
load edm_si2.dat -ascii
loc=edm_si2(:,1);
disp=edm_si2(:,2);

% fit a function
[P,S]=polyfit(loc, disp, 1);
disp_new=polyval(P,loc);

% now subtract the fitted line from the data
disp_norm=disp-disp_new;

x = ones(size(disp));

% now find the RMS error
y = sqrt(sum(disp_norm(:).^2)/length(disp_norm(:)));
RMS_roughness = y * 1e-4

% plot the corrected function plus the RMS limits

RMS_line = x.*RMS_roughness./2;
loc = loc./10000;
plot(loc, disp_norm.*1e-4, loc, RMS_line, loc, -RMS_line)
xlabel('Location (mm)')
ylabel('Surface height (microns)')
```

Bibliography

[1] *Honeywell.* 101 Columbia Road, Morristown, NJ 07962.

[2] *Igus, Inc.* P.O. Box 14349 E. Providence, RI 02914, USA, Tel: 1-800-521-2747, http://www.igus.com/.

[3] *Leech Carbide, Inc.* P.O.Box 539, 1061 Lamont Drive, Meadville,PA 16335, Phone: (800)441-7385, http://www.leechcarbide.com/.

[4] *Maple V Release 4.00b.* Waterloo Maple, 57 Erb St. W., Waterloo, Ontario, N2L 6C2, Canada, Tel: 519-737-2373.

[5] *Mathcad 2000 Professional.* MathSoft, Inc. 101 Main Street, Cambridge, MA 02142-152.

[6] *Mathematica.* Wolfram Research, Inc. 100 Trade Center Drive, Champaign, IL 61820, USA.

[7] *MATLAB.* The Mathworks, 3 Apple Hill Drive, Natick, MA 01760-2098.

[8] *MSC Industrial Supply Co.* 75 Maxess Road, Melville, NY 11747-3151.

[9] *New Way Bearings.* 4009-I Market Street, Aston, PA 19014 , USA, Tel: 1-800-394-1046, http://www.newwaybearings.com/.

[10] *Parametric Technology Corporation.* 128 Technology Drive,Waltham, MA 02453.

[11] *Patent #5501893: Method of Anisotropically Etching Silicon.*

[12] *Perkin Elmer Biosystems, Inc.* 761 Main Avenue, Norwalk, CT 06859,Phone 800-762-4000, http://www.pecorporation.com/.

[13] *System 3R USA.* 40-D Commerce Way, Totowa, NJ 07512.

[14] *Thomson Industries, Inc.* 2 Channel Drive, Port Washington, NY 11050, USA, Tel: 1-800-554-8466, http://www.thomsonindustries.com.

[15] *TYGH Silicon, Inc.* 135 Lindbergh Ave. Bldg.A, Livermore, CA 94550.

[16] M.F. Ashby. *Material Selection in Mechanical Design.* Butterworth-heinemann Ltd., Jordan Hill, Oxford, England, year =.

[17] D. Banks. *Introduction to Microengineering.*

[18] S. H. Crandall and et al. *An Introduction to the Mechanics of Solids.* McGraw-Hill, Inc., New York, New York., second edition, .

[19] G. Gruenwald. *Plastics: How Structure Determines Properties.* Carl Hanser Verlag, New York, New York, 1993.

[20] P. G. Hartwell and et al. *Deep Silicon RIE with Profile Control.* Ithaca, NY 14853, USA, http://fatmac.ee.cornell.edu/ defish/avstalk/posterindex.html, October 1997.

[21] P. Herren, D. Reynaerts, H. Van Brussel, C. Beuret, O. Larsson, and A. Bertholds. Microstructuring silicon by electro-discharge machining (edm) - part 2: Application. *Sensors and Actuators*, 61:379–386, 1997.

[22] R.C Hibbeler. *Mechanics of Materials.* Prentice-Hall, Inc., Upper Saddle River, New Jersey, third edition, 1997.

[23] T. S. Kanigan, C. J. Brenan, S. Lafontaine, L. Sosnowski, P. Madden, and I. W. Hunter. Living chips for drug discovery. *Advances in Nucleic Acid and Protein Analyses, Manipulation and Sequencing*, 1(20):172–180, January 2000.

[24] J. Marafona and C. Wykes. A new method for optimizing material removal rate using edm with copper-tungsten electrodes. *International Journal of Machine Tools and Manufacture*, 40:153–164, 2000.

[25] A.F. Mills. *Basic Heat and Mass Transfer.* Richard D. Irwin, Inc., Boston, Massachusetts, 1995.

[26] E. Oberg and et al. *Machinery's Handbook.* Industrial Press, New York, New York, 25th edition, 1996.

[27] D. Reynaerts, P. Herren, and H. Van Brussel. Microstructuring silicon by electro-discharge machining (edm) - part 1: Theory. *Sensors and Actuators*, 60:212–218, 1997.

[28] D. Reynaerts, W. Meeusen, and H. Van Brussel. Machining of three-dimensional microstructures in silicon by electro-discharge machining. *Sensors and Actuators*, 67:159–165, 1998.

[29] P. Shankar, V.K. Jain, and T. Sundararajan. Analysis of spark profiles during edm process. *Machining Science and Technology*, 1(2):195–217, 1997.

[30] M.A. Sills and et al. Future considerations in hts: the acute effect of chronic dillemas. *Drug Discovery Today*, 3(7):304+, July 1998. *http://www.ieice.or.jp/*.

[31] A. H. Slocum. *Precision Machine Design.* Society of Manufacturing Engineers, Dearborn, Michigan, 1992.

[32] K. Takahata, S. Aoki, and T. Sato. Fine surface finishing method for 3-dimensional micro structures. *IEICE Transactions Online*, (2):291+, February 1997. *http://www.ieice.or.jp/*.

[33] G. Van Wylen, R. Sonntag, and C. Borgnakke. *Fundamentals of Classical Thermodynamics.* John Wiley and Sons, Inc., New Youk, New York, 1994.

[34] Y.S. Wong, L.C. Lim, I. Rahuman, and W.M. Tee. Near-mirror-finish phenomenon in edm using powder-mixed dielectric. *Journal of Material Processing Technology*, 79:30–40, 1998.